Application of Hypersonic Vehicle Flying Qualities Criteria and Computational Considerations

by

June Choi

B.S., Aeronautical Engineering, Rensselaer Polytechnic Institute (1992)

Submitted to the Department of Aeronautics and Astronautics in partial fulfillment of the requirements for the degree of

Master of Science in Aeronautics and Astronautics

at the

MASSACHUSETTS INSTITUTE OF TECHNOLOGY

May 1994

Author .....
Department of Aeronautics and Astronautics
May 2, 1994

Certified by .....
Professor Rudrapatna V. Ramnath
Adjunct Professor of Aeronautics and Astronautics
Thesis Supervisor

Accepted by .....
Professor Harold Y. Wachman
Chairman, Departmental Committee on Graduate Students

Application of Hypersonic Vehicle Flying Qualities Criteria and Computational Considerations

by

June Choi

Submitted to the Department of Aeronautics and Astronautics
on May 2, 1994, in partial fulfillment of the
requirements for the degree of
Master of Science in Aeronautics and Astronautics

Abstract

The longitudinal stability and flying qualities as well as a parameter estimation approach are investigated for the Generic Hypersonic Aerodynamic Model Example (GHAME) vehicle along an optimal trajectory. The stability parameter provides very accurate stability information based on three simple aerodynamic coefficients and ambient density. The accuracy of the stability parameter is investigated in two approaches. One is a numerical solution and the other is the bound of an asymptotic solution derived from the Generalized Multiple Scales (GMS) technique. The stability parameter shows that the stability improves along the trajectory. The numerical solution and the bound of the solution based on the GMS theory also show the same results. Extended flying qualities criteria (EFQC) are based on the GMS theory, which provides analytical solutions for time-varying systems. The EFQC specify flying qualities in terms of variable system responses. The EFQC are applied to the GHAME vehicle to analyze the flying qualities of the short-period, phugoid, dutch-roll, spiral and roll modes. The spiral mode is the only mode which has adequate flying quality during the entire trajectory. Finally, a parameter estimation approach using the GMS theory is investigated. The advantages of the GMS method over the direct-integration (DI) method to estimate initial states are examined in terms of computational time. For the second order dynamics, the GMS method is 419 times faster than the DI reference case. For the fourth order dynamics of the GHAME vehicle, the GMS method is 447 times faster than the reference case. The benefit of using the GMS method in computing time is substantial and it will expedite the parameter estimation process.

Thesis Supervisor: Professor Rudrapatna V. Ramnath
Title: Adjunct Professor of Aeronautics and Astronautics

Acknowledgment

I sincerely wish to thank many people who made this thesis possible. First of all, I would like to express my deepest gratitude to Professor Rudrapatna V. Ramnath for his guidance and inspiration throughout the course of this study. I enjoyed his very interesting and wonderful stories related to the science and engineering fields.

I would like to thank Jon Anh, Bryan Kang, Seung Jin Song and other KGSA members for their consideration and encouragement. I would like to thank my friends Hansuk, Hunwook, Hyuck, Ian, Jinkyu, Mike, Minsuk, Sangjun, Shin-Juh, TJ, Yongki and others for their phone calls and encouragement. I also would like to thank my friends in Korea Donghee, Hosik, Jaehwa, Jiho, Kyungduk and others for their letters and Christmas cards.

Special thanks go to all of my professors at MIT and Rensselaer Polytechnic Institute. I owe thanks to all the teachers at Glen Rock High and Kyunggi High. I wish to thank Mr. Lee who was my fifth grade teacher years ago and who is now a Professor at a college. He inspired me to pursue life-long education.

I also wish to thank Rev. Kim, brothers and sisters of the Korean Church in Cambridge.

A great deal of appreciation must go to my grandparents and other relatives for their love, support and advice.

I thank God for his everlasting love, and I praise the Lord who made this study possible from the beginning.

My very special thanks go to Jiyean for her phone calls, prayer and encouragement throughout this study.

Finally, I would like to express deepest thanks to my parents and sister, Yoona, for their constant love, prayer and support. I would not have been here without them, and their love and support goes beyond my ability to express through words.

In memory of my grandfather,

Han Ki Choi,

who gave so much but expected nothing in return.

Contents

List of Figures

List of Tables

Chapter 1

Introduction

1.1 Background

With the emergence of new technology, human exploration and the development of space are expanding enterprises of the future, such as missions to Mars and space stations. These new explorations require advanced space vehicles. Since the first voyage of the space shuttle Columbia on April 12th, 1981, space shuttles have completed numerous successful missions, including the recent repair mission on the Hubble telescope. The space shuttle has been successful as a research and multipurpose spacecraft on many flights. However, the space shuttle program requires special and expensive launch facilities and rocket boosters that must be recovered from the ocean after each launch.

The present research interest has been focused on the development of fully reusable space vehicles, which will have single-stage-to-orbit (SSTO) capabilities and will be able to take off and land horizontally on conventional runways. These space vehicles will fly from subsonic through hypersonic speeds in excess of Mach 6. These improved modifications will provide increased versatility and lower costs of operation. The National Aeronautics and Space Administration (NASA) has proposed several hypersonic vehicles with these capabilities; perhaps the best known is the National Aerospace Plane (NASP). A successful flight of the NASP would represent the next generation of aerospace development and significant achievements in many engineer-

ing fields.

In the development of this vehicle, one of the difficult issues is the problem of predicting the dynamics and flying qualities of a hypersonic vehicle during its reentry into the Earth's atmosphere. The equations of motion describing the dynamics of the space vehicle are non-linear time-varying differential equations because the flight conditions of a vehicle change drastically during its reentry. It is impossible to obtain exact analytical solutions to these equations, and many approximation solutions have been attempted. In the past, such approximations to reentry dynamics have been developed by many restricting assumptions on the nature of the vehicle and reentry trajectory [8, 9].

In this thesis, the Generalized Multiple Scales (GMS) theory, which was developed by Ramnath [3, 6] on the basis of asymptotic analysis, is used to analyze the dynamics and flying qualities, and the GMS theory is also used to expedite the parameter estimation process. The major advantages of using the GMS theory are that it eliminates restrictions on the nature of vehicle and trajectory, and that it provides asymptotic solutions in the form of simple elementary functions. The GMS theory has been used to predict dynamics in various applications including the space shuttle, satellites and Vertical Take-Off and Landing (VTOL) aircraft [3, 4, 5].

In this study, the Generic Hypersonic Aerodynamics Model Example (GHAME) [1] along a space shuttle's trajectory has been used. The GHAME vehicle, which was developed at the Dryden Flight Research Facility in 1988, is a computer simulation model designed to estimate aerodynamic coefficients for a generic hypersonic vehicle.

1.2 Thesis Overview

This thesis is organized into seven chapters. The current chapter describes the background and motivation for this thesis.

Chapter 2 describes the GHAME vehicle and the trajectory on which the GHAME vehicle is studied. The reentry trajectory was designed to minimize the weight of the thermal protection system of the space shuttle orbiter 049 vehicle [2].

The conceptual foundation of the GMS theory is presented in Chapter 3. The analytical approximations of the GMS solutions for the second order and fourth order linear time-varying (LTV) differential equations are detailed.

In Chapter 4, the second order and fourth order longitudinal equations of motion as well as the fourth order lateral equation of the motion of the GHAME vehicle are presented. The stability parameter for longitudinal dynamics based on the GMS theory is also presented. The angle-of-attack perturbation dynamics are used for this investigation. The stability of the GHAME vehicle is investigated along the trajectory, and changes in degree of stability along the trajectory are investigated.

Application of the extended flying qualities criteria for the GHAME vehicle for the longitudinal and lateral modes are demonstrated in Chapter 5. The flying qualities of the GHAME vehicle are analyzed based on the extended flying qualities criteria.

Chapter 6 presents the parameter estimation process with the GMS method in initial state estimation. The advantages of the GMS method in the state estimation process are investigated in the second order system. The fourth order longitudinal and the fourth order lateral dynamics of the GHAME vehicle are also investigated for the state estimation process with the GMS method. The use of the initial state estimation with the GMS method in the parameter estimation is discussed.

The results are summarized and discussed in Chapter 7.

Chapter 2

GHAME Vehicle and Trajectory

2.1 Description of the GHAME Vehicle

The need for realistic hypersonic aerodynamic data increased with the recent interest in the development of hypersonic vehicles. The Generic Hypersonic Aerodynamic Model Example (GHAME) was developed at NASA Ames Research Center, Dryden Flight Research Facility, to provide realistic hypersonic aerodynamic data [1].

The GHAME model was developed as a combination of existing vehicles and theories. The sources were actual data from the space shuttle orbiter, a lifting body type vehicle, a swept double-delta configuration, and a 6^o half-angle cone using a modified Newtonian impact flow method. The longitudinal aerodynamic coefficients were a mix of various sources at all Mach numbers. The lateral aerodynamic coefficients were taken from space shuttle data and a swept double-delta configuration except for Mach numbers greater than 8, when the lateral aerodynamic coefficients were taken from space shuttle data only. The drag coefficients were modified in order to provide a realistic L/D ratio when compared with that of the space shuttle. The longitudinal and lateral aerodynamic coefficients were adjusted for reference span and reference area.

The GHAME model was developed for a single stage-to-orbit (SSTO) mission. This mission consists of a powered horizontal takeoff from conventional runways, and acceleration to orbital velocities with air-breathing engines to reach a low-Earth-orbit

(LEO). After completing its mission in orbit, the vehicle would reenter the Earth's atmosphere and maneuver to a gliding horizontal landing.

The configuration of the GHAME model consisted of simple geometrical shapes as seen in Fig. 2-1. The fuselage was modeled as a cylinder 20 ft in diameter and 120 ft in length. A pair of 10^o half-angle cones were attached to form a nose and a boat-tail in the fuselage. The delta wings and vertical tail were modeled as thin triangular plates. The GHAME model had a mid-wing configuration, and there was no dihedral on the wings. The engine module was wrapped around the lower surface of the fuselage and strakes were extended behind the wings. The reference area was 6000 ft^2, the reference chord was 75 ft and the reference span was 80 ft.

The mass properties of the GHAME model were assumed to be on the same order of magnitude as existing supersonic cruise aircraft and the estimates of the GHAME model were derived from the XB-70. The takeoff gross weight was estimated to be 300,000 lb and 60% of this weight was assumed to be the liquid hydrogen fuel. For the purpose of this study, the GHAME model is considered at the fuel burnout weight of 120,000 lb and the moments of inertia are also taken at fuel burnout condition. The complete set of parameters of the GHAME vehicle is shown in Table 2.1.

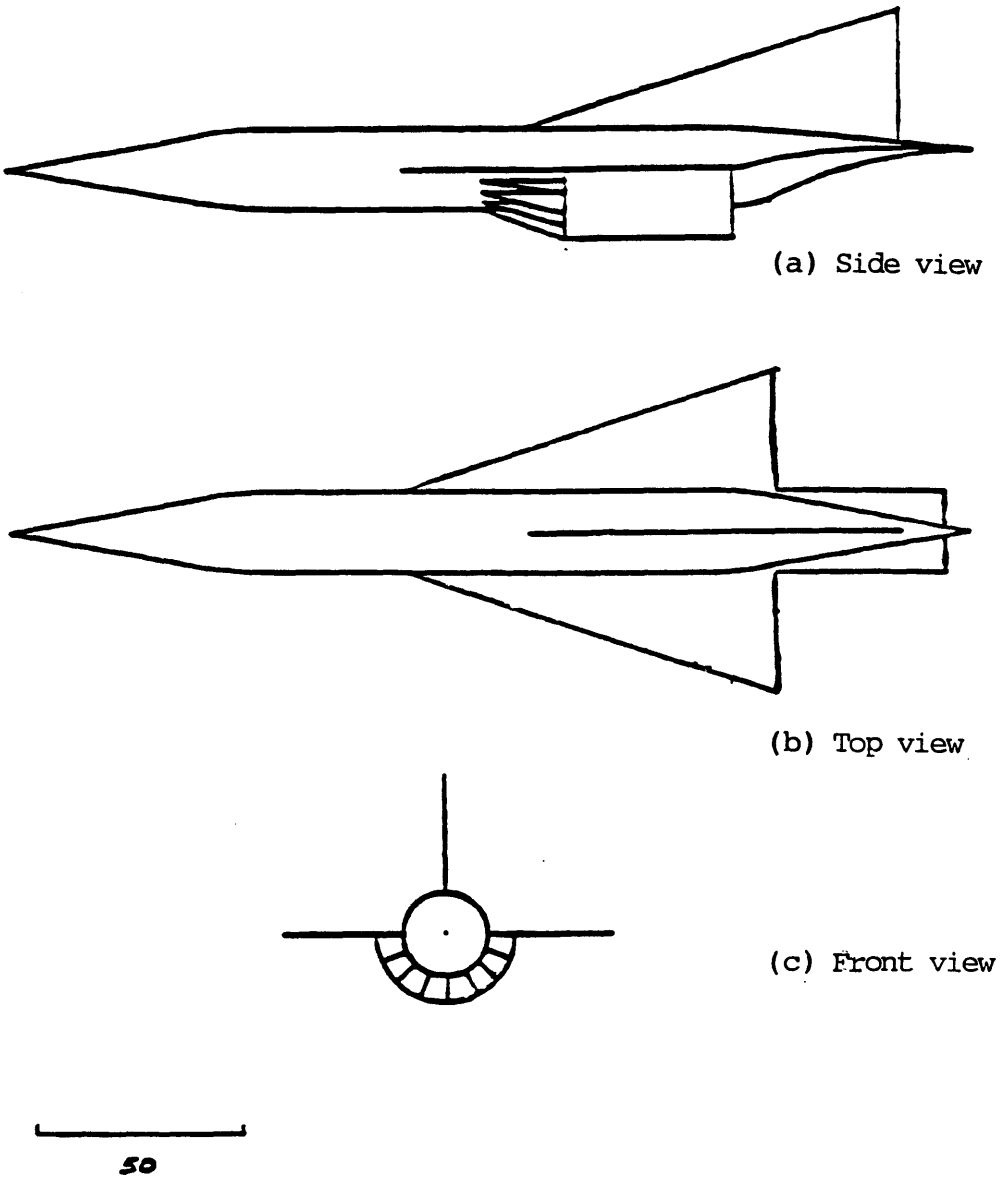

Figure 2-1: Configuration of GHAME vehicle

Table 2.1: Parameters of the GHAME vehicle

Length, l	233.4 ft
Reference area, S	6000 ft^2
Reference chord, c	75 ft
Reference span, b	80 ft
Weight,W_0 (At takeoff)	300,000 lb
Mass, m_0	300,000 slug
I_{xx}	1.16×10^6 slug-ft^2
I_{yy}	23.3×10^6 slug-ft^2
I_{zz}	24.0×10^6 slug-ft^2
I_{xz}	0.28×10^6 slug-ft^2
Weight, W_e (At fuel burnout)	120,000 lb
Mass, m_e	120,000 slug
I_{xx}	0.87×10^6 slug-ft^2
I_{yy}	14.2×10^6 slug-ft^2
I_{zz}	14.9×10^6 slug-ft^2
I_{xz}	0.28×10^6 slug-ft^2

2.2 Description of Trajectory

The dynamics of the GHAME vehicle are studied as it re-enters the Earth's atmosphere along a prescribed trajectory which was originally designed to minimize the thermal-protection-system (TPS) weight of the space shuttle orbiter 049 vehicle [2]. In order to obtain the optimal trajectory, the method of steepest descent was applied to minimize the total heat load.

This optimal trajectory was studied by Ramnath [3], and angle-of-attack, flight path angle, velocity, altitude, and time are shown as functions of a non-dimensional variable ξ in Fig. 2-2. The non-dimensional variable is the number of vehicle lengths traveled along the trajectory.

The space shuttle orbiter trajectory covers a range of 0 to 290,000 vehicle lengths and an altitude from 400,000 ft to 100,000 ft. The angle-of-attack varies from 53° to 19°, and the flight path angle varies from 0° to -4°. The reentry starts at Mach number 25.7 and it terminates at Mach number 3.1. The total time of the reentry trajectory is 1886 seconds.

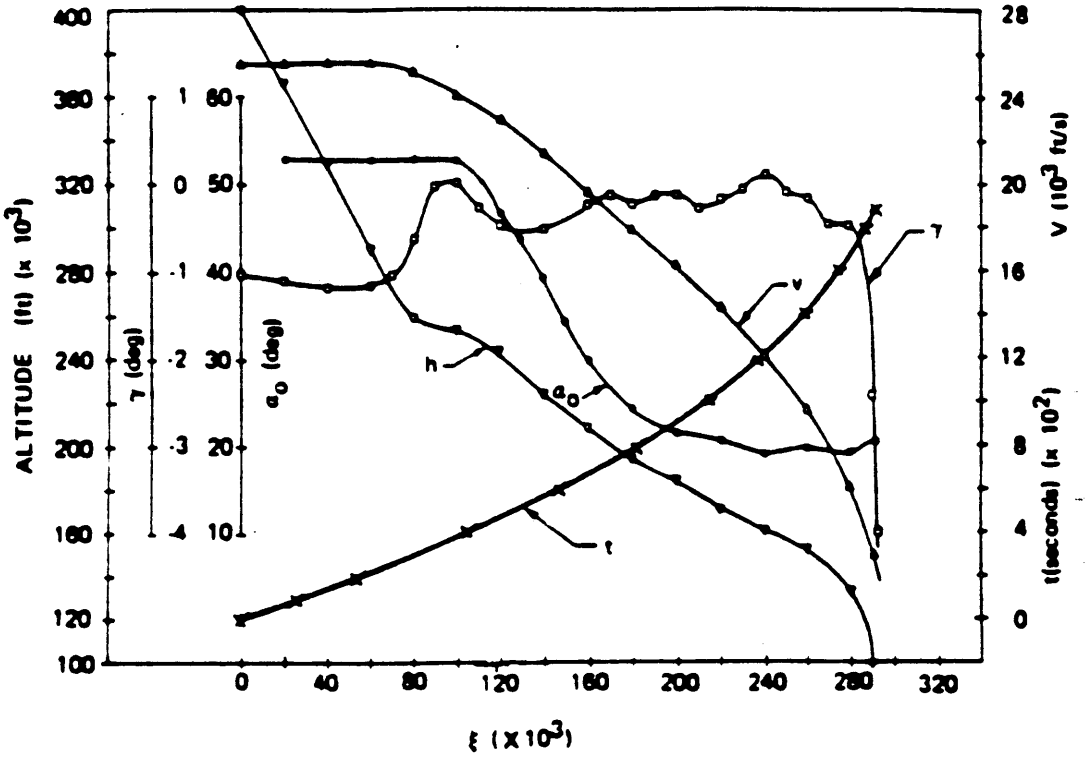

Figure 2-2: Characteristics of reentry trajectory

Chapter 3

Generalized Multiple Scales Theory

3.1 Description of General Theory

The General Multiple Scales (GMS) theory, which was developed by Ramnath [6, 7], is an asymptotic approach for approximating solutions for linear and non-linear time-varying systems. The concept of asymptotic solutions is based on the work of Poincarè [10, 11] and has been applied to many fields such as astrodynamics and fluid mechanics. The GMS theory has been used to study dynamics of various applications including the space shuttle, satellites and VTOL aircraft [3, 4, 5].

One very useful application of the GMS theory is that of approximate solutions for linear time-varying (LTV) differential equations. Although the first order LTV differential equations in general have exact solutions in terms of simple mathematical functions (such as exponential), only some higher order LTV differential equations have exact solutions in terms of functions such as Bessel or Mathieu functions, which are usually available in tabulated forms. The GMS theory provides approximate solutions to higher order LTV differential equations in terms of simple mathematical functions.

The GMS theory is based on the extension of the independent variable to a set of new independent scale functions. In this approach, the general solution is separated

into several modes which occur at different rates. The extension allows the dynamics to be separated into several modes which are then combined to make a complete solution. Applying the extension to an ordinary differential equation generates a set of partial differential equations with new independent variables.

3.2 Second Order GMS Solution

In this section, the GMS theory is applied to a second order LTV differential equation and the GMS solution is obtained by two time scales such as fast and slow scales [3]. Consider the second order LTV differential equation,

$$\frac{d^2y}{dt^2} + Z_1(t)\frac{dy}{dt} + Z_0(t)y = 0. \tag{3.1}$$

The characteristic roots which describe the solution of Eq. 3.1 are given by the second order algebraic equation,

$$S^2 + Z_1 S + Z_0 = 0. \tag{3.2}$$

As developed by Ramnath, the GMS solution for Eq. 3.1 is obtained by using two time scales. The fast part of the solution provides frequency information and the slow part of the solution provides correction for the amplitude. The GMS solution for Eq. 3.1 is given by

$$y(t) = y_s(t)y_f(t) \tag{3.3}$$

where the fast solution is

$$y_f(t) = C_1 exp(\int_{t_0}^{t} K_r(t)dt) sin(\int_{t_0}^{t} K_i(t)dt) + C_2 exp(\int_{t_0}^{t} K_r(t)dt) cos(\int_{t_0}^{t} K_i(t)dt) \tag{3.4}$$

and the slow solution is

$$y_s(t) = \left|4Z_0(t) - Z_1(t)^2\right|^{-1/4}. \tag{3.5}$$

Based on the initial condition, arbitrary constants C_1 and C_2 are determined, and K_i and K_r are the imaginary and real parts of the characteristic roots of Eq. 3.2.

3.3 Fourth Order GMS Solution

In this section, the two-time scales GMS theory is applied to a fourth order LTV differential equation [6, 7]. Consider the fourth order LTV differential equation,

$$\frac{d^4y}{dt^4} + Z_3\frac{d^3y}{dt^3} + Z_2\frac{d^2y}{dt^2} + Z_1(t)\frac{dy}{dt} + Z_0(t)y = 0. \tag{3.6}$$

The characteristic roots which describe the solution of Eq. 3.6 are given by the fourth order algebraic equation,

$$S^4 + Z_3S^3 + Z_2S^2 + Z_1S + Z_0 = 0. \tag{3.7}$$

Since the coefficients of the equation are time-varying, it is clear that the characteristic roots of this system also vary with time. Depending on the nature of the coefficients, the four roots of the algebraic equation are consisted of pairs of complex conjugate or real roots. A particular mode is represented by either a pair of complex conjugate roots or a single real root.

As developed by Ramnath, the GMS solution for Eq. 3.6 is obtained by using two time scales. The fast part of the solution provides frequency information and the slow part of the solution provides correction for the amplitude. If a mode is represented by a single real root, K, then the GMS solution is given by

$$y(t) = C_1 exp\int_{t_0}^{t} K(t)dt. \tag{3.8}$$

If a mode is represented by a complex conjugate pair of roots, $K = K_r \pm iK_i$, then the GMS solution is given by

$$y(t) = y_s(t)y_f(t) \tag{3.9}$$

where the fast solution is

$$y_f(t) = C_1 exp(\int_{t_0}^{t} K_r(t)dt) sin(\int_{t_0}^{t} K_i(t)dt) + C_2 exp(\int_{t_0}^{t} K_r(t)dt) cos(\int_{t_0}^{t} K_i(t)dt) \tag{3.10}$$

and the slow solution is

$$y_s(t) = exp(\int_{t_0}^{t} \left| \frac{\dot{K_r}(t)}{2iK_i(t)} \right| dt). \tag{3.11}$$

The complete GMS solution to the fourth order equation Eq. 3.6 is obtained by a linear combination of the approximations to each of the modes. For example, consider a system which contains three modes consisting of a pair of complex roots and two real roots. If the complex parts are given by $K = K_r \pm iK_i$ and the real roots are K_1 and K_2, then the full GMS solution to the system is given by

$$\begin{aligned} y_(t) &= C_1 exp(\int_{t_0}^{t} K_1(t)dt) + C_2 exp(\int_{t_0}^{t} K_2(t)dt) \\ &+ C_3 exp(\int_{t_0}^{t} \left| \frac{\dot{K_r}(t)}{2iK_i(t)} \right| dt) exp(\int_{t_0}^{t} K_r(t)dt) sin(\int_{t_0}^{t} K_i(t)dt) \\ &+ C_4 exp(\int_{t_0}^{t} \left| \frac{\dot{K_r}(t)}{2iK_i(t)} \right| dt) exp(\int_{t_0}^{t} K_r(t)dt) cos(\int_{t_0}^{t} K_i(t)dt). \end{aligned} \tag{3.12}$$

The arbitrary constants C1, C2, C3 and C4 are determined by initial conditions of the differential equation.

Chapter 4

Equations of Motion and Stability Parameter of the GHAME Vehicle

4.1 Introduction

In this chapter, the second order and the fourth order longitudinal equations of the motion as well as the fourth order lateral equation of the motion of the GHAME vehicle are presented. The stability of the second order longitudinal dynamics of the GHAME vehicle is investigated later in this chapter. The stability of a variable system such as the GHAME vehicle is difficult to predict in most cases. The GMS theory provides analytical insight into the dynamics in simple mathematical functions and the stability parameter, which was developed by Ramnath, is presented based on the second order GMS solution.

4.2 The Second Order Equation of the Motion for Longitudinal Dynamics

Under the assumption that a vehicle experiences lift without rolling or yawing motion, the equations describing the longitudinal motion of a vehicle are developed. The x-axis is tangential to the instantaneous flight path in this coordinate system and the

equations of the motion in the plane of the symmetry are described by [3, 8, 10]

$$\frac{dV}{dt} \equiv \dot{V} = -\frac{\rho S C_D V^2}{2m} - g sin\gamma \tag{4.1}$$

$$V\dot{\gamma} = \frac{\rho S C_L V^2}{2m} - (g - \frac{V^2}{R}) cos\gamma \tag{4.2}$$

$$\dot{q} = \frac{\rho S l C_m V^2}{2I_{yy}} - \frac{3g}{2R}(\frac{I_{xx} - I_{zz}}{I_{yy}}) sin2\theta \tag{4.3}$$

and the kinematic relations are

$$\dot{\theta} = q + \frac{V}{R} cos\gamma \tag{4.4}$$

$$\dot{R} = V sin\gamma \tag{4.5}$$

$$\theta = \gamma + \alpha. \tag{4.6}$$

After the Taylor series expansion about the nominal trajectory, and elimination of θ and q in Eqs. 4.1-4.3, a change of the variable is made [3, 8]. The independent variable time is replaced by a non-dimensional variable ξ with the relationship

$$\xi = \frac{1}{l}\int_0^t V(t)dt. \tag{4.7}$$

The new independent variable is the number of the vehicle lengths traveled along the trajectory. This change of the variable leads to a general equation for the angle-of-attack perturbation,

$$\frac{d^2\alpha}{d\xi^2} + Z_1(\xi)\frac{d\alpha}{d\xi} + Z_0(\xi)\alpha = 0 \tag{4.8}$$

where

$$Z_1(\xi) = \delta(C_{L\alpha} - \sigma(C_{M\dot{\alpha}} + C_{Mq})) + \frac{V'}{V} \tag{4.9}$$

$$\begin{aligned} Z_0(\xi) \;=\; & -\delta(\sigma C_{m\alpha} + \frac{gl}{V^2} C_{D\alpha} cos\gamma) + \delta' C_{L\alpha} + \delta\frac{V'}{V} C_{L\alpha} \\ & -\delta^2(C_{L\alpha}(\sigma C_{mq} + C_{D0}) + C_{L0} C_{D\alpha}) \end{aligned}$$

$$+\frac{3l}{R}\frac{gl}{V^2}\nu cos2(\gamma+\alpha_0) \tag{4.10}$$

and

$$\delta = \frac{\rho Sl}{2m} \tag{4.11}$$

$$\sigma = \frac{ml^2}{I_y} \tag{4.12}$$

$$\nu = \frac{I_{xx} - I_{zz}}{I_{yy}}. \tag{4.13}$$

The prime represents the differentiation with respect to the new independent variable ξ.

4.3 The Fourth Order Equation of Motion for Longitudinal Dynamics

In this section, the fourth order equations of motion for longitudinal dynamics and the lateral dynamics of the GHAME vehicle are presented. The state space form of equations of motion can be transformed into the differential equation in a scalar form which describes the dynamics of the vehicle [10, 12]. The longitudinal dynamics of the GHAME vehicle are represented by [10]

$$\frac{d^4y}{dt^4} + Z_3\frac{d^3y}{dt^3} + Z_2\frac{d^2y}{dt^2} + Z_1(t)\frac{dy}{dt} + Z_0(t)y = 0. \tag{4.14}$$

where

$$Z_3 = \frac{L_\alpha}{V_0} - M_{\dot\theta} + D_V \tag{4.15}$$

$$Z_2 = D_V\frac{L_\alpha}{V_0} - D_V M_{\dot\theta} - M_{\dot\theta}\frac{L_\alpha}{V_0} - M_\alpha - D_\alpha\frac{L_\alpha}{V_0} + g\frac{L_V}{V_0} \tag{4.16}$$

$$Z_1 = M_V D_\alpha - M_\alpha D_V - D_V M_{\dot\theta}\frac{L_\alpha}{V_0} + D_\alpha M_{\dot\theta}\frac{L_V}{V_0} - gM_{\dot\theta}\frac{L_V}{V_0} \tag{4.17}$$

$$Z_0 = g(M_V \frac{L_\alpha}{V_0} - M_\alpha \frac{L_V}{V_0}) \tag{4.18}$$

The fourth order GMS solutions, which are detailed in Chapter 3, approximate solutions of a differential equation by separately approximating the dynamics of the each mode of the motion. These approximations require those characteristic roots associated with each of the GHAME vehicle's modes. The characteristic roots of the longitudinal equation of motion are determined by solving the algebraic equation

$$S^4 + Z_3 S^3 + Z_2 S^2 + Z_1 S + Z_0 = 0. \tag{4.19}$$

The roots associated with the modes of motion will not remain stationary because coefficients of Eq. 4.19 are time-varying.

Fig. 4-1 clearly illustrates the roots of the short-period mode and the time-varying characteristics during the entire trajectory. The roots of the short-period mode remain in the left-half plane throughout the entire trajectory. The damping associated with short-period increases as the GHAME vehicle traverses further into the atmosphere and the frequency associated with this mode increases until 1200 seconds then it decreases.

Fig. 4-2 clearly illustrates the roots of the phugoid mode and the time-varying characteristics during the entire trajectory. It is clear that the roots of the phugoid mode behave in a non-conventional manner. In the beginning of the GHAME vehicle's reentry, the roots are in the right-half plane as a pair of complex conjugate roots. As the vehicle progresses into the atmosphere, a pair of complex conjugate roots moves into left-half plane and then returns to the right-half plane at 312 seconds. At 400 seconds into the reentry trajectory, the pair of complex conjugate roots suddenly becomes a pair of real roots. One of them is a positive root and the other is a negative root. These real roots move towards the origin, then two roots become a pair of complex conjugate roots at 685 seconds. The roots stay as a pair of complex conjugate roots until 1670 seconds and then these roots become two real roots again at the end of the trajectory.

The peculiar behavior of the phugoid mode requires more careful use of the GMS theory to study the vehicle dynamics. The points at which the roots transform from complex conjugate roots to real roots, or the reverse, are known as the 'turning points' and represent a change in the nature of the mode between oscillatory and non-oscillatory behavior.

The lateral dynamics of the GHAME vehicle are represented by [10]

$$\frac{d^4y}{dt^4} + Z_3\frac{d^3y}{dt^3} + Z_2\frac{d^2y}{dt^2} + Z_1(t)\frac{dy}{dt} + Z_0(t)y = 0. \tag{4.20}$$

where

$$Z_3 = -L_p - N_r - Y_v \tag{4.21}$$

$$Z_2 = VN_v - L_rN_p + Y_vL_p + N_r(L_p + Y_v) \tag{4.22}$$

$$Z_1 = Y_v(L_rN_p - N_rL_p) - gL_v + VN_pL_v - VL_pN_v \tag{4.23}$$

$$Z_0 = g(L_vN_r - N_vL_r) \tag{4.24}$$

The fourth order GMS solution, which is shown in Chapter 3, requires that the each mode of motion and its corresponding roots be identified. The characteristic roots of the lateral equation of motion are determined by solving the algebraic equation

$$S^4 + Z_3S^3 + Z_2S^2 + Z_1S + Z_0 = 0. \tag{4.25}$$

The roots associated with the modes of motion will not remain stationary because coefficients of Eq. 4.25 are time-varying.

Fig. 4-3 clearly illustrates the roots of the dutch-roll mode and the time-varying characteristics during the entire trajectory. The roots of the dutch-roll mode remain in the left-half plane throughout the entire trajectory. The damping associated with

dutch-roll increases as the GHAME vehicle traverses further into the atmosphere and the frequency associated with this mode increases until 1200 seconds, then it decreases.

Figs. 4-5 and 4-7 clearly illustrate the roots of the spiral mode and the time-varying characteristics during the entire trajectory. The roots of the spiral mode remain in the right-half plane throughout the entire trajectory. The root moves toward origin until 800 seconds and then it moves away from the origin until the end of the trajectory.

Figs. 4-4 and 4-6 clearly illustrate the roots of the roll mode and the time-varying characteristics during the entire trajectory. The roots of the roll mode remain in the left-half plane and the roots move away from the origin throughout the trajectory.

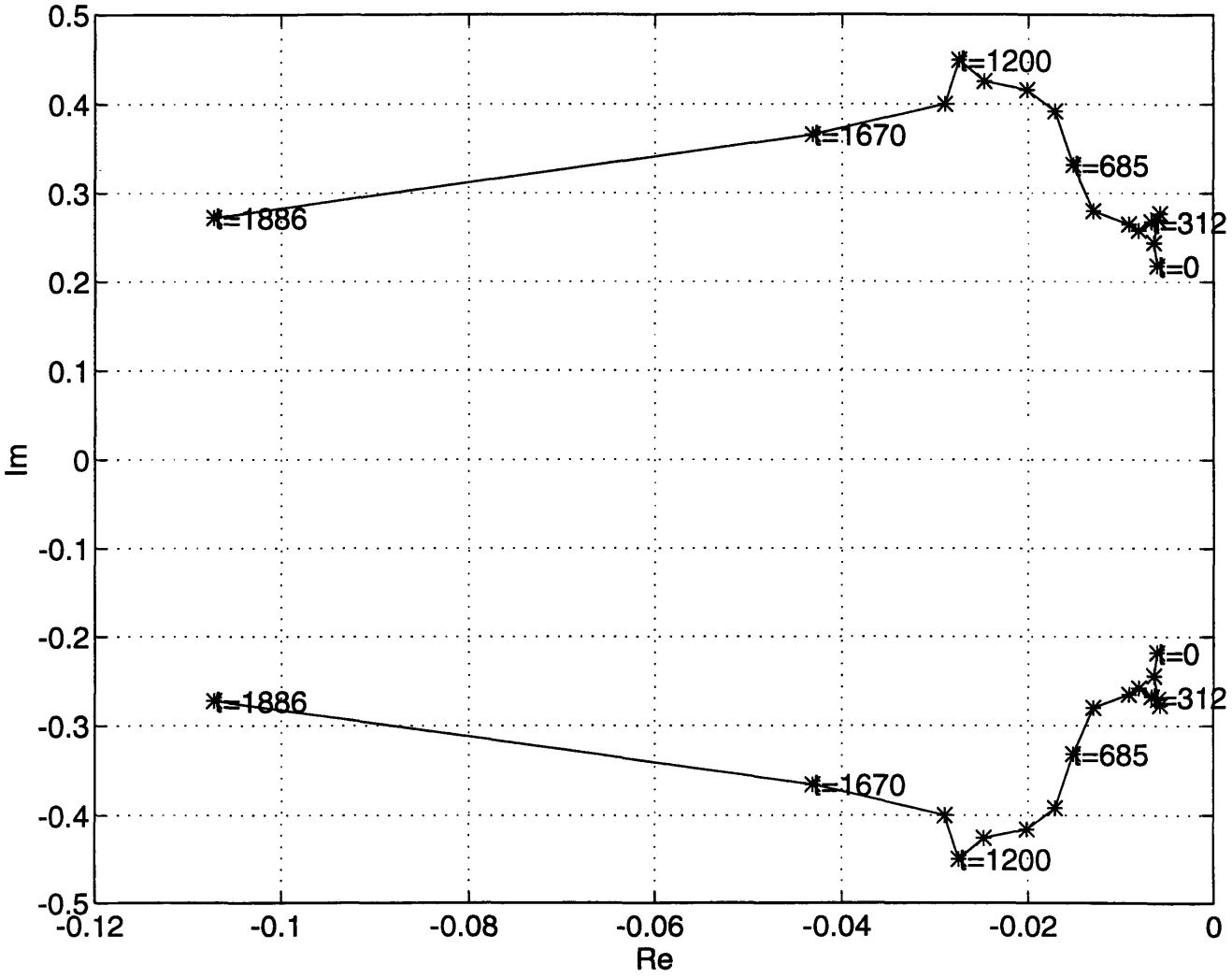

Figure 4-1: Roots of Short-period Mode

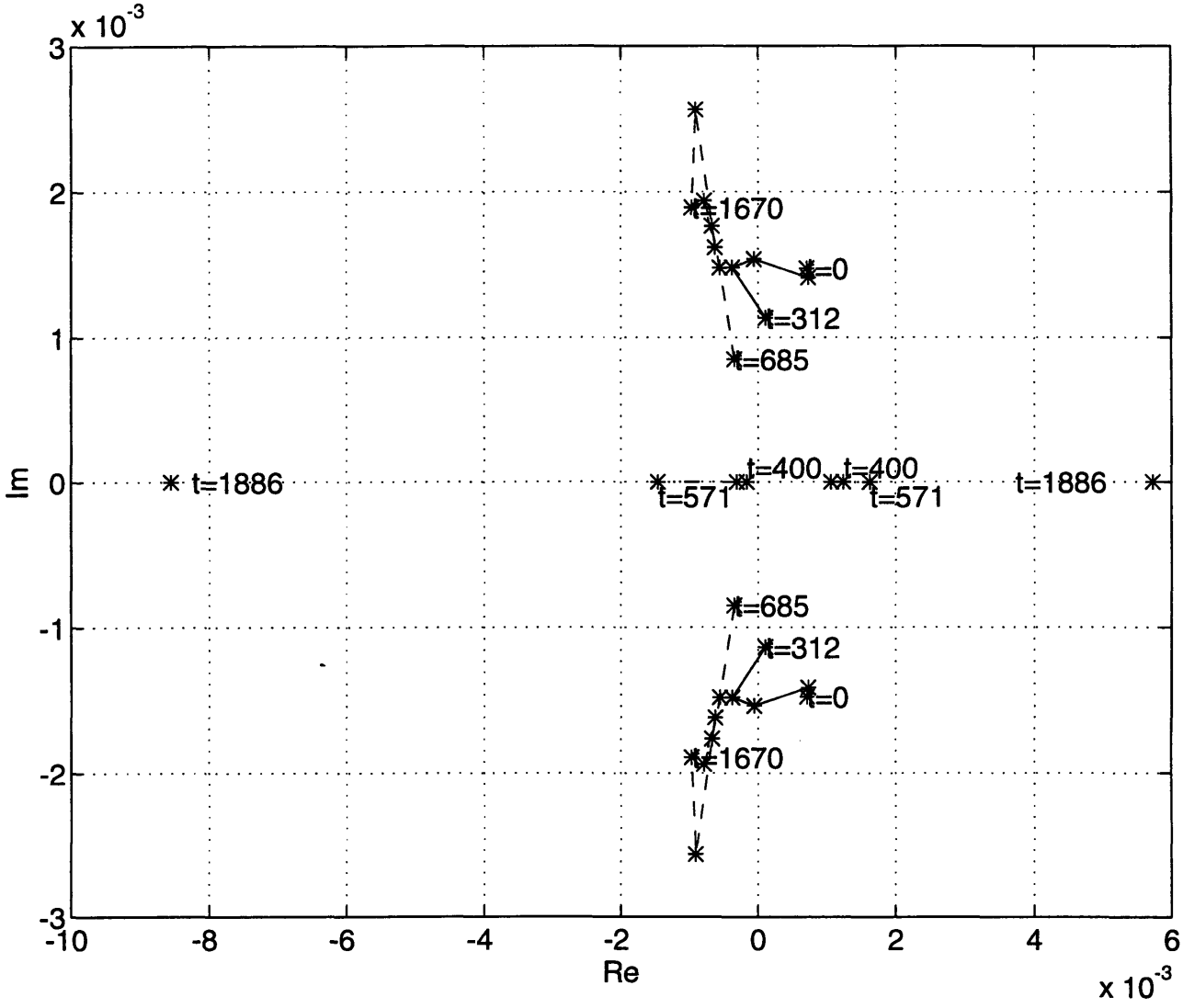

Figure 4-2: Roots of Phugoid Mode

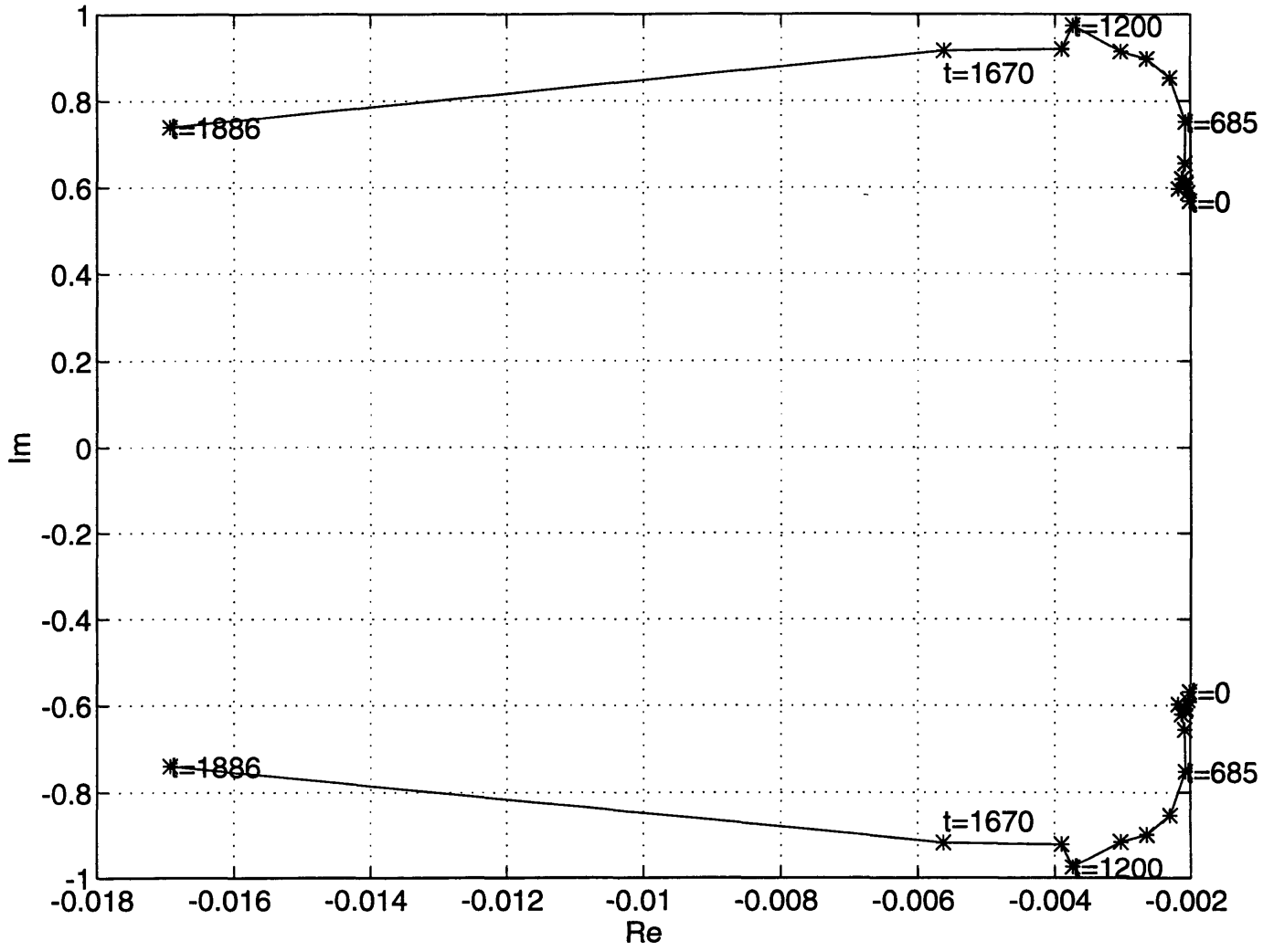

Figure 4-3: Roots of Dutch-roll Mode

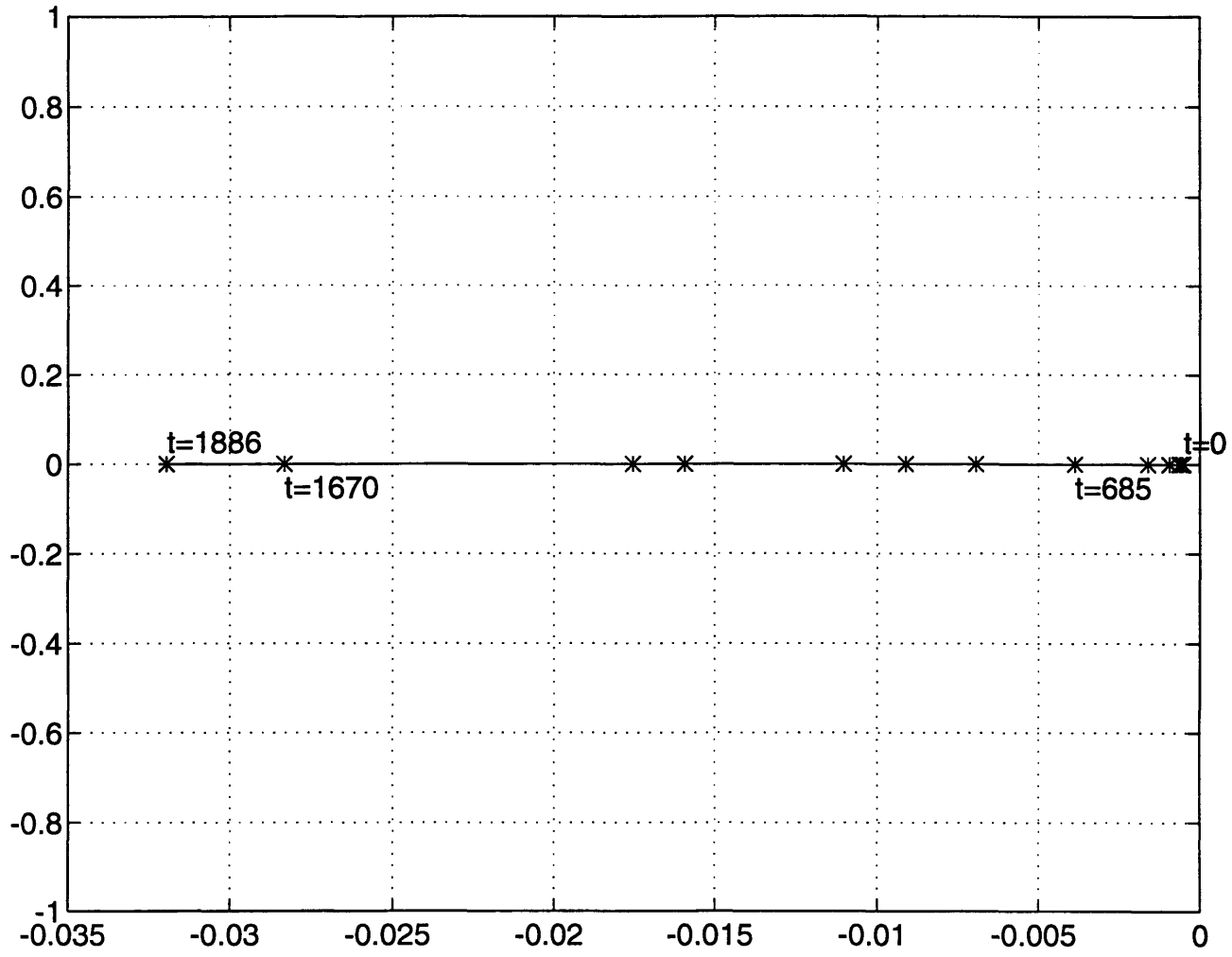

Figure 4-4: Root of Roll Mode

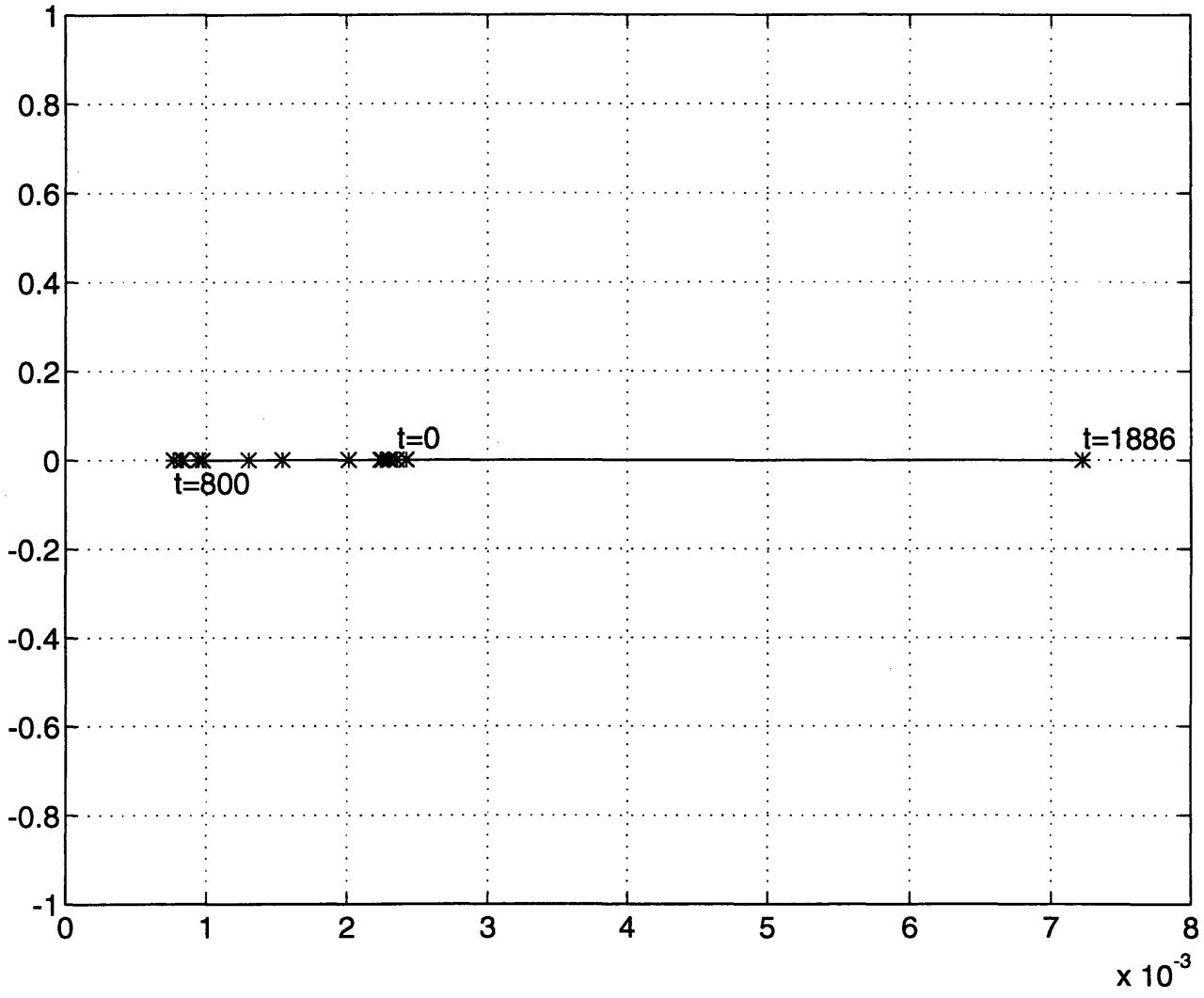

Figure 4-5: Root of Spiral Mode

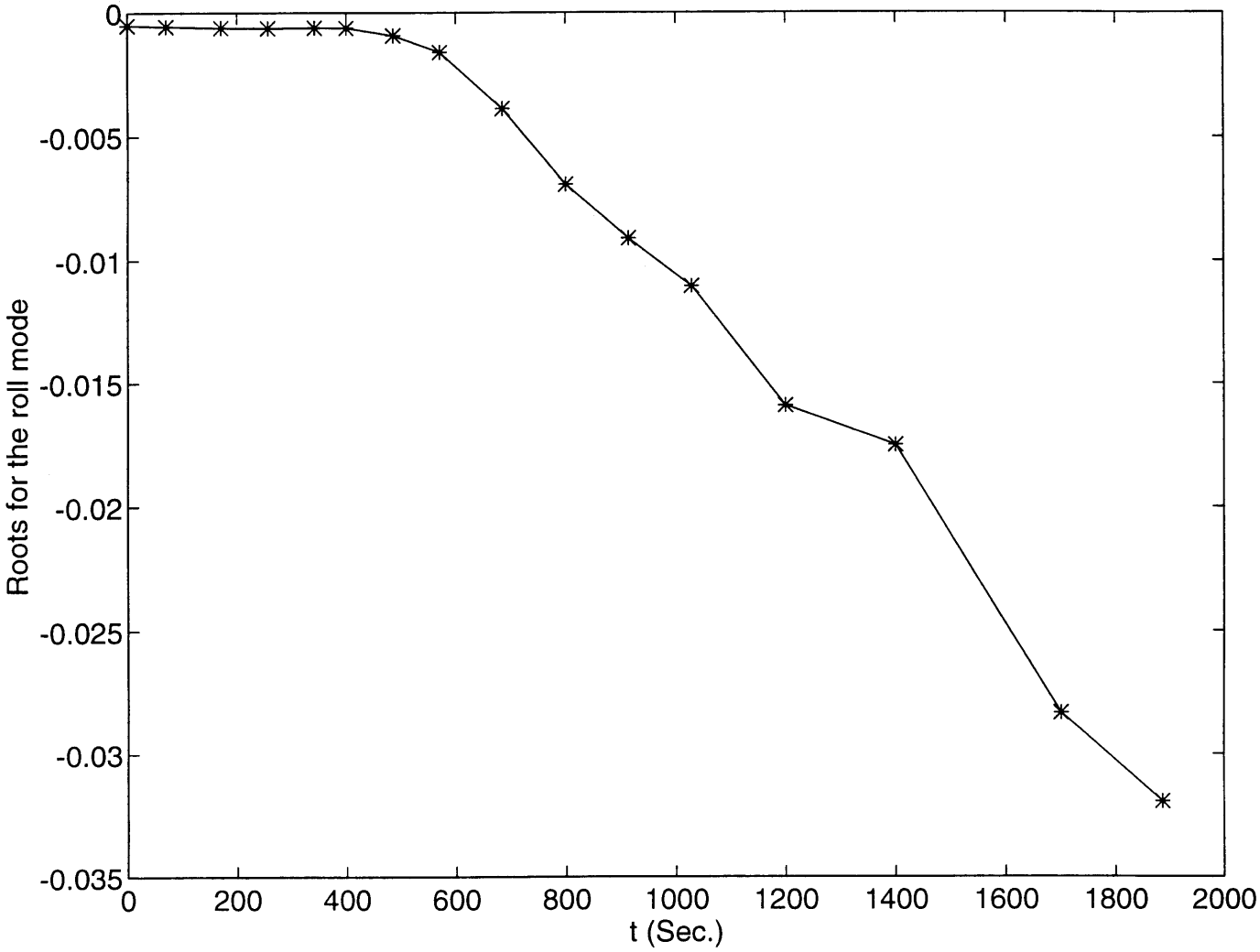

Figure 4-6: Roots of Roll Mode vs. t (sec)

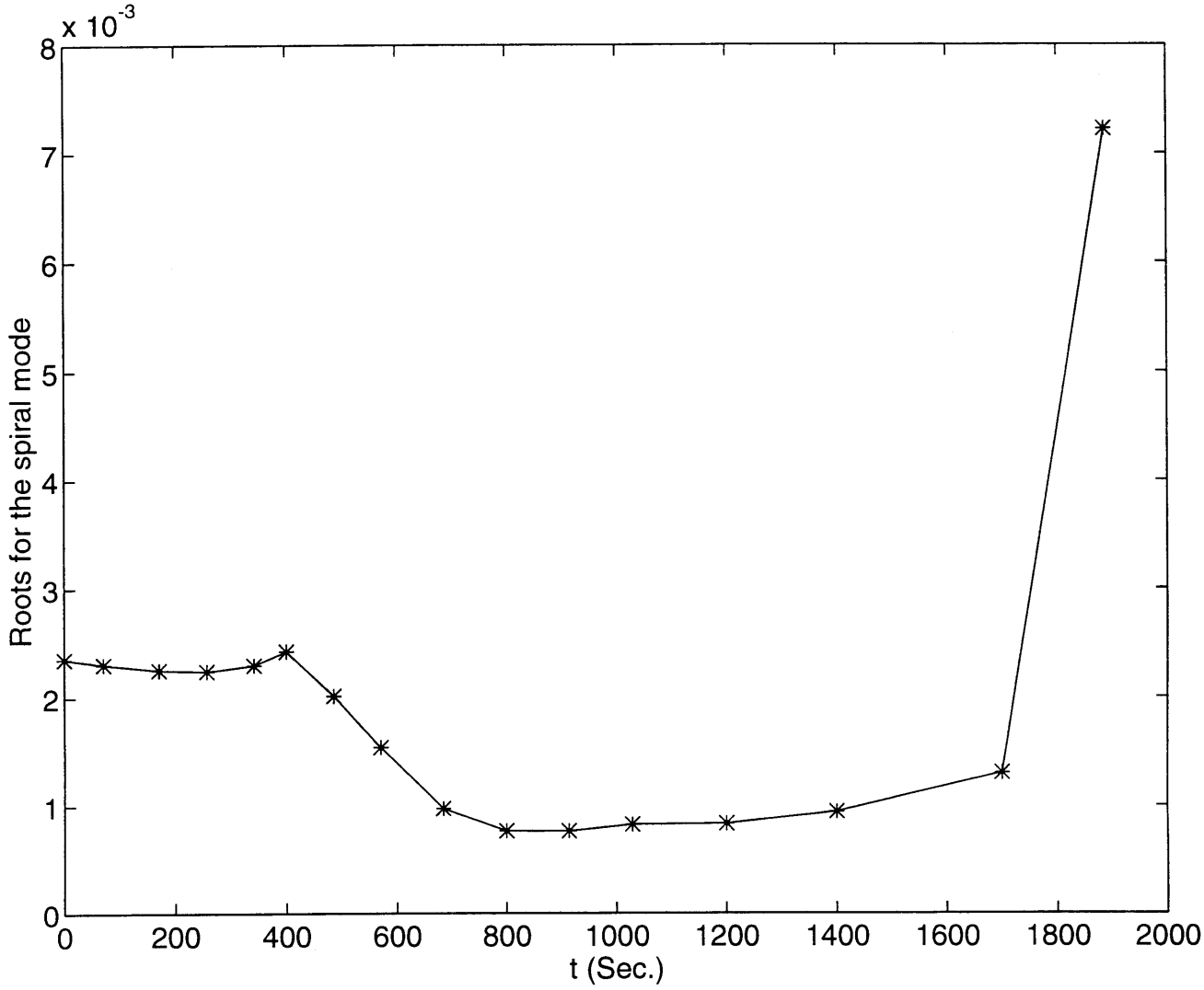

Figure 4-7: Roots of Spiral Mode vs. t (sec)

4.4 Stability Parameter for Longitudinal Dynamics

A second order LTV differential equation, which describes the GHAME vehicle's angle-of-attack perturbation, is used in this section [3]. The stability of a system with time-varying coefficients such as the GHAME vehicle is very difficult to predict in most cases. Simple stability criteria applicable to this case had been developed by Ramnath.

$$\frac{d^2\alpha}{d\xi^2} + Z_1(\xi)\frac{d\alpha}{d\xi} + Z_0(\xi)\alpha = 0 \tag{4.26}$$

where ξ, a non-dimensional variable, is the number of vehicle lengths traveled along the trajectory. Based on the GMS solution, the bound of α can be defined in the following form:

$$\mid \alpha(\xi) \mid = \left|4Z_0(\xi) - Z_1(\xi)^2\right|^{-1/4} exp\int_{\xi_0}^{\xi} K_r(\xi)d\xi \tag{4.27}$$

It is clear that α is stable when K_r is negative, and K_r can be written in terms of aerodynamic coefficients in Eq. 4.28

$$K_r = \frac{-Z_1}{2} = \frac{-1}{2}(\delta(C_{L\alpha} - \sigma(C_{M\dot{\alpha}} + C_{Mq})) + \frac{V'}{V}) \tag{4.28}$$

where

$$\frac{V'}{V} = -\delta C_D - \frac{gl}{V^2}sin\gamma \tag{4.29}$$

$$C_D = C_{D0} + C_{D\alpha}\alpha \tag{4.30}$$

$$\delta = \frac{\rho Sl}{2m} \tag{4.31}$$

$$\sigma = \frac{ml^2}{I_y} \tag{4.32}$$

After substitution of Eq. 4.29 and Eq. 4.30 into Eq. 4.28, this yields Eq. 4.33:

$$K_r = \frac{-1}{2}(\delta(C_{L\alpha} - (C_{D0} + C_{D\alpha}\alpha) - \sigma(C_{M\dot{\alpha}} + C_{Mq})) - \frac{gl}{V^2}sin\gamma)) \tag{4.33}$$

Since $C_{D\alpha}$, $C_{M\dot{\alpha}}$ and γ are negligible, these values are assumed to be zero for simplification. Then K_r is simplified as,

$$K_r = \frac{-1}{2}(\delta(C_{L\alpha} - C_{D0} - \sigma C_{Mq})). \tag{4.34}$$

Based on Eq. 4.34, the stability parameter (P) is defined as

$$P = \delta(C_{L\alpha} - C_{D0} - \sigma C_{Mq}) \tag{4.35}$$

When P is positive, α is stable and α is unstable when P is negative.

The stability parameter (P) and aerodynamic coefficients ($C_{L\alpha}, C_{D0}, C_{Mq}$) are shown in Fig. 4-8(a). Fig. 4-8(b) shows that ambient density, ρ, plays a significant role in the stability parameter because the density changes significantly (from 5.545 $\times 10^{-10}$ to 1.061 $\times 10^{-3} lb/ft^3$) from altitude 400,000 ft to 100,000 ft. Therefore, the density term, which is included in δ, must be included in the stability parameter. Figs. 4-9 and 4-10 show the stability parameter (P) vs. ξ and vs. time, respectively, which show the stability increases as the trajectory progresses.

4.5 Stability of GHAME Vehicle

The stability of the GHAME vehicle on the given trajectory is investigated in two other methods. One is the comparison of numerical solutions along the trajectory in terms of the relative stability. The other method is the bound of the solution throughout the trajectory. In order to investigate the stability, the trajectory is divided into six segments and their relative stabilities are compared. Figs. 4-11 - 4-16 illustrate that the solution becomes more stable as the trajectory progresses. This result is consistent with the result from Fig. 4-9, which shows increasing P as the

trajectory progresses. From Figs. 4-11 - 4-16, 'settling trajectory length' for 0.5 and 0.1 amplitude are compared between six segments of the trajectory. For the range 0 to $5 \times 10^4 \xi$, the convergence is very slow. For instance, it takes 30220 ξ to satisfy 0.5 amplitude bound for cosine-like solution and 22020 ξ to satisfy 0.5 amplitude bound for sine-like solution. For this range, 0.1 amplitude bound does not meet for both cosine-like and sine-like solutions. For the range 5×10^4 to $1 \times 10^5 \xi$, the convergence is faster than in the previous case. The 0.5 amplitude bound is satisfied within 11900 ξ and 10420 ξ for cosine-like and sine-like solutions, respectively. The 0.1 amplitude bound is satisfied within 22460 ξ and 21660 ξ for cosine-like and sine-like solution, respectively. The summary is given in Table 4.1.

The same conclusion can be drawn from Figs. 4-17 - 4-19, which show the bound of α. Fig. 4-17 shows a rapid decrease and the plot reaches zero after 70,000 ξ, and Fig. 4-18 also shows the decreasing plot. Therefore, the solution becomes more stable as the trajectory progresses and the major contribution for the α bound comes from $exp(\int_{\xi_0}^{\xi} K_r(\xi) d\xi)$. Fig. 4-20 shows that the K_r term is negative throughout the trajectory and K_r decreases as the trajectory progresses. As a consequence, K_r dominates the stability of the solution and the stability parameter, P, which was derived from K_r in Eqs. 4.34 and 4.35. The stability of this trajectory increases as the trajectory progresses. This result can be shown from the stability parameter (Fig. 4-9) and the solution for the trajectory (Figs. 4-11 - 4-16). This result also can be shown from the bound of α (Fig. 4-19). Therefore, all three methods agree and the stability parameter P is the easiest way to estimate stability information of a vehicle during the flight because it only requires three aerodynamic coefficients and ambient density.

Another interesting result can be obtained from the comparison of the Figs. 4-17 - 4-19. From the GMS theory, it is known that the fast solution provides frequency information. The change of the frequency is most significant between ranges 0 - $5 \times 10^4 \xi$ and 5×10^4 - $1 \times 10^5 \xi$ according to the Figs. 4-11-4-16. From Fig. 4-17, it is shown clearly that the slope of the plot is changed most significantly between ranges 0 - $5 \times 10^4 \xi$ and 5×10^4 - $1 \times 10^5 \xi$.

In conclusion, the stability parameter (P) provides accurate stability information with three simple aerodynamic coefficients and ambient density. Therefore, this stability parameter can be obtained easily with existing flight measurement systems, and the stability parameter can be available to the pilot during the flight.

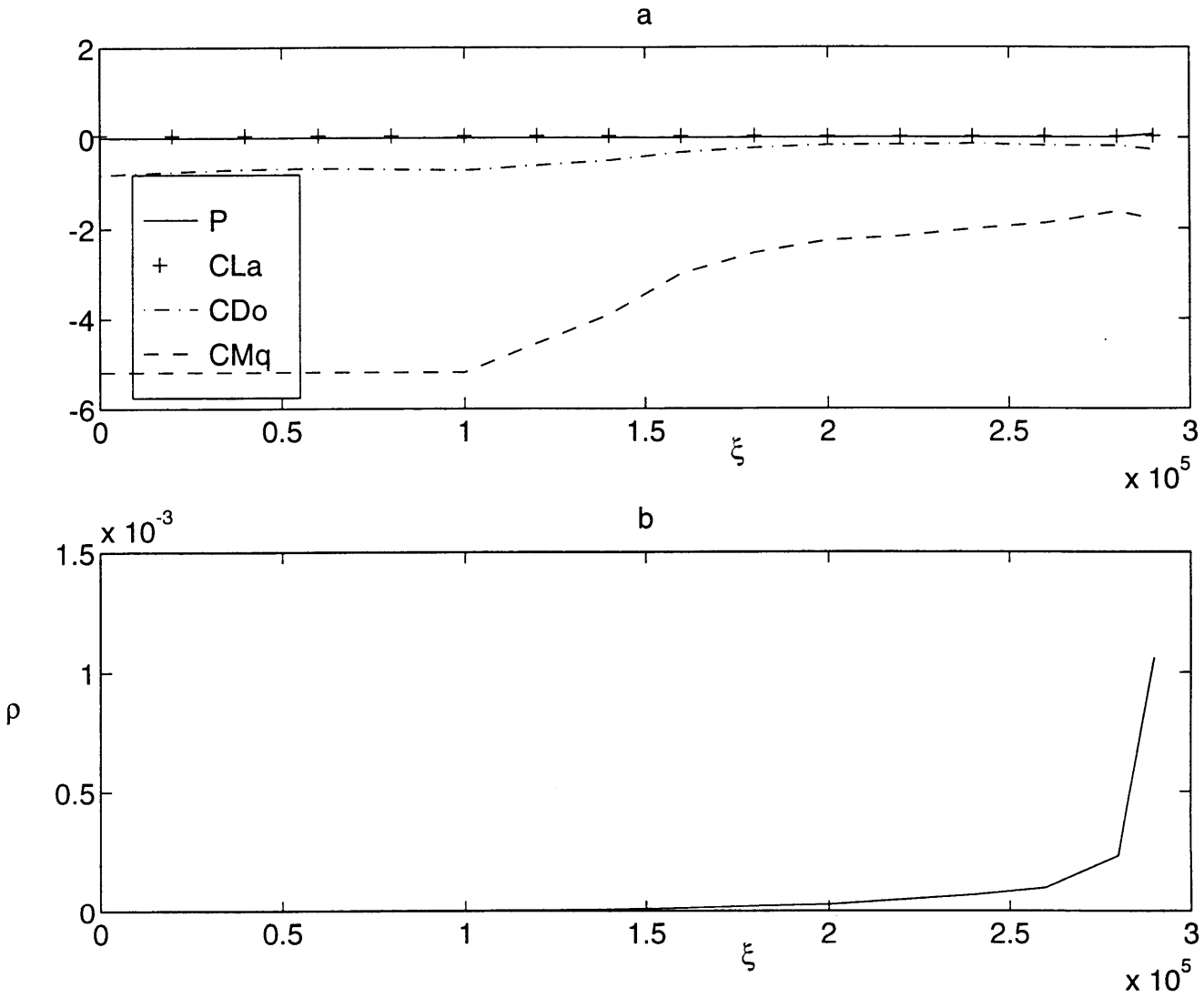

Figure 4-8: (a) Stability parameter (P) and aerodynamic coefficients vs. ξ, (b) Ambient density (ρ) vs. ξ

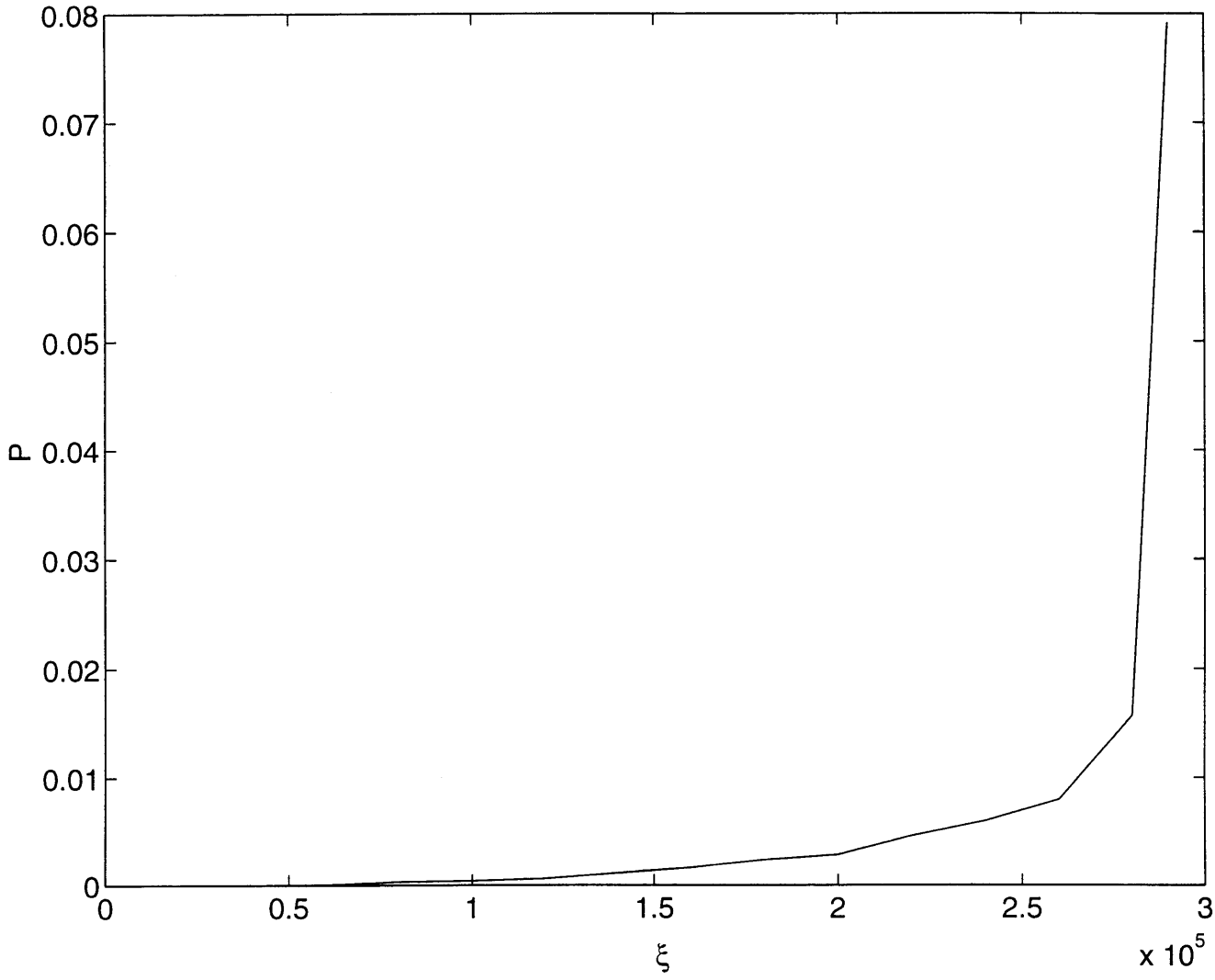

Figure 4-9: Stability parameter (P) vs. ξ

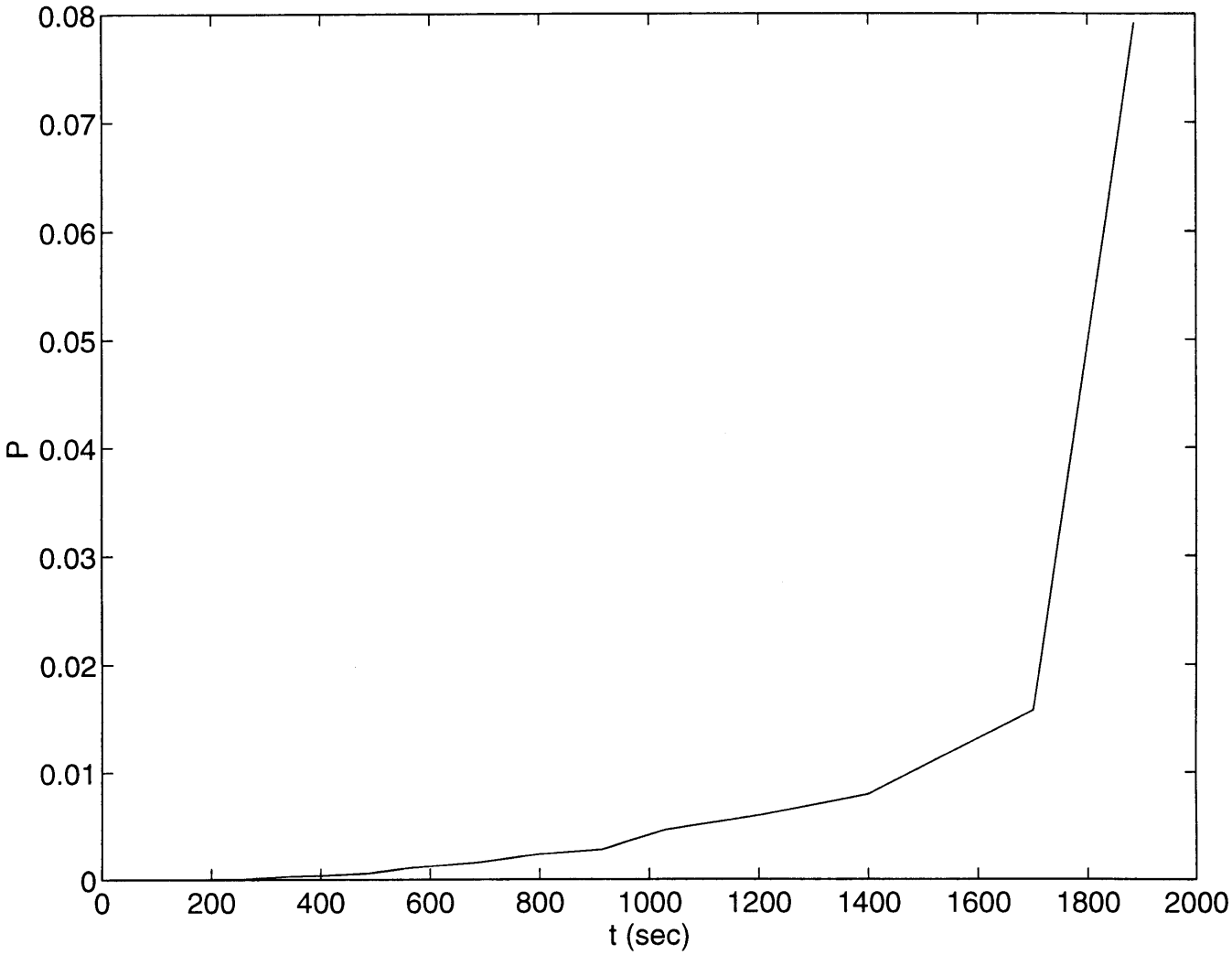

Figure 4-10: Stability parameter (P) vs. time

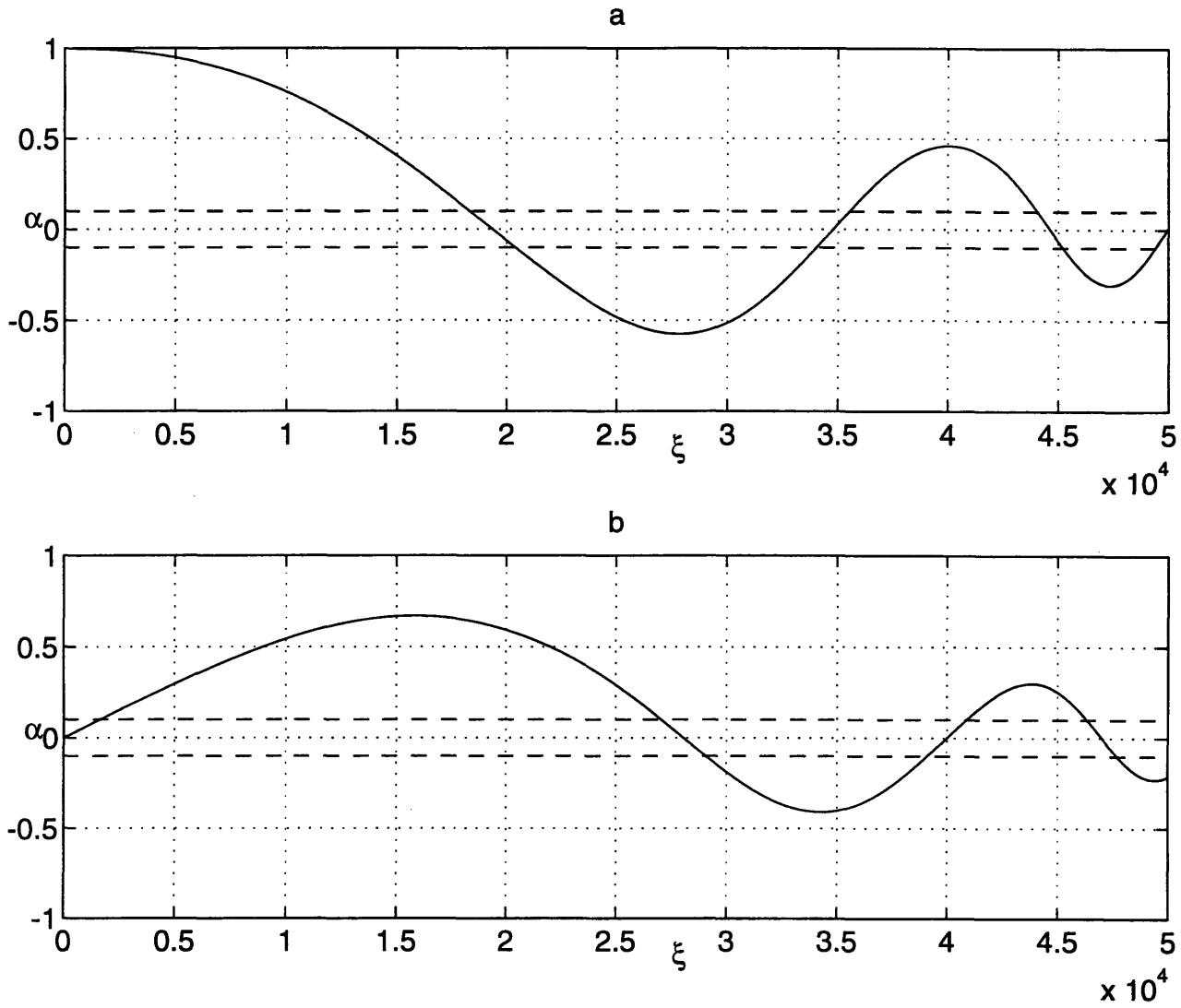

Figure 4-11: (a) Cosine-like numerical solution, (b) Sine-like numerical solution for ξ (0 to 5.0 $\times$ 10^4)

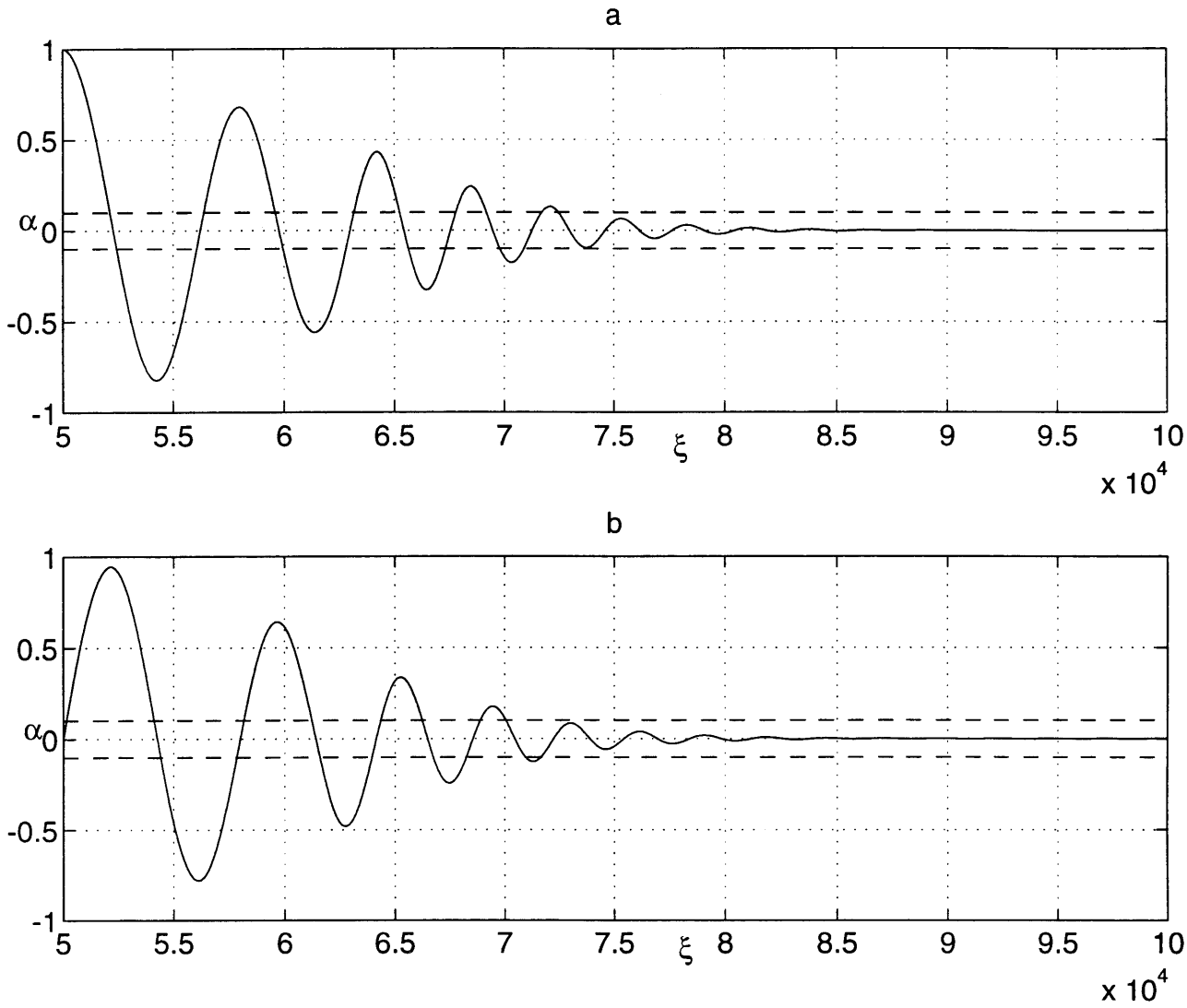

Figure 4-12: (a) Cosine-like numerical solution, (b) Sine-like numerical solution for ξ (5.0×10^4 to 1.0×10^5)

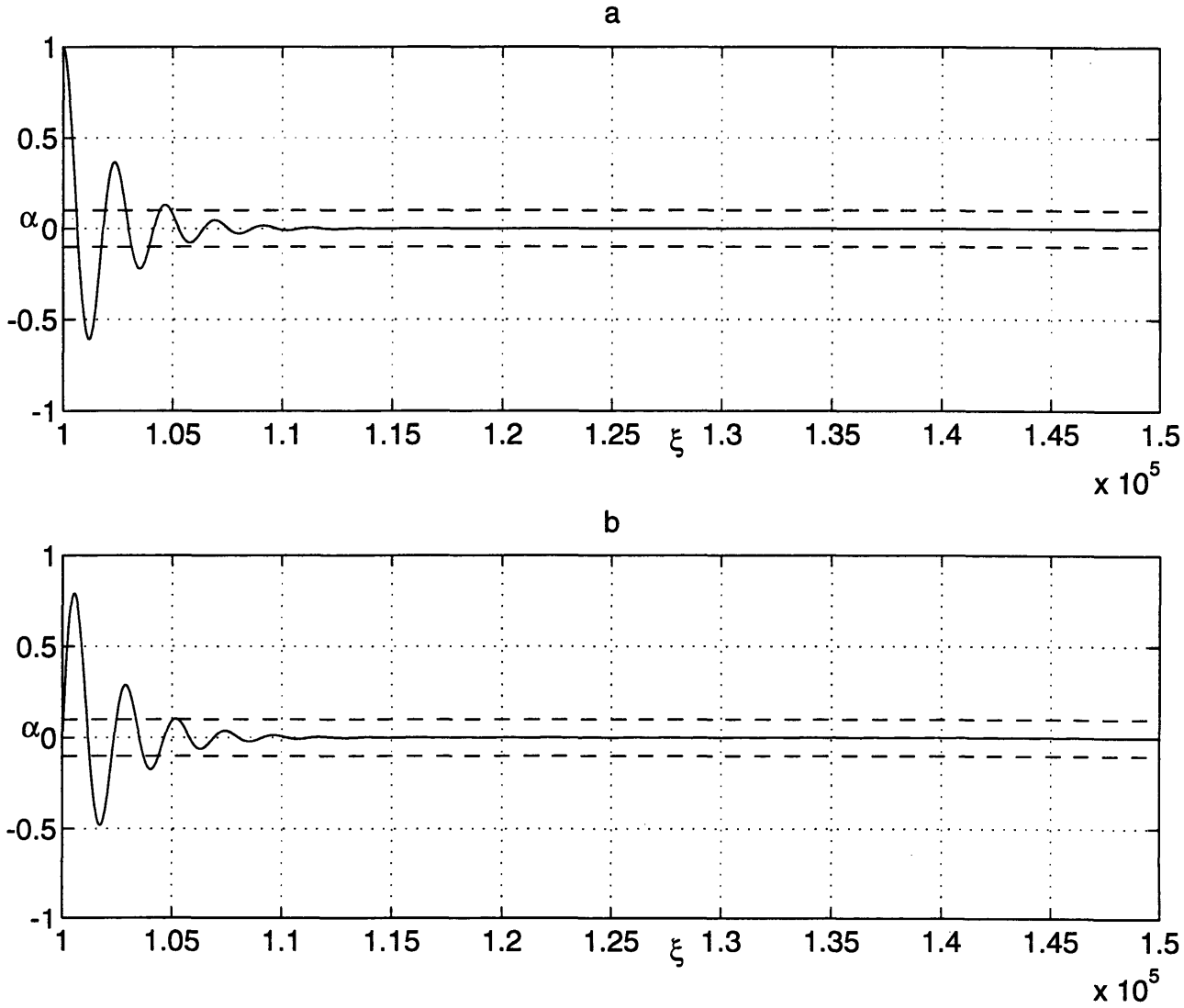

Figure 4-13: (a) Cosine-like numerical solution, (b) Sine-like numerical solution for ξ (1.0×10^5 to 1.5×10^5)

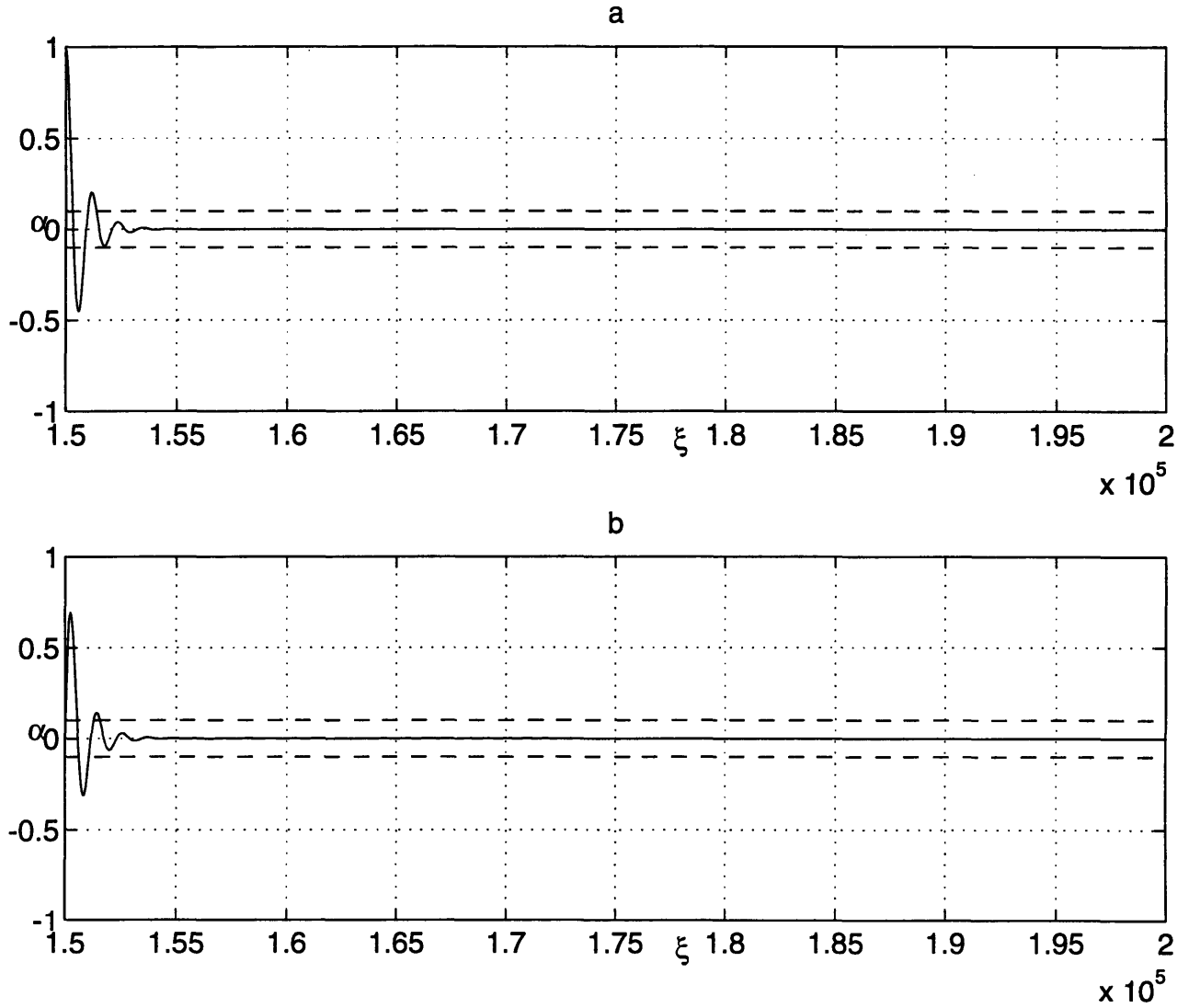

Figure 4-14: (a) Cosine-like numerical solution, (b) Sine-like numerical solution for ξ (1.5×10^5 to 2.0×10^5)

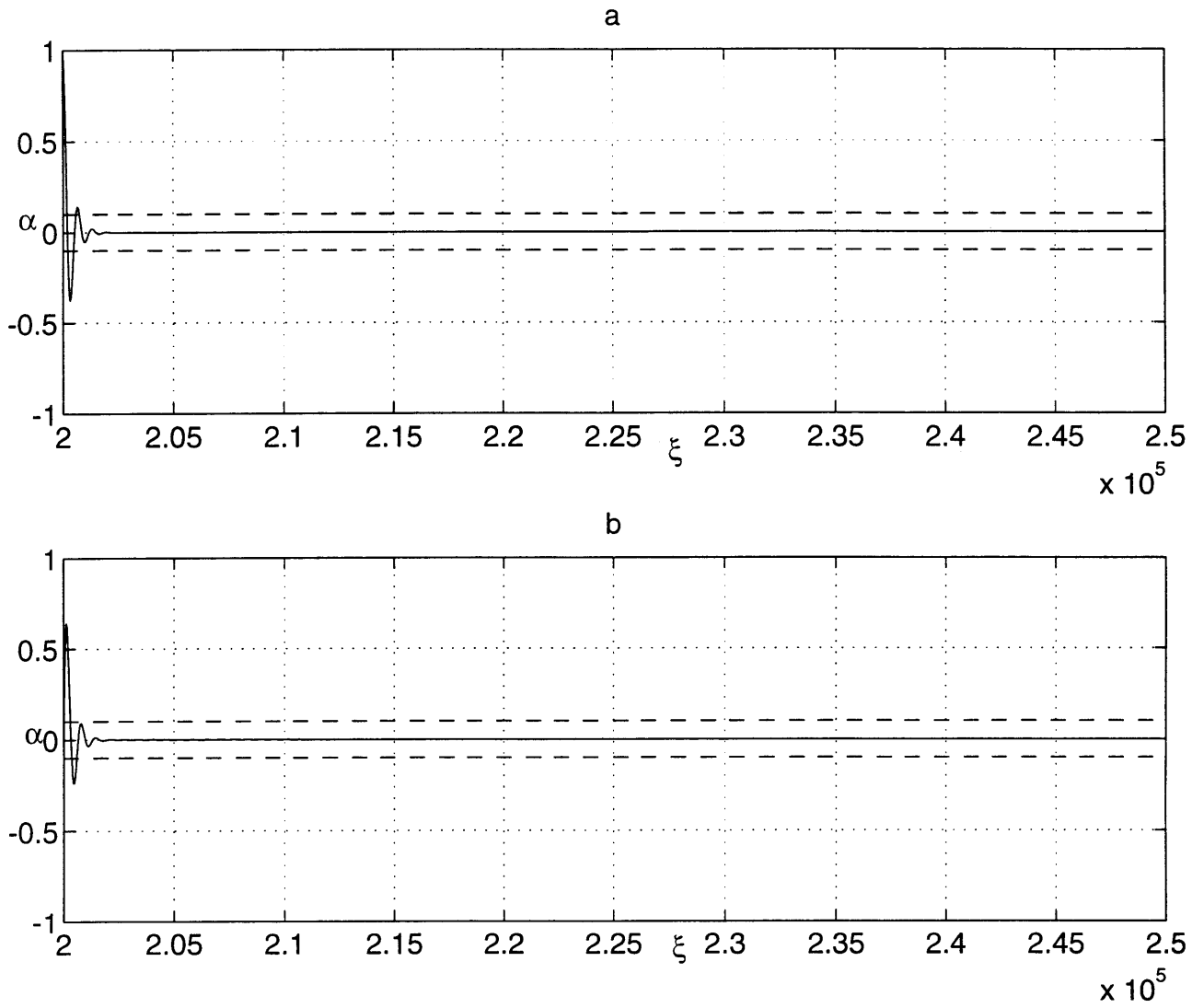

Figure 4-15: (a) Cosine-like numerical solution, (b) Sine-like numerical solution for ξ (2.0×10^5 to 2.5×10^5)

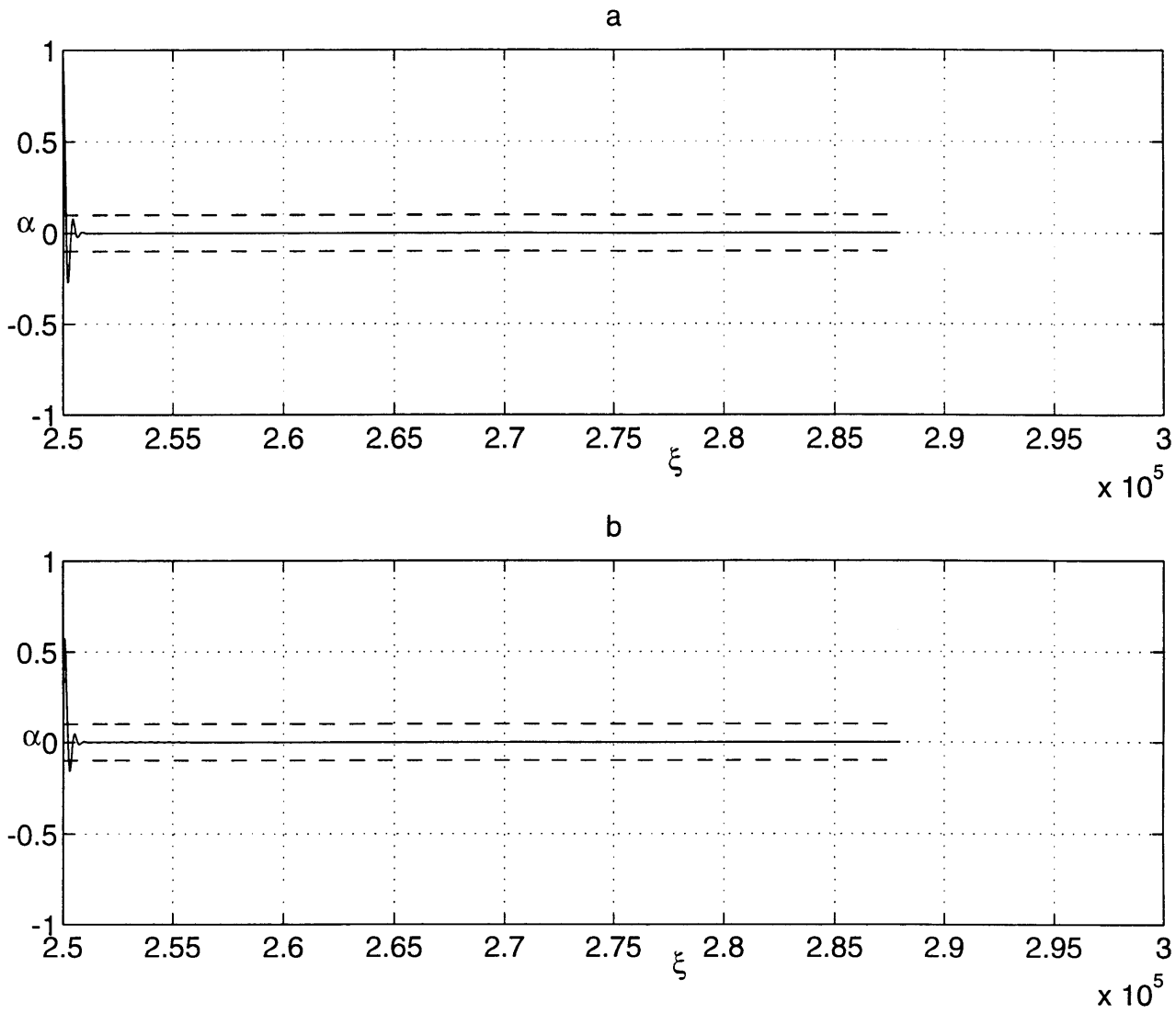

Figure 4-16: (a) Cosine-like numerical solution, (b) Sine-like numerical solution for ξ (2.5×10^5 to 3.0×10^5)

Table 4.1: Comparison for Settling Trajectory Length

Range (ξ)	Cosine-like solution (ξ)		Sine-like solution (ξ)	
	0.5 Amp.	0.1 Amp.	0.5 Amp.	0.1 Amp.
0 to 5×10^4	30220	NA	22020	NA
5×10^4 to 1.0×10^5	11900	22460	10420	21660
1.0×10^5 to 1.5×10^5	1420	4900	860	5260
1.5×10^5 to 2.0×10^5	210	1380	380	1580
2.0×10^5 to 2.5×10^5	110	710	210	590
2.5×10^5 to 3.0×10^5	70	310	110	370

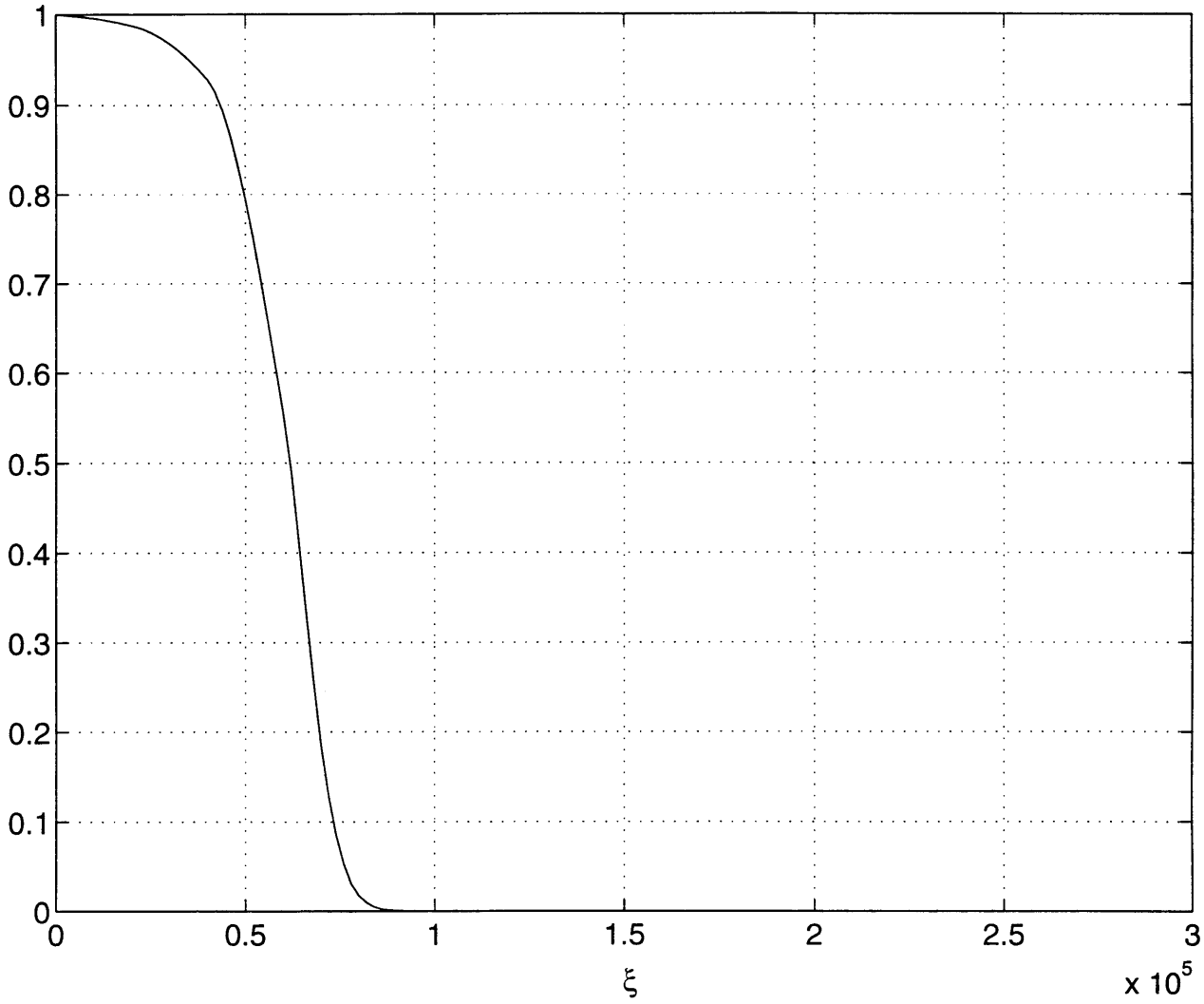

Figure 4-17: $exp(\int_{\xi_0}^{\xi} K_r(\xi)d\xi)$ vs. ξ

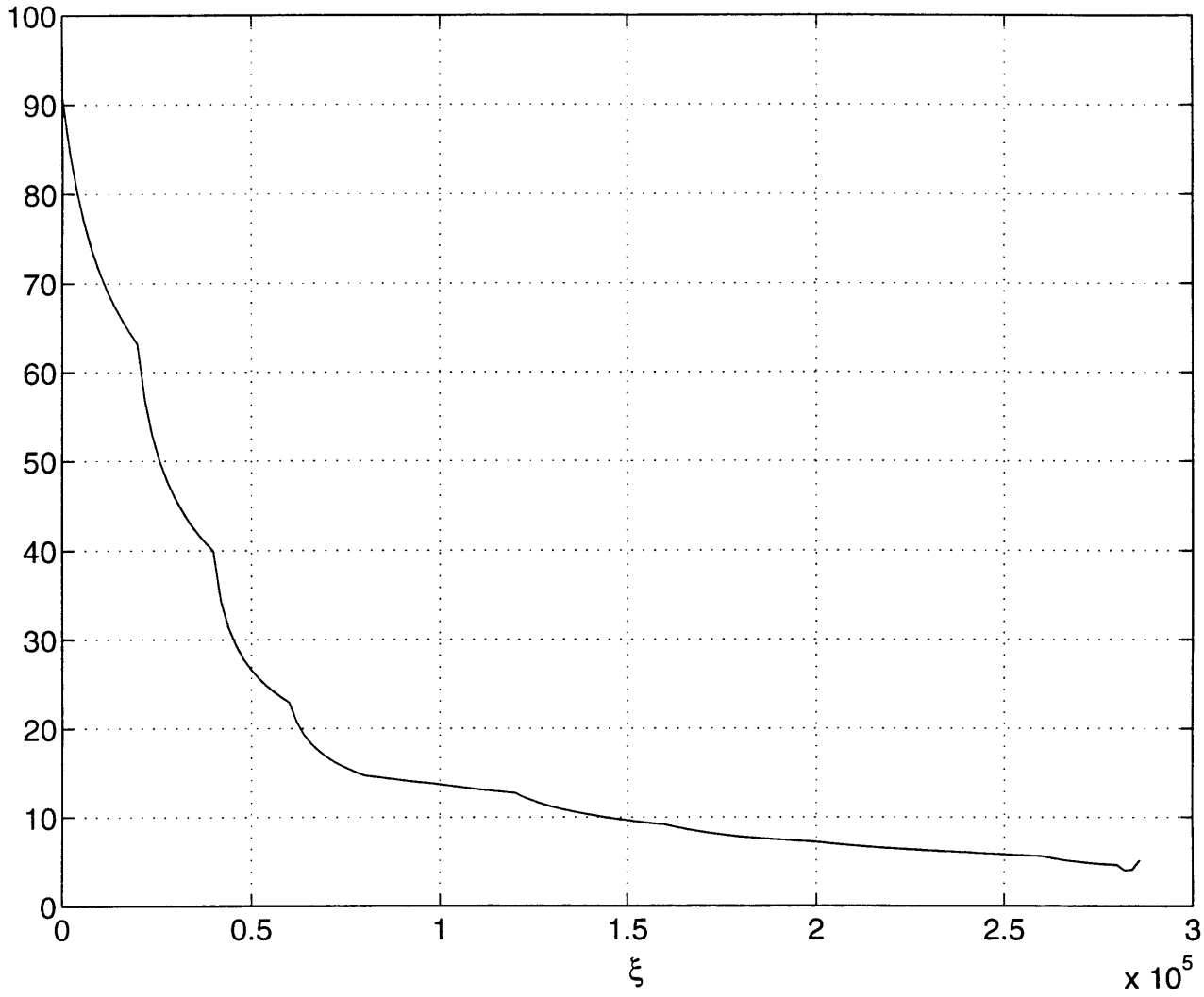

Figure 4-18: $\mid 4Z_0(\xi) - Z_1(\xi)^2 \mid^{-1/4}$ vs. ξ

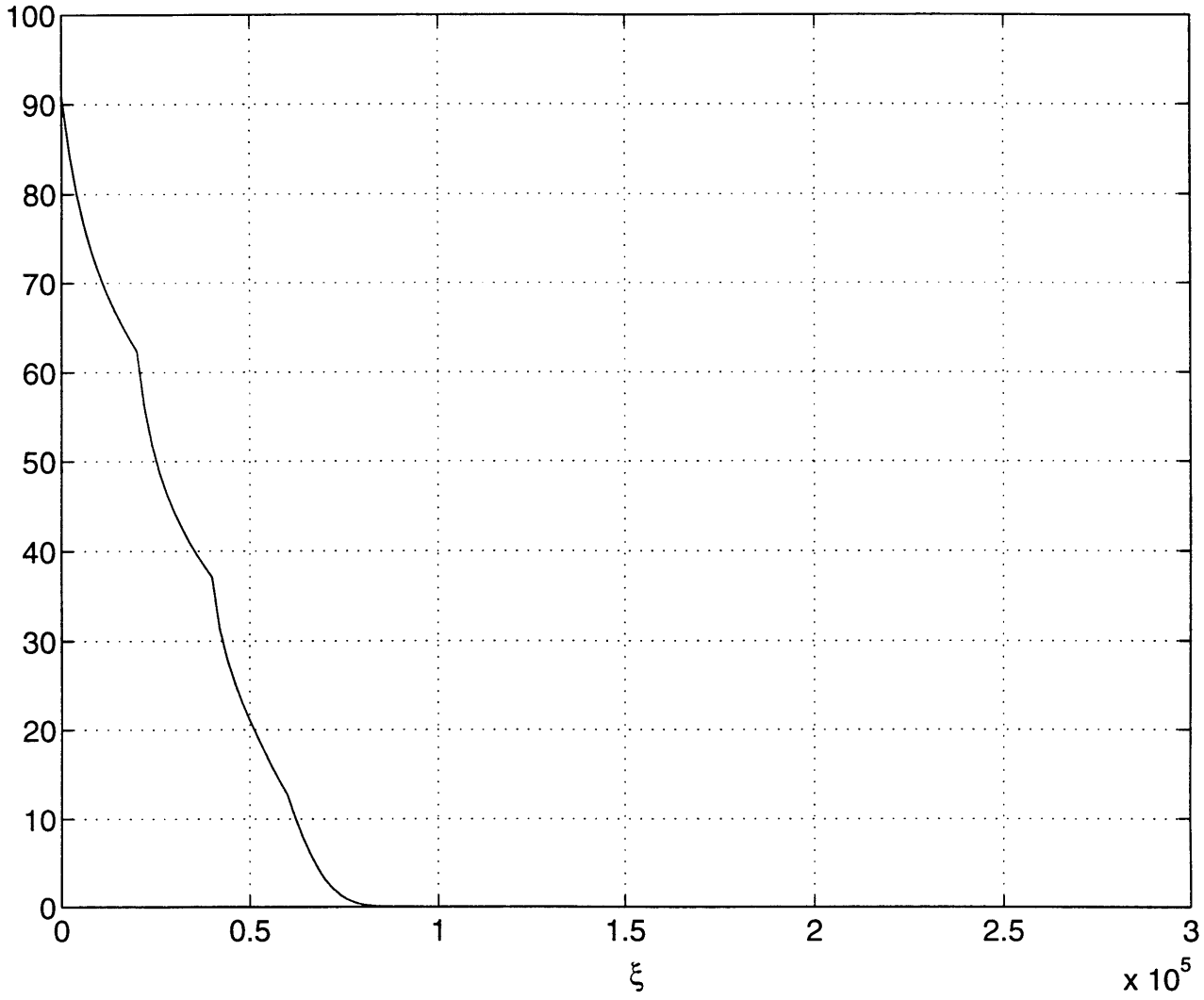

Figure 4-19: $\mid 4Z_0(\xi) - Z_1(\xi)^2 \mid^{-1/4} exp(\int_{\xi_0}^{\xi} K_r(\xi)d\xi)$ vs. ξ

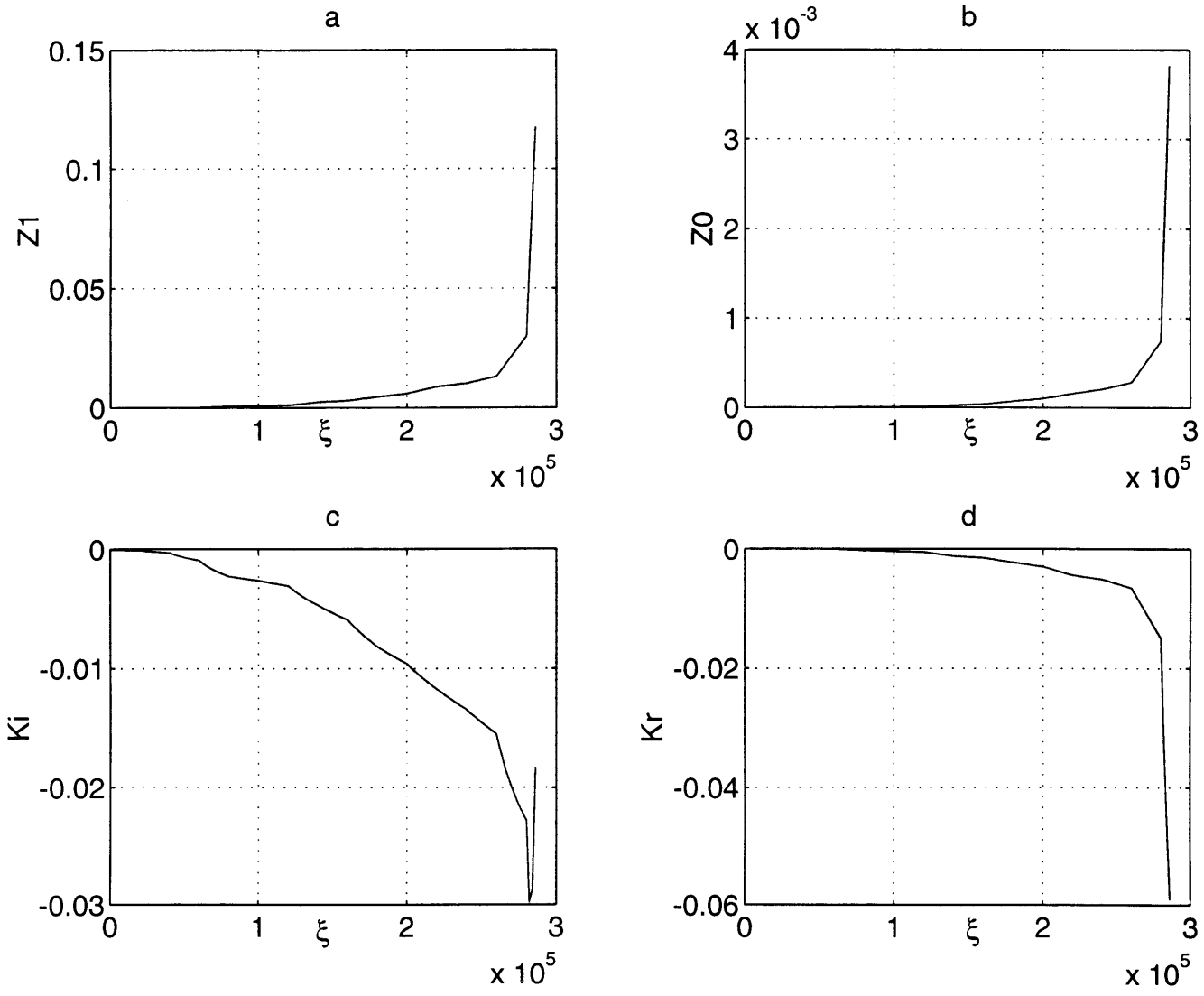

Figure 4-20: (a) Z_1 vs. ξ, (b)Z_0 vs. ξ, (c) K_i vs. ξ, (d)K_r vs. ξ

Chapter 5

Application of Extended Flying Qualities Criteria to the GHAME Vehicle

5.1 Introduction

From the beginning of manned flight, the flying qualities of aircraft have been a topic of significant research interest [13]. The analysis of the equation of motion has provided information about the flying qualities. Until now, the analysis of flying qualities has been based on constant flight conditions. However, the nature of flight vehicles has changed drastically. For example, hypersonic vehicles, such as the National Aerospace Plane (NASP) and the High Speed Civil Transport (HSCT), have time-varying systems and they also have very large flight envelopes. Therefore, the conventional flying qualities criteria may not be appropriate for these hypersonic vehicles, and it is necessary to develop an analytical approach to specify complete flying qualities for these vehicles.

5.2 Description of the Flying Qualities

The flying qualities can be defined as the stability and control characteristics that have an important bearing on the safety of flight and on the pilot's impressions of the ease of flying [13]. The pilot expects the flying qualities of the aircraft according to the flight phase and the type of aircraft. The aircraft are classified into four classes as shown in Table 5.1, and the flight phases are categorized into three categories as shown in Table 5.2 [14].

The specifications of the flying qualities are separated into three levels [14].

Level 1: Flying qualities clearly adequate for the mission flight phase.

Level 2: Flying qualities adequate to accomplish the mission flight phase, but some increase in pilot workload or degradation in mission effectiveness, or both, exists.

Level 3: Flying qualities such that the airplane can be controlled safely, but pilot workload is excessive or mission effectiveness is inadequate, or both Category A flight phases can be terminated safely, and Category B and C flight phase can be completed.

These levels can be related to a well known subjective rating system, Copper-Harper handling qualities rating scales [15].

Level 1: Copper-Harper Scale = 1 - 3.5

Level 2: Copper-Harper Scale = 3.5 - 6.5

Level 3: Copper-Harper Scale = 6.5 - 9+

Table 5.1: Classification of aircraft

Class I	Small, light airplanes, such as light utility, primary trainer, and light observation aircraft
Class II	Medium-weight, low-to-medium maneuverability airplanes, such as heavy utility/search and rescue. light or medium transport/cargo/tanker, reconnaissance, tactical bomber, heavy attack and trainer for Class II
Class III	Large, heavy, low-to-medium maneuverability airplanes, such as heavy transport/cargo/tanker, heavy bomber and trainer for Class III
Class IV	High-maneuverability airplanes, such as fighter/interceptor, attack, tactical reconnaissance, observation and trainer or Class IV

Table 5.2: Flight phase categories

Nonterminal flight phase	
Category A	Nonterminal flight phase that requires rapid maneuvering, precision tracking, or precise flight-path control. Included in the category are air-to-air combat ground attack, weapon delivery/launch, aerial recovery, reconnaissance, in-flight refueling (receiver), terrain-following, antisubmarine search, and close formation flying
Category B	Nonterminal flight phase that are normally accomplished using gradual maneuvers and without precision tracking, although accurate flight-path control may be required. Included in the category are climb, cruise, loiter, in-flight refueling (tanker), descent, emergency descent, emergency deceleration, and aerial delivery
Terminal flight phase	
Category C	Terminal flight phase are normally accomplished using gradual maneuvers and usually require accurate flight-path control. Included in the category are takeoff, catapult takeoff, approach, wave-off/go-around and landing

5.3 Flying Qualities for Steady Flight Conditions

The flying qualities specifications for a steady flight condition are discussed in this section. Consider a second order linear time-invariant (LTI) differential equation which describes the dynamics of the short-period, phugoid or dutch-roll mode in steady flight conditions,

$$\frac{d^2y}{dt^2} + Z_1\frac{dy}{dt} + Z_0 y = \frac{d^2y}{dt^2} + 2\zeta\omega_n\frac{dy}{dt} + \omega_n^2 y = 0 \tag{5.1}$$

where ζ is the damping ratio and ω_n is the undamped natural frequency. The solution can be written as

$$y(t) = C_1 \exp(-\zeta\omega_n(t))[sin(\omega_n\sqrt{1-\zeta^2}(t) + \phi)]. \tag{5.2}$$

Therefore, the characteristics of a second order linear time-invariant (LTI) system can be obtained in terms of $\zeta\omega_n$ and $\omega_n\sqrt{(1-\zeta^2)}$, and simplified flying quality criteria can be defined following Hagelauer [16]:

Level 1	$AA1_{min} \leq \zeta\omega_n \leq AA1_{max}$	and	$BB1_{min} \leq \omega_n\sqrt{1-\zeta^2} \leq BB1_{max}$
Level 2	$AA2_{min} \leq \zeta\omega_n \leq AA2_{max}$	and	$BB2_{min} \leq \omega_n\sqrt{1-\zeta^2} \leq BB2_{max}$
Level 3	$AA3_{min} \leq \zeta\omega_n \leq AA3_{max}$	and	$BB3_{min} \leq \omega_n\sqrt{1-\zeta^2} \leq BB3_{max}$

Consider a first order linear time-invariant (LTI) differential equation which describes the dynamics of the spiral or roll mode in steady flight conditions,

$$\frac{dy}{dt} + Zy = 0. \tag{5.3}$$

The solution can be written as

$$y(t) = C_1 \exp(-Z(t)). \tag{5.4}$$

Therefore, the characteristics of a first order linear time-invariant (LTI) system

can be obtained from Z, which is related to the time constant (t_c) as

$$Z = -t_c. \tag{5.5}$$

The first order system dynamics are described by time for the doubling (t_2) or halving ($t_{1/2}$) amplitude, and these are defined as

$$t_{1/2} \; or \; t_2 = \frac{\ln 2}{\mid t_c \mid} \tag{5.6}$$

Based on the above results, simplified flying quality criteria can be defined as,

Level 1 $\quad AA1_{min} \leq \frac{\ln 2}{|t_c|} \leq AA1_{max}$

Level 2 $\quad AA2_{min} \leq \frac{\ln 2}{|t_c|} \leq AA2_{max}$

Level 3 $\quad AA3_{min} \leq \frac{\ln 2}{|t_c|} \leq AA3_{max}$

5.4 Flying Qualities for Variable Flight Conditions

The basis of the extension of handling qualities to time varying systems was developed by Hagelauer, who developed extended handling quality criteria for the short-period mode with Level 1 and Level 2 requirements [16]. Consider a second order linear time-varying (LTV) differential equation which describes the dynamics of the short-period, phugoid or dutch-roll mode in variable flight conditions,

$$\frac{d^2y}{dt^2} + Z_1(t)\frac{dy}{dt} + Z_0(t)y = \frac{d^2y}{dt^2} + 2\zeta(t)\omega_n(t)\frac{dy}{dt} + \omega_n^2(t)y = 0. \tag{5.7}$$

Based on the Generalized Multiple Scales theory, the fast part of the asymptotic approximation is written in the following way,

$$y(t) = C_1 \exp(-\int_{t_0}^{t} \zeta(\tau)\omega_n(\tau)d\tau)[sin(\int_{t_0}^{t} \omega_n(\tau)\sqrt{1-\zeta^2(\tau)}d\tau) + \phi]. \tag{5.8}$$

The extended flying quality criteria for variable flight conditions can be defined as,

Level 1 $AA1_{min} \leq AA \leq AA1_{max}$ and $BB1_{min} \leq BB \leq BB1_{max}$

Level 2 $AA2_{min} \leq AA \leq AA2_{max}$ and $BB2_{min} \leq BB \leq BB2_{max}$

Level 3 $AA3_{min} \leq AA \leq AA3_{max}$ and $BB3_{min} \leq BB \leq BB3_{max}$

where

$$AA = \frac{1}{T}\int_t^{t+T} \zeta(\tau)\omega_n(\tau)d\tau, \quad BB = \frac{1}{T}\int_t^{t+T} \omega_n(\tau)\sqrt{1-\zeta^2(\tau)}d\tau. \tag{5.9}$$

A first order linear time-varying (LTV) differential equation describes the dynamics of the spiral or roll mode in variable flight conditions,

$$\frac{dy}{dt} + Z(t)y = 0. \tag{5.10}$$

The solution is

$$y(t) = C_1 \exp(-\int_{t_0}^{t} Z(\tau)d\tau) = C_1 \exp(\int_{t_0}^{t} t_c(\tau)d\tau). \tag{5.11}$$

Based on the above results, the extended flying quality criteria for variable flight conditions can be defined as,

Level 1 $AA1_{min} \leq AA \leq AA1_{max}$

Level 2 $AA2_{min} \leq AA \leq AA2_{max}$

Level 3 $AA3_{min} \leq AA \leq AA3_{max}$

where

$$AA = \frac{1}{T}\int_t^{t+T} \frac{\ln 2}{\mid t_c(\tau) \mid}d\tau. \tag{5.12}$$

5.5 Extended Flying Qualities Criteria for Longitudinal Dynamics

In this section, the extended flying qualities criteria for the longitudinal dynamics are developed, first for the short-period mode, and second for the phugoid mode. The EFQC are developed for the GHAME vehicle, which is classified as Class III according to Table 5.1 and the trajectory is Category B according to Table 5.2.

5.5.1 Extended Flying Qualities Criteria for Short-Period Mode

The values of ζ and ω_n (rad/sec) of the short period are obtained from MIL-STD-1797A.

Level 1	$0.30 \leq \zeta \leq 2.00$	and	$0.46 \leq \omega_n \leq 3.50$
Level 2	$0.20 \leq \zeta \leq 2.00$	and	$0.36 \leq \omega_n \leq 6.00$
Level 3	$0.05 \leq \zeta$	and	$0.36 \leq \omega_n$

The appropriate choice for T is a complete period of the short-period mode. Since the period of the short-period mode is about 6 seconds, T is used as 6 seconds in this study. Based on this, the EFQC for the short-period mode is written as,

Level 1	$0.14 \leq A \leq 7.00$	and	$0 \leq B \leq 3.30$
Level 2	$0.07 \leq A \leq 12.0$	and	$0 \leq B \leq 5.90$
Level 3	$0.02 \leq A$		

where

$A = \frac{1}{6}\int_t^{t+6} \omega_n(\tau)\zeta(\tau)d\tau$

$B = \frac{1}{6}\int_t^{t+6} \omega_n(\tau)\sqrt{1-\zeta(\tau)^2}d\tau$

5.5.2 Extended Flying Qualities Criteria for Phugoid Mode

The flying quality specification for the phugoid mode is the following. The values of ζ and T_2 of phugoid are obtained from MIL-STD-1797A.

Level 1 $\zeta > 0.04$

Level 2 $\zeta > 0$

Level 3 $T_2 \geq 55$ seconds (for unstable root)

The Level 3 requirement can be written in terms of $\zeta\omega_n$ in Eq. 5.13.

$$| -\zeta\omega_n | \leq 0.0126 \tag{5.13}$$

The appropriate choice for T is a complete period of the phugoid mode. Since the period of the phugoid is about 30 seconds, T is used as 30 seconds in this study. Based on this, the EFQC for the phugoid mode is written as,

Level 1 $0.04 < C$

Level 2 $0 < C$

Level 3 $0.0126 \geq D$ (for unstable root)

where

$C = \frac{1}{30} \int_t^{t+30} \zeta(\tau) d\tau$

$D = \frac{1}{30} \int_t^{t+30} | -\zeta(\tau)\omega_n(\tau) | d\tau.$

5.6 Extended Flying Qualities Criteria for Lateral Dynamics

In this section, the extended flying qualities criteria for the lateral dynamics are developed. The extended flying quality criteria, first for the dutch-roll mode, second for the spiral mode, and finally for the roll mode are developed.

5.6.1 Extended Flying qualities Criteria for Dutch-Roll Mode

The flying quality specification for the dutch-roll mode is following. The values of ζ, ω_n and $\zeta\omega_n$ of the dutch-roll are obtained from MIL-STD-1797A.

Level 1	$0.08 \leq \zeta$	$0.40 \leq \omega_n$	$0.15 \leq \zeta\omega_n$
Level 2	$0.02 \leq \zeta$	$0.40 \leq \omega_n$	$0.10 \leq \zeta\omega_n$
Level 3	$0 \leq \zeta$	$0.40 \leq \omega_n$	

The appropriate choice for T is a complete period of the dutch-roll mode. Since the period of the dutch-roll is about 3 seconds, T is used as 3 seconds in this study. Based on this, the EFQC for the dutch-roll mode is written as,

Level 1	$0.15 \leq E$ and $0.08 \leq F$
Level 2	$0.10 \leq E$ and $0.02 \leq F$
Level 3	$0 \leq E$ and $0 \leq F$

where

$E = \frac{1}{3}\int_t^{t+3} \omega_n(\tau)\zeta(\tau)d\tau$

$F = \frac{1}{3}\int_t^{t+3} \zeta(\tau)d\tau.$

5.6.2 Extended Flying Qualities Criteria for Spiral Mode

The flying quality specification for the spiral mode follows. The value of t_2 of the spiral mode is obtained from MIL-STD-1797A.

Level 1	$20 \leq t_2$
Level 2	$8 \leq t_2$
Level 3	$4 \leq t_2$

The appropriate choice for T is a time constant for the spiral mode, and the time constant of the spiral mode is about 20 seconds. Therefore, T is used as 20 seconds in this study. Based on this, the EFQC for the spiral mode is written as,

Level 1 $20 \leq G$

Level 2 $8 \leq G$

Level 3 $4 \leq G$

where

$G = \frac{1}{20} \int_t^{t+20} \frac{\ln 2}{|t_c(\tau)|} d\tau.$

5.6.3 Extended Flying Qualities Criteria for Roll Mode

The flying quality specification for the roll mode follows. The value of $t_{1/2}$ of the roll is obtained from MIL-STD-1797A.

Level 1 $1.4 \geq t_{1/2}$

Level 2 $3.0 \geq t_{1/2}$

Level 3 $10 \geq t_{1/2}$

The appropriate choice for T is a time constant for the roll mode, and the time constant of the roll mode is about 2 seconds. Therefore, T is used as 2 seconds in this study. Based on this, the EFQC for the roll mode is written as,

Level 1 $1.4 \geq H$

Level 2 $3.0 \geq H$

Level 3 $10 \geq H$

where

$H = \frac{1}{2} \int_t^{t+2} \frac{\ln 2}{|t_c(\tau)|} d\tau.$

5.7 Flying Qualities for GHAME Vehicle based on EFQC

In this section, the flying qualities for the GHAME vehicle are investigated. Fig. 5-1 illustrates the flying quality for the short-period mode based on the EFQC. The flying

quality on the short-period mode starts from below Level 3. Until 900 seconds, the flying quality remains below Level 3 then the flying quality enters Level 3 after 900 seconds. The first half of the flight is below Level 3 and it reaches Level 2 at the end of the trajectory. Therefore, the short-period mode is not safely controllable for the pilot during the first half of the flight, and the second half of the flight is controllable with excessive workload for the pilot.

Fig. 5-2 illustrates the flying quality for the phugoid mode. Due to the 'turning point', which was discussed in Chapter 4, flying quality was not analyzed for the entire trajectory in the phugoid mode. Fig. 5-3 shows the detail of Fig. 5-2. The flying quality of the phugoid mode starts from Level 3 then it enters Level 2 and Level 1. However, the flying quality degrades to Level 3 at 312 seconds. Between 312 seconds and 685 seconds the flying quality is not investigated due to the 'turning point'. From 685 seconds the flying quality remains at Level 1 until 1670 seconds then the 'turning point' occurs again. These analyses show that flying quality of the phugoid mode fluctuates between Level 1 and Level 3. Therefore, it will be very useful to have a flight display window for the pilot to provide information about flying qualities during the flight, especially for the phugoid mode.

From Fig. 5-4, it is clear that the flying quality for the dutch-roll mode is inadequate because it satisfies only the Level 3 requirement during the entire trajectory. Therefore, workload for the pilot is excessive for the dutch-roll mode.

Fig. 5-5 illustrates the flying quality for the spiral mode. The extended flying quality for the spiral mode meets the Level 1 requirement during the entire trajectory. However, the roll mode does not satisfy the Level 3 requirements. Therefore, the roll mode is not safely controllable for the pilot. The spiral mode is the only mode which has adequate flying quality throughout the trajectory.

Based on these analyses, the GHAME vehicle is not safely controllable for the pilot or the workload for the pilot will be excessive. Therefore, the GHAME vehicle needs augmented control systems. In addition, the flight display window for the pilot will be very useful especially for the phugoid mode which fluctuates between level 1 and Level 3. Figs. 5-7 and 5-8 illustrate extended flying qualities for each mode in

the flight display window. For the safety reason, the 'turning point' is considered as Level 3 in the phugoid mode because the dynamics of the 'turning point' have to be investigated further. The investigation of the 'turning point' is not carried out because it is beyond scope of this thesis.

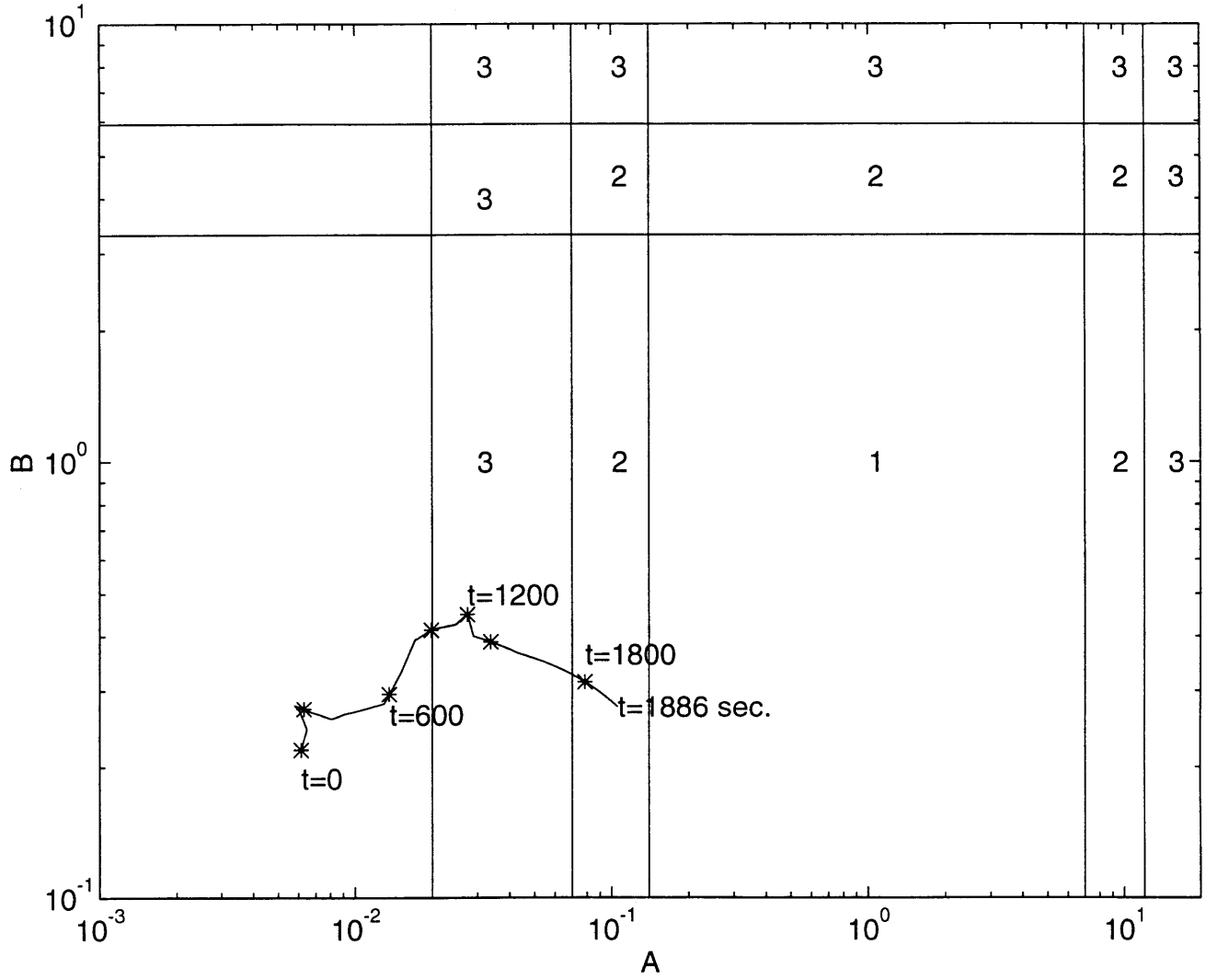

Figure 5-1: Flying Quality for Short-Period Mode by EFQC

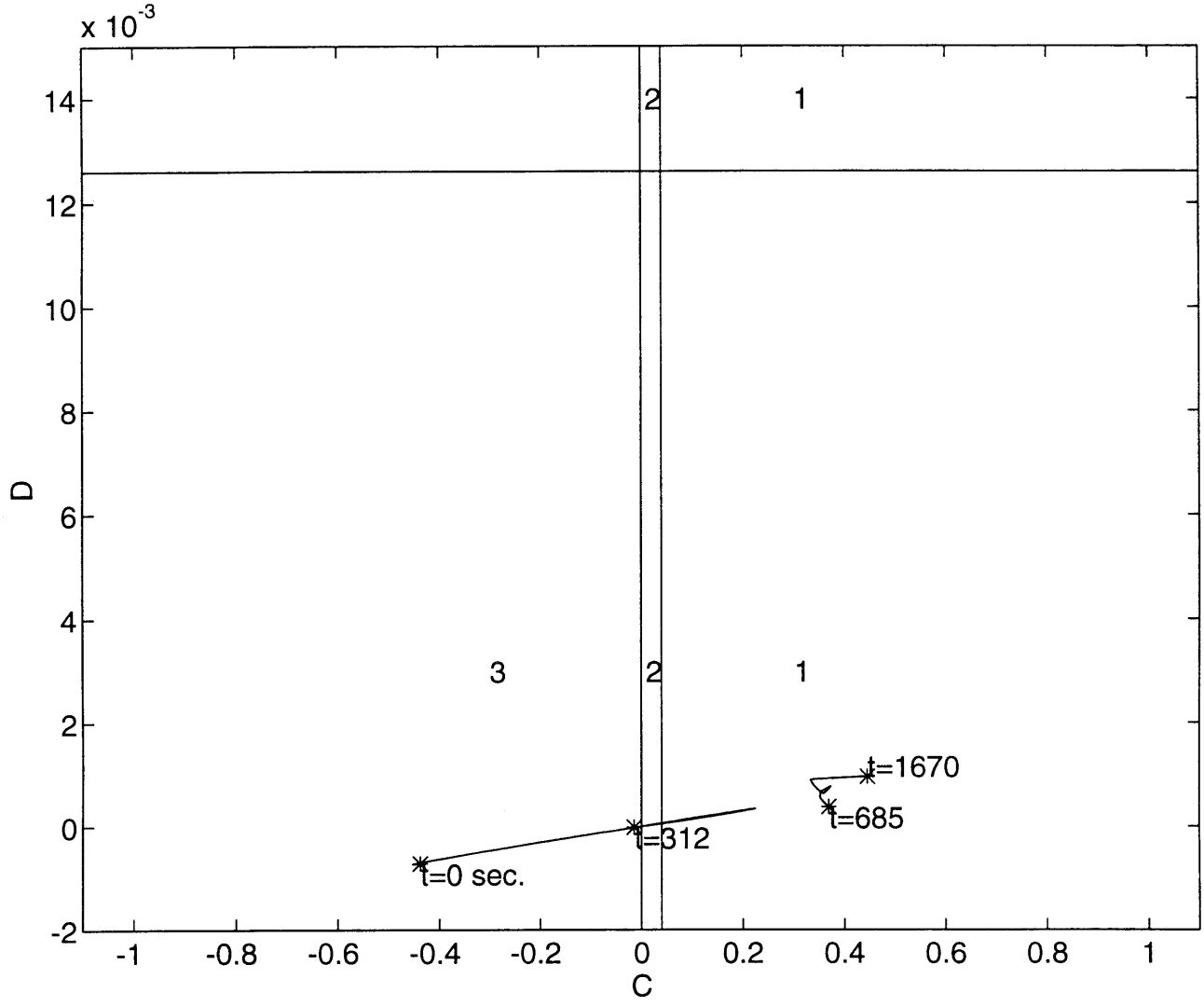

Figure 5-2: Flying Quality for Phugoid Mode by EFQC

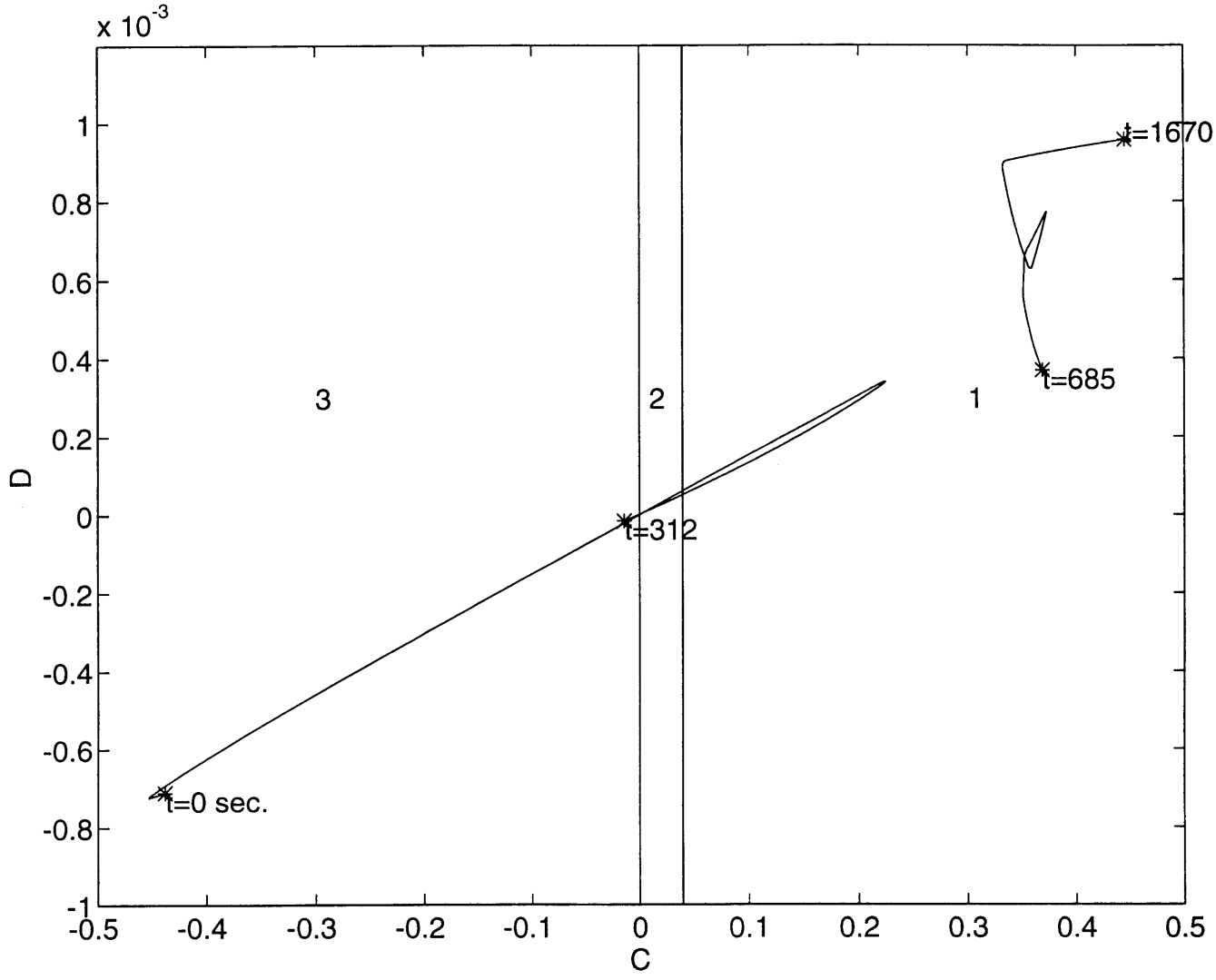

Figure 5-3: Flying Quality for Phugoid Mode by EFQC (In detail)

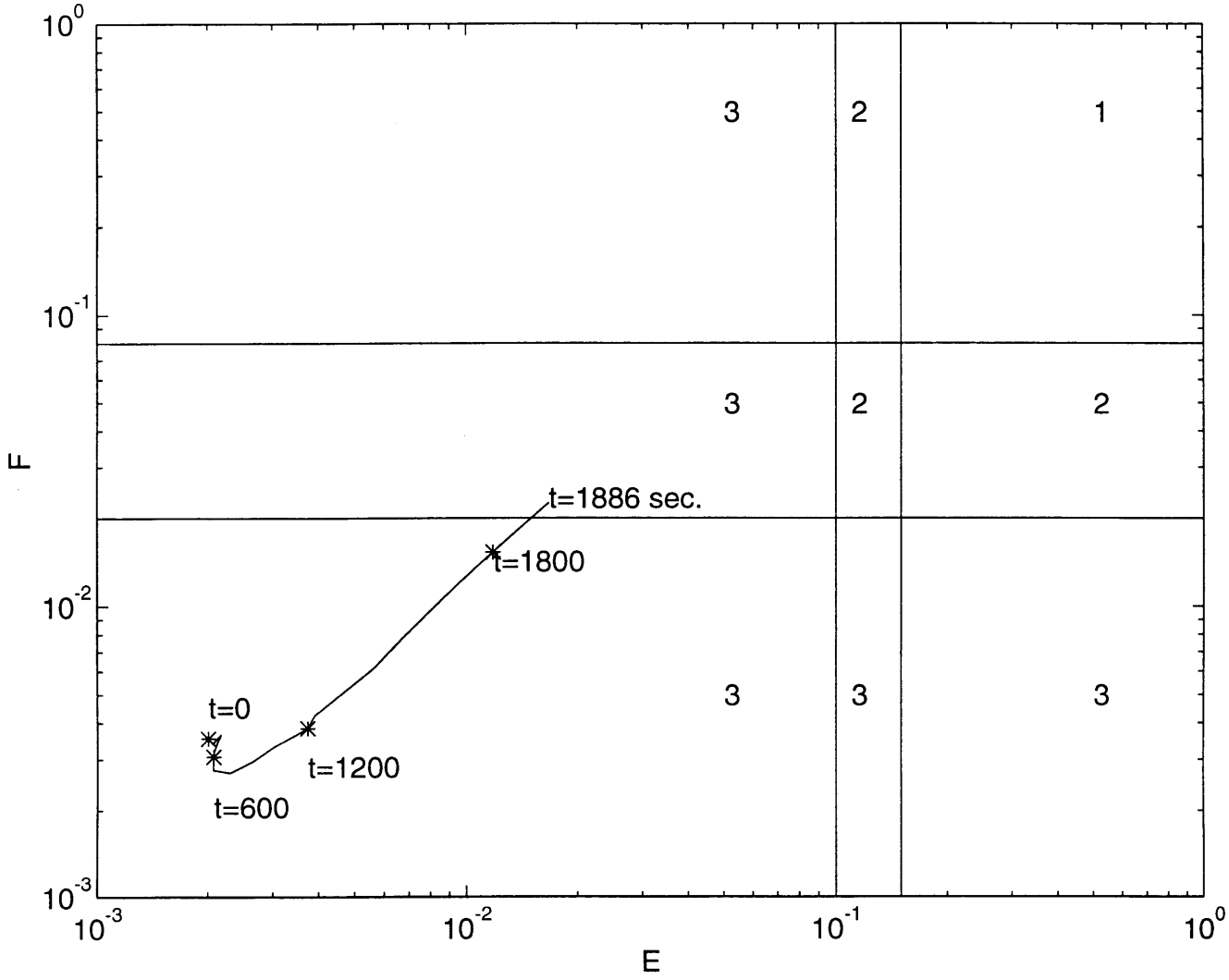

Figure 5-4: Flying Quality for Dutch-Roll Mode by EFQC

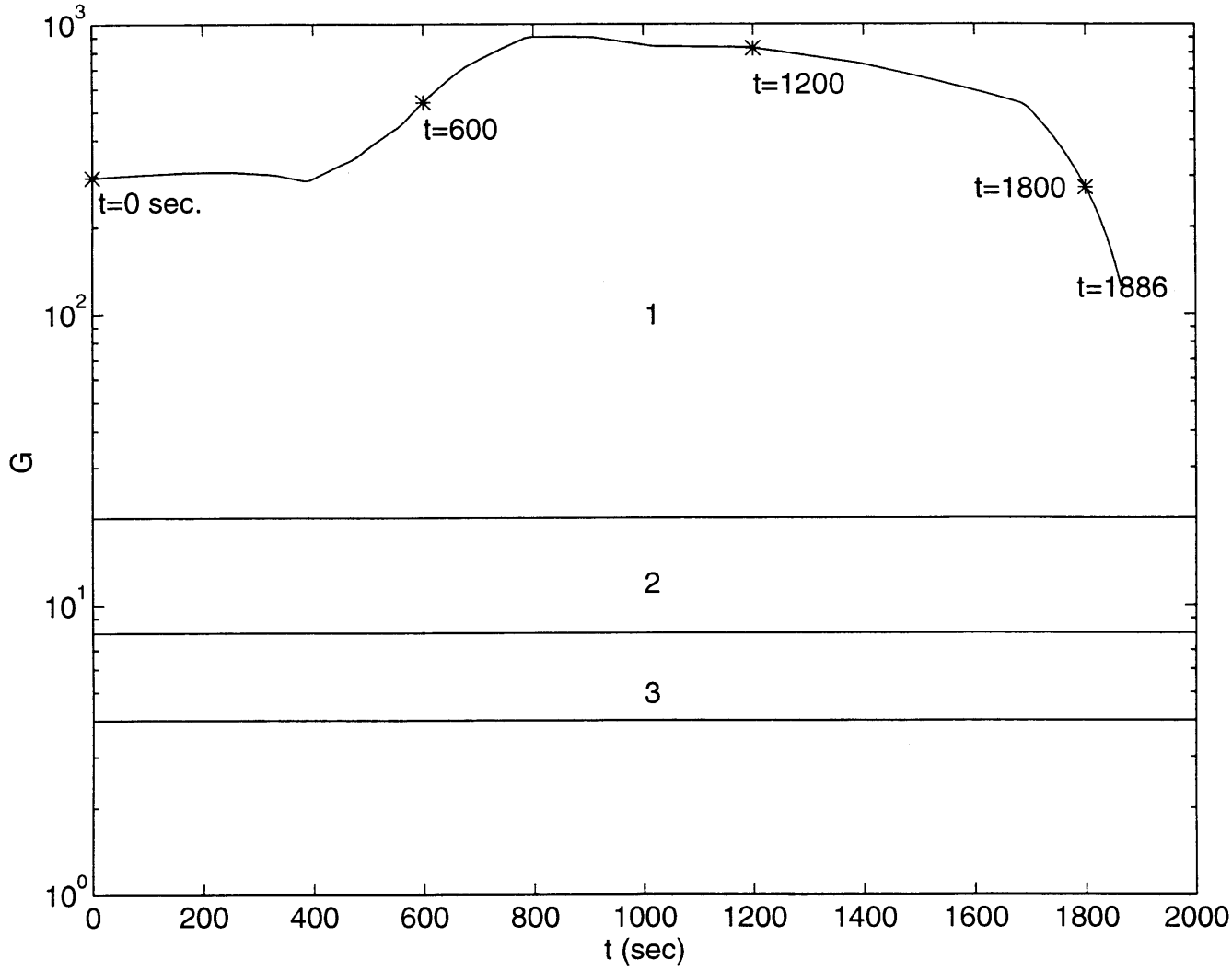

Figure 5-5: Flying Quality for Spiral Mode by EFQC

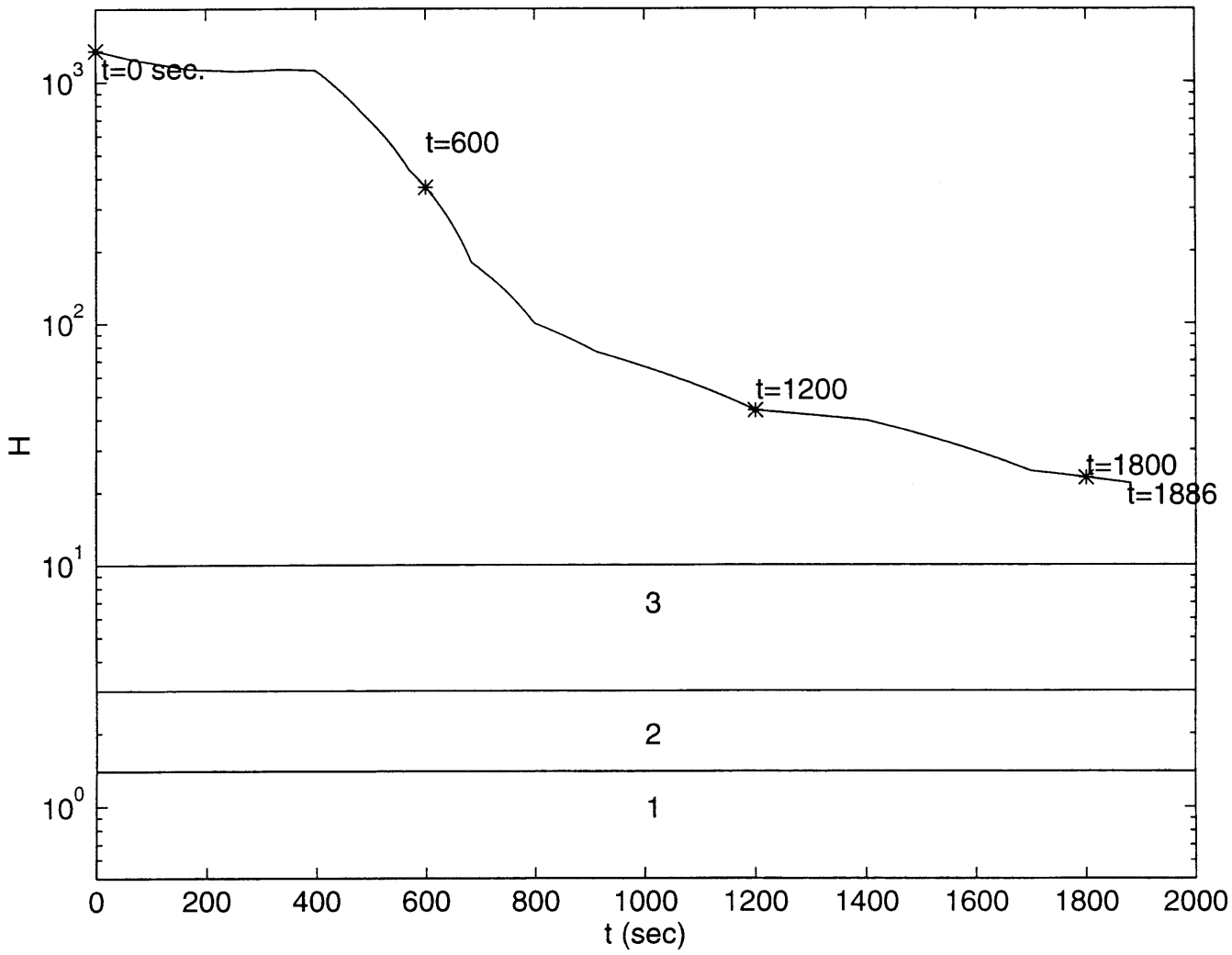

Figure 5-6: Flying Quality for Roll Mode by EFQC

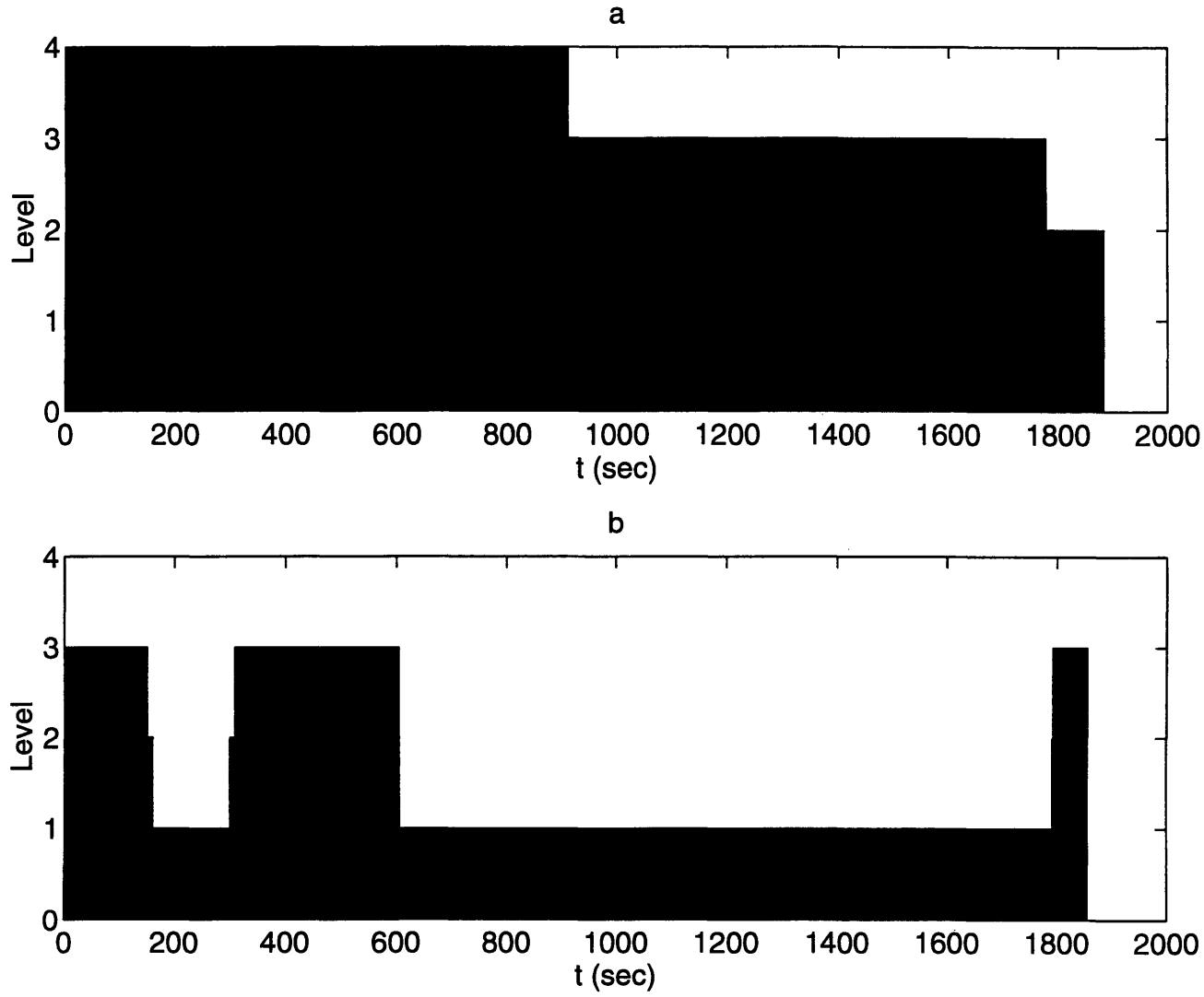

Figure 5-7: Flying Quality Level for Longitudinal Dynamics by EFQC: (a) Short-Period Mode, (b) Phugoid Mode

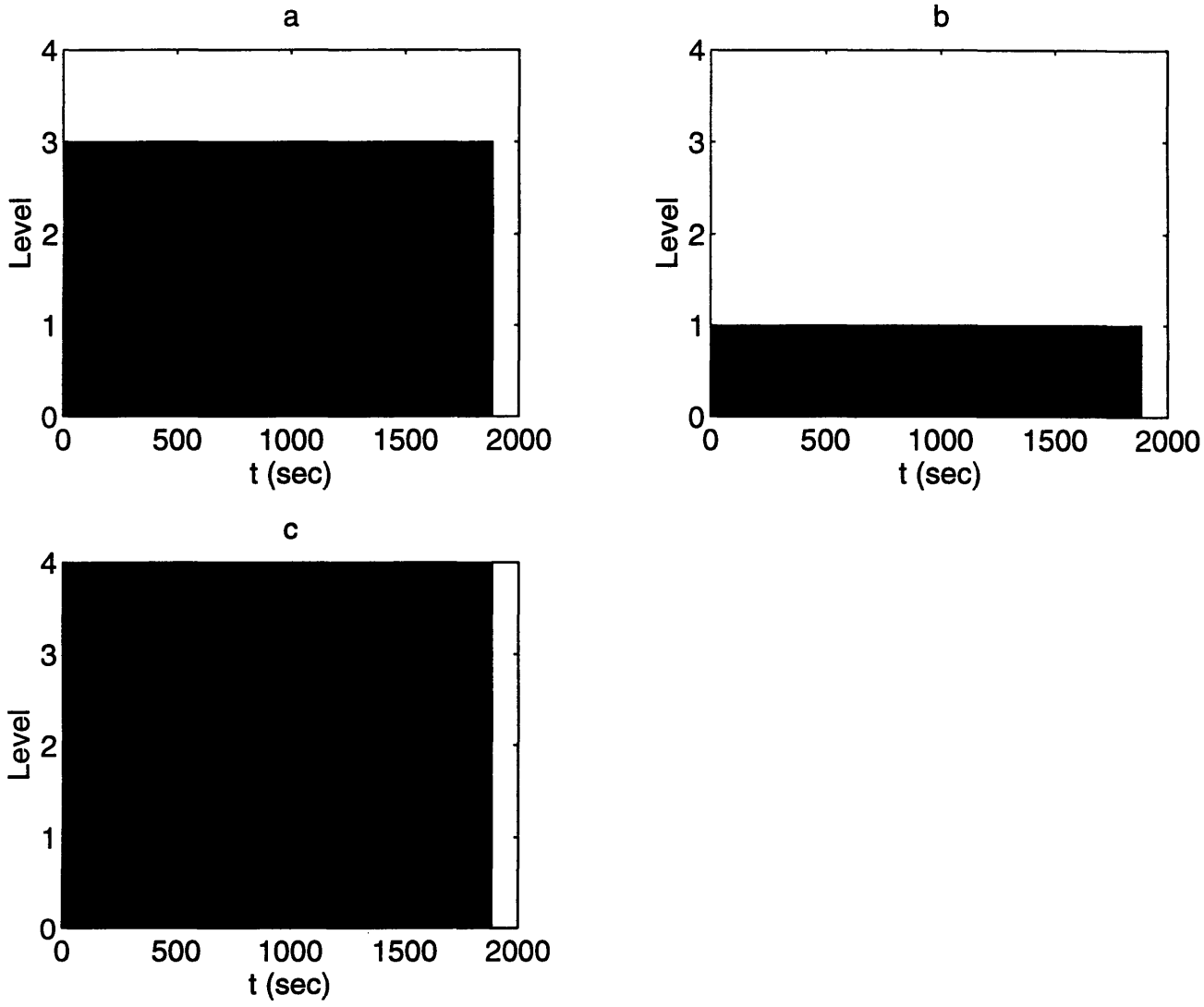

Figure 5-8: Flying Quality Level for Lateral Dynamics by EFQC: (a) Dutch-Roll Mode, (b) Spiral Mode, (c) Roll Mode

Chapter 6

Parameter Estimation using Generalized Multiple Scales Theory

6.1 Introduction

The extraction of unknown stability and control derivatives from flight data has been of interest since the early 1920's [17, 18, 20]. The stability and control derivatives play a very important role in development and modification of aircraft. For example, these derivatives are used in the flight planning, flight control system modification and verification of aircraft performance and characteristics. The systematic method of obtaining the stability and control derivatives is parameter estimation. The parameter estimation is explained in the following section.

6.2 Parameter Estimation

A set of differential equations with unknown parameters describes an aircraft system. The unknown parameters are determined by the following procedures. The system is excited by a given input, and the input and the output are measured. The values of the unknown parameters are deduced based on results from the actual system

response and the model response with the given input. The unknown parameters can be identified easily through this approach. There are many parameter estimation techniques available including the maximum-likelihood and the Kalman filter techniques.

In this thesis, the maximum-likelihood estimator, which has been used for space shuttle vehicles and the F-14, is used for parameter estimation [17, 21, 22]. A brief explanation of the maximum-likelihood method is following [17, 19, 22, 23, 24]. The first procedure is to define the system (equations of motion) in the form as

$$x(t_0) = x_0 \tag{6.1}$$

$$\dot{x}(t) = f[x(t), u(t), \zeta] + F(\zeta)n(t) \tag{6.2}$$

$$z(t_i) = g[x(t_i), u(t_i), \zeta] + G(\zeta)\eta_i \tag{6.3}$$

where

x = state vector	u = control input vector
ζ = vector of unknowns	n = state noise vector
z = observation vector	η_i = measurement noise vector

The measurement noise vector is assumed as a sequence of independent Gaussian random variables with zero mean and identity covariance, and the state noise vector is assumed as zero-mean white Gaussian and stationary. The maximum-likelihood estimator minimizes the cost function

$$J(\zeta) = 1/2 \sum_{i=1}^{N} [z(t_i - \tilde{z}_\zeta(t_i)]^T (GG^T)^{-1} [z(t_i - \tilde{z}_\zeta(t_i)] + 1/2(\zeta - m_\zeta)^T P^{-1} (\zeta - m_\zeta) \tag{6.4}$$

where

$\tilde{}$ = predicted estimate	GG^T = measurement noise covariance matrix
P = covariance	m_ζ = mean of the prior distribution of ζ
$\tilde{z}_\zeta$ = computed response	

If Eqs. 6.2 and 6.3 are linearized,

$$x(t_0) = x_0 \tag{6.5}$$

$$\dot{x}(t) = Ax(t) + Bu(t) + Fn(t) \tag{6.6}$$

$$z(t_i) = Cx(t_i) + Du(t_i) + G\eta_i. \tag{6.7}$$

The $\tilde{z_\zeta}(t_i)$ term of Eq. 6.4 can be approximated by

$$\tilde{x_\zeta}(t_0) = x_0(\zeta) \tag{6.8}$$

$$\tilde{x_\zeta}(t_{i+1}) = \phi\tilde{x_\zeta}(t_i) + \psi[u(t_i) - u(t_{i+1})]/2 \tag{6.9}$$

$$\tilde{z_\zeta}(t_i) = C\tilde{x_\zeta}(t_i) + Du(t_i) \tag{6.10}$$

where the transition matrix ϕ and the integral of the transition matrix ψ are given by

$$\phi = exp[A(t_{i+1} - t_i)] \tag{6.11}$$

$$\psi = \int_{t_i}^{t_{i+1}} exp(A\tau)d\tau. \tag{6.12}$$

Then the minimization technique is used to minimize the cost and in this case the Gauss-Newtonian algorithm is used. The maximum-likelihood estimator estimates unknown parameters by iterative procedures. The accurate initial states lead to accurate parameter estimation results and this minimizes computational time. In order to obtain accurate initial states, the direct-integration method has been used. However, this method is time-consuming. Therefore, an alternative method is needed for saving CPU time.

6.3 Importance of the Initial State in Parameter Estimation

In this section, the importance of the initial state is investigated in the parameter estimation. A first order LTV differential equation (Eq. 6.13), which describes the GHAME vehicle's pitch rate, is used for investigation.

$$\frac{dq}{dt} + M_q(t)q = M_{\delta e}(t)\delta e \tag{6.13}$$

Fig. 6-1 shows the time varying nature of coefficients, which are M_q and $M_{\delta e}$, in Eq. 6.13. Fig. 6-2 shows the input and output during one second. The input for δe is repeated every second for simulation.

The maximum-likelihood estimator is used for the comparison test. The correct value of the initial state q is 10 deg/second in this case. The error is introduced into the initial state and errors on the parameter estimation are compared. When the correct initial state is given, the estimations of M_q and $M_{\delta e}$ are correct. When 0.1 % error is introduced into the initial state, error in the M_q is 4.5 % and error in the $M_{\delta e}$ is 6.0 %. When 1 % error is introduced into the initial state, error in the M_q is 45.2 % and error in the $M_{\delta e}$ is 59.4 %. When 10 % error is introduced into the initial state, error in the M_q is 447.9 % and error in the $M_{\delta e}$ is 586.5 %. Therefore, the initial state estimation plays a very important role in the parameter estimation and the initial state error is proportional to the error in the parameter estimation. The summary is given in Table 6.1 The parameter estimation is shown in Tables 6.2 - 6.4 and the iteration plots are shown in Figs. 6-3 - 6-5.

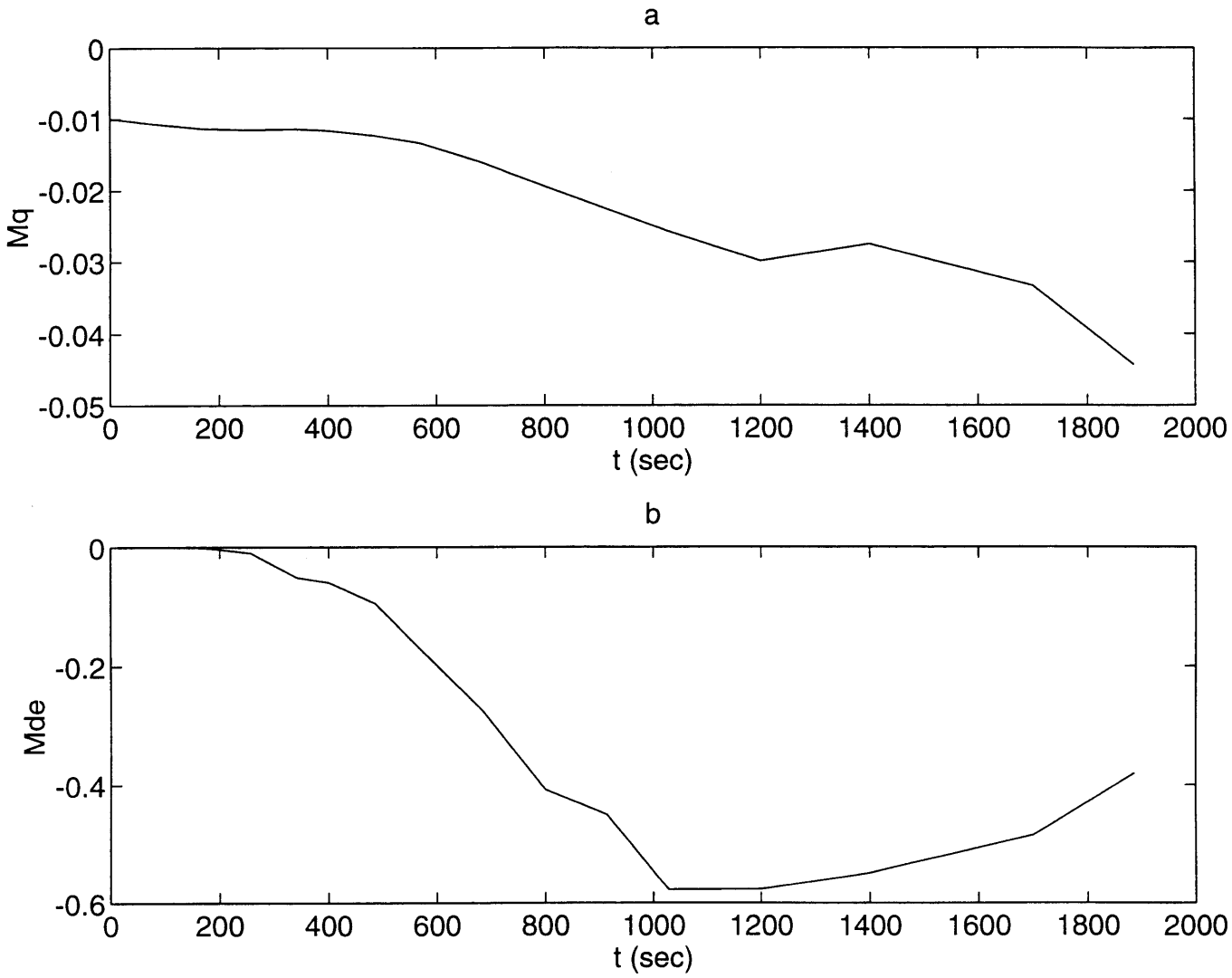

Figure 6-1: (a) M_q vs. time, (b) $M_{\delta e}$ vs. time

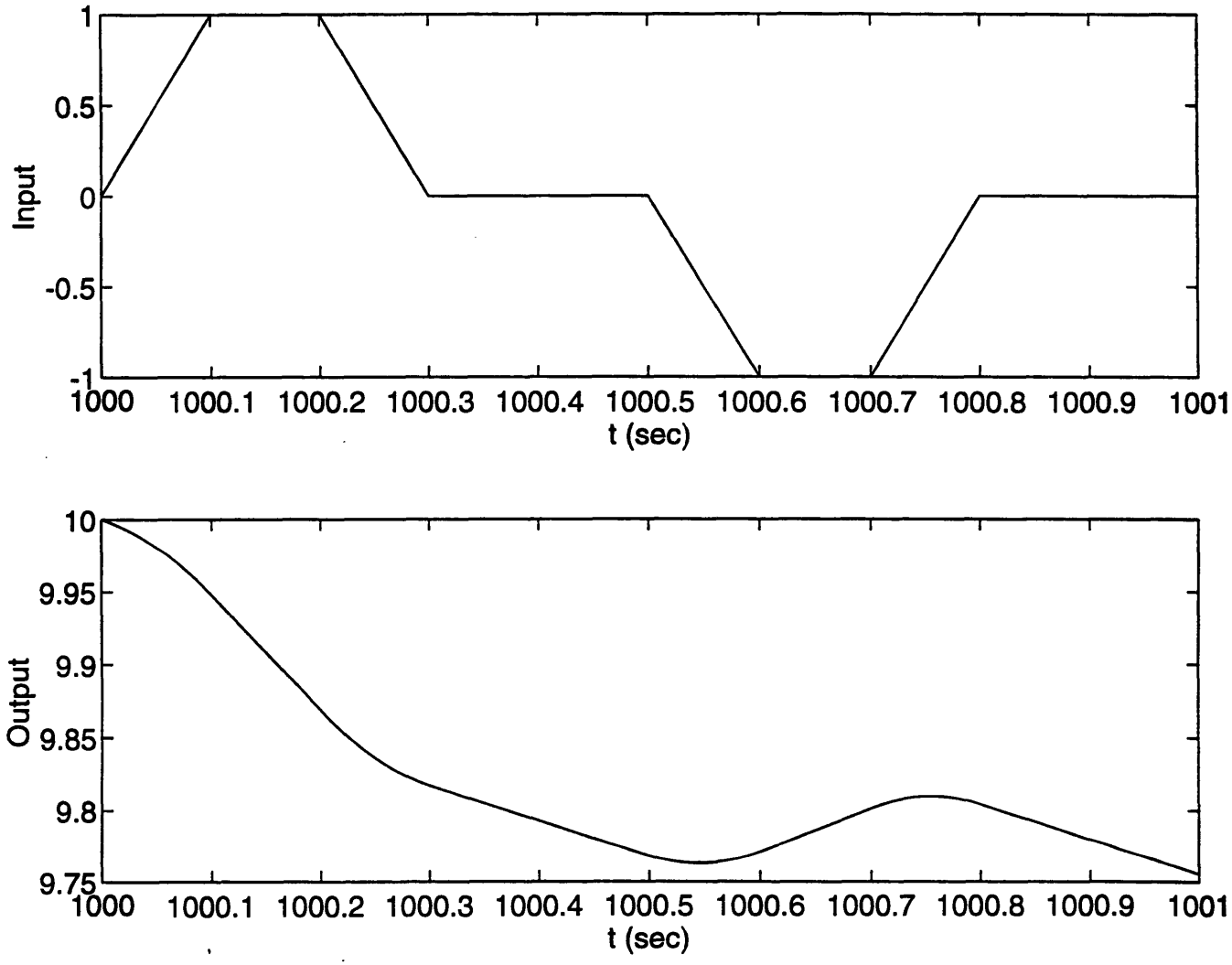

Figure 6-2: Input and Output

Table 6.1: Comparison between error of initial state and error of parameter estimation

% error of initial state	% error of M_q	% error of $M_{\delta e}$
0.1	4.5	6.0
0.2	9.1	12.0
0.3	13.6	17.9
0.4	18.1	23.8
0.5	22.6	29.8
0.6	27.1	35.7
0.7	31.7	41.7
1	45.2	59.4
2	90.3	118.7
10	447.9	586.5
20	887.1	1153.8

Table 6.2: Parameter estimation for correct initial state

# of iteration	J	M_q	$M_{\delta e}$	$\tilde{M}_q$	$\tilde{M}_{\delta e}$
1	4.2908×10^{-1}	-2.4894×10^{-2}	-5.4424×10^{-1}	-2.4786×10^{-2}	-5.4492×10^{-1}
2	1.5888×10^{-5}	-2.4894×10^{-2}	-5.4424×10^{-1}	-2.4894×10^{-2}	-5.4424×10^{-1}
3	2.0609×10^{-13}	-2.4894×10^{-2}	-5.4424×10^{-1}	-2.4894×10^{-2}	-5.4424×10^{-1}
4	1.8560×10^{-13}	-2.4894×10^{-2}	-5.4424×10^{-1}	-2.4894×10^{-2}	-5.4424×10^{-1}

Table 6.3: Parameter estimation for 0.1 % error in the initial state

# of iteration	J	M_q	$M_{\delta e}$	$\tilde{M}_q$	$\tilde{M}_{\delta e}$
1	3.4917×10^{-1}	-2.4894×10^{-2}	-5.4424×10^{-1}	-2.5932×10^{-2}	-5.7721×10^{-1}
2	6.2807×10^{-4}	-2.4894×10^{-2}	-5.4424×10^{-1}	-2.6020×10^{-2}	-5.7664×10^{-1}
3	6.1756×10^{-4}	-2.4894×10^{-2}	-5.4424×10^{-1}	-2.6020×10^{-2}	-5.7664×10^{-1}
4	6.1756×10^{-4}	-2.4894×10^{-2}	-5.4424×10^{-1}	-2.6020×10^{-2}	-5.7664×10^{-1}

Table 6.4: Parameter estimation for 1 % error in the initial state

# of iteration	J	M_q	$M_{\delta e}$	$\tilde{M}_q$	$\tilde{M}_{\delta e}$
1	6.3781×10^{-2}	-2.4894×10^{-2}	-5.4424×10^{-1}	-3.6147×10^{-2}	-8.6788×10^{-1}
2	6.1684×10^{-2}	-2.4894×10^{-2}	-5.4424×10^{-1}	-3.6147×10^{-2}	-8.6786×10^{-1}
3	6.1684×10^{-2}	-2.4894×10^{-2}	-5.4424×10^{-1}	-3.6147×10^{-2}	-8.6786×10^{-1}
4	6.1684×10^{-2}	-2.4894×10^{-2}	-5.4424×10^{-1}	-3.6147×10^{-2}	-8.6786×10^{-1}

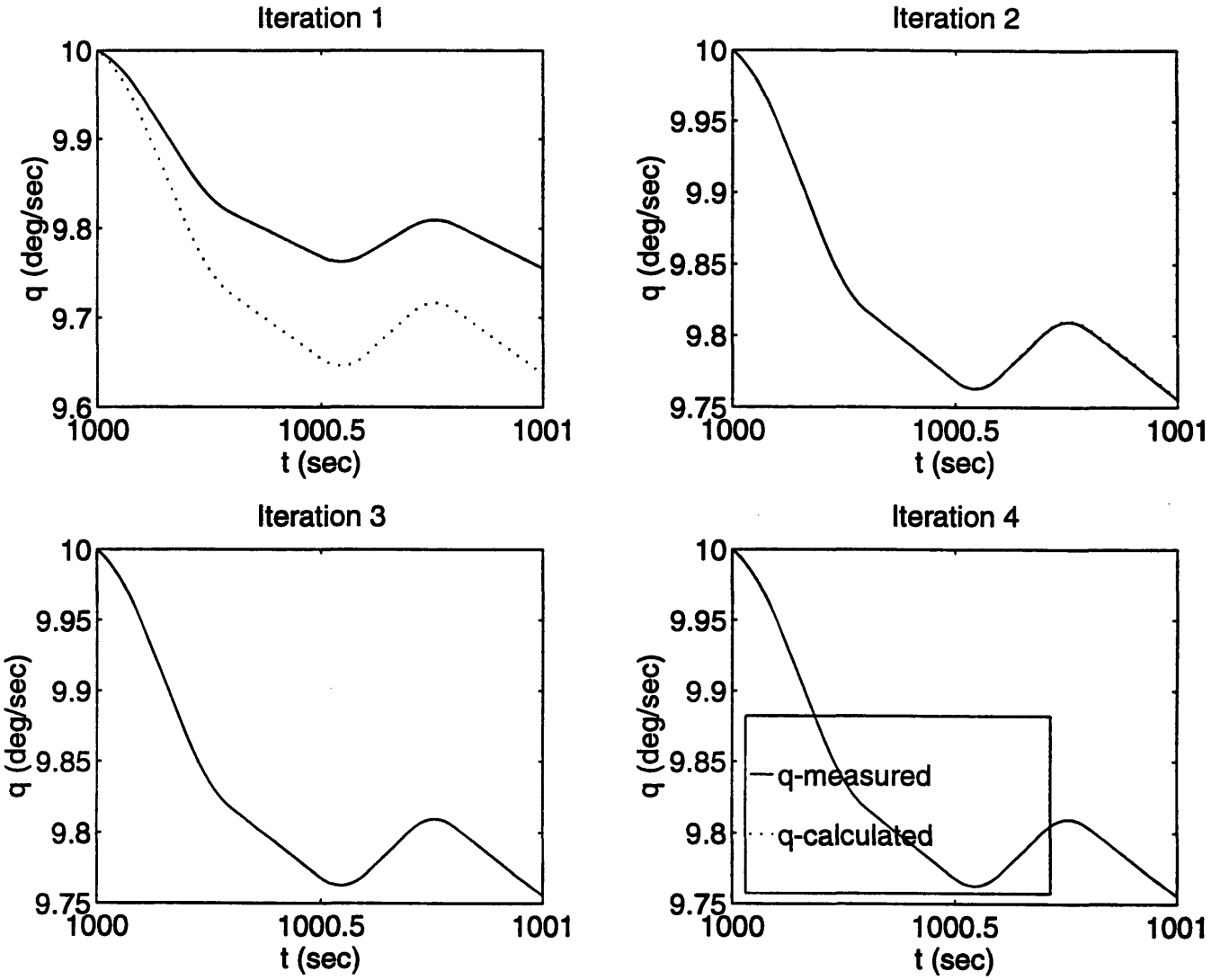

Figure 6-3: Parameter estimation for correct initial state

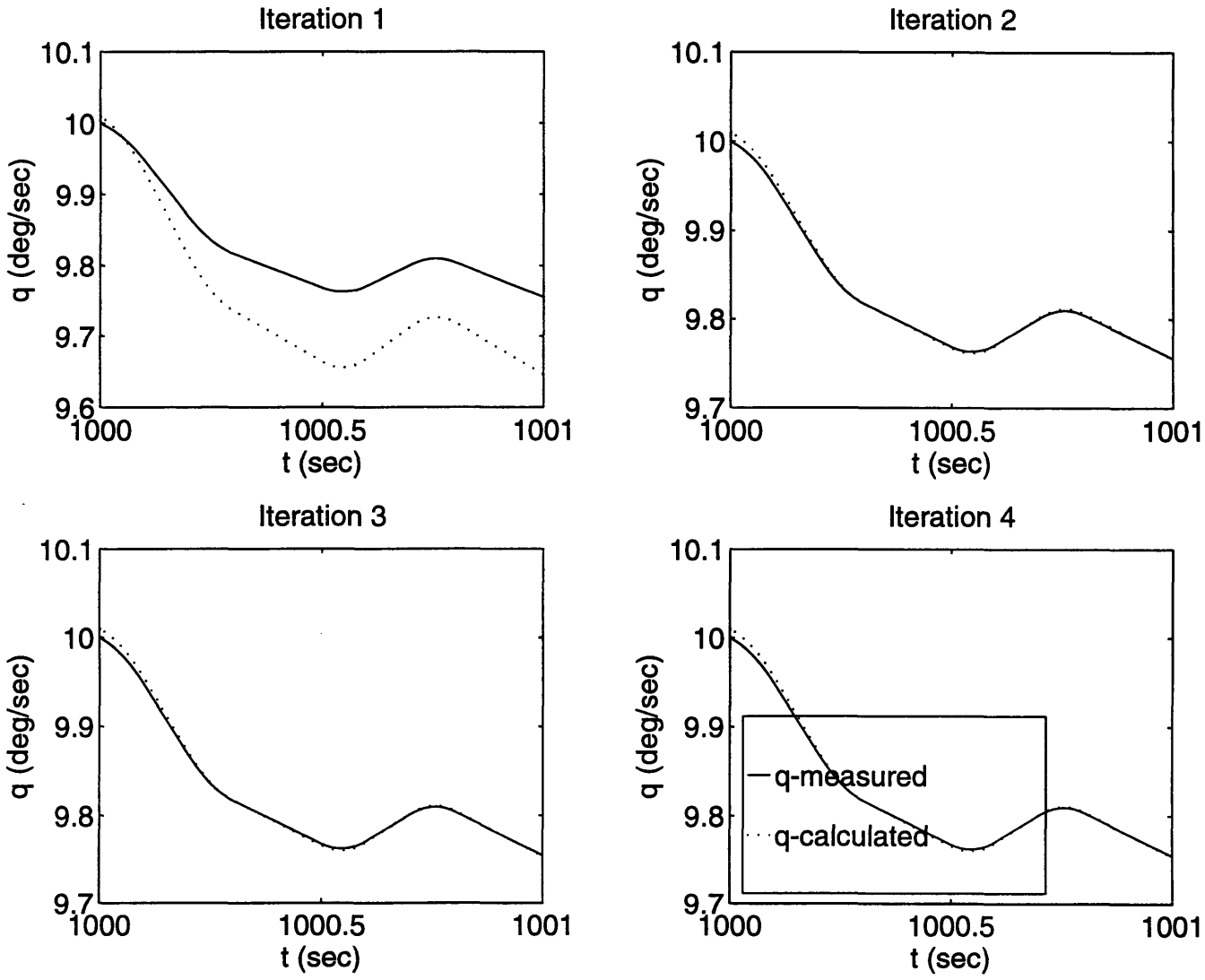

Figure 6-4: Parameter estimation for 0.1 % error in the initial state

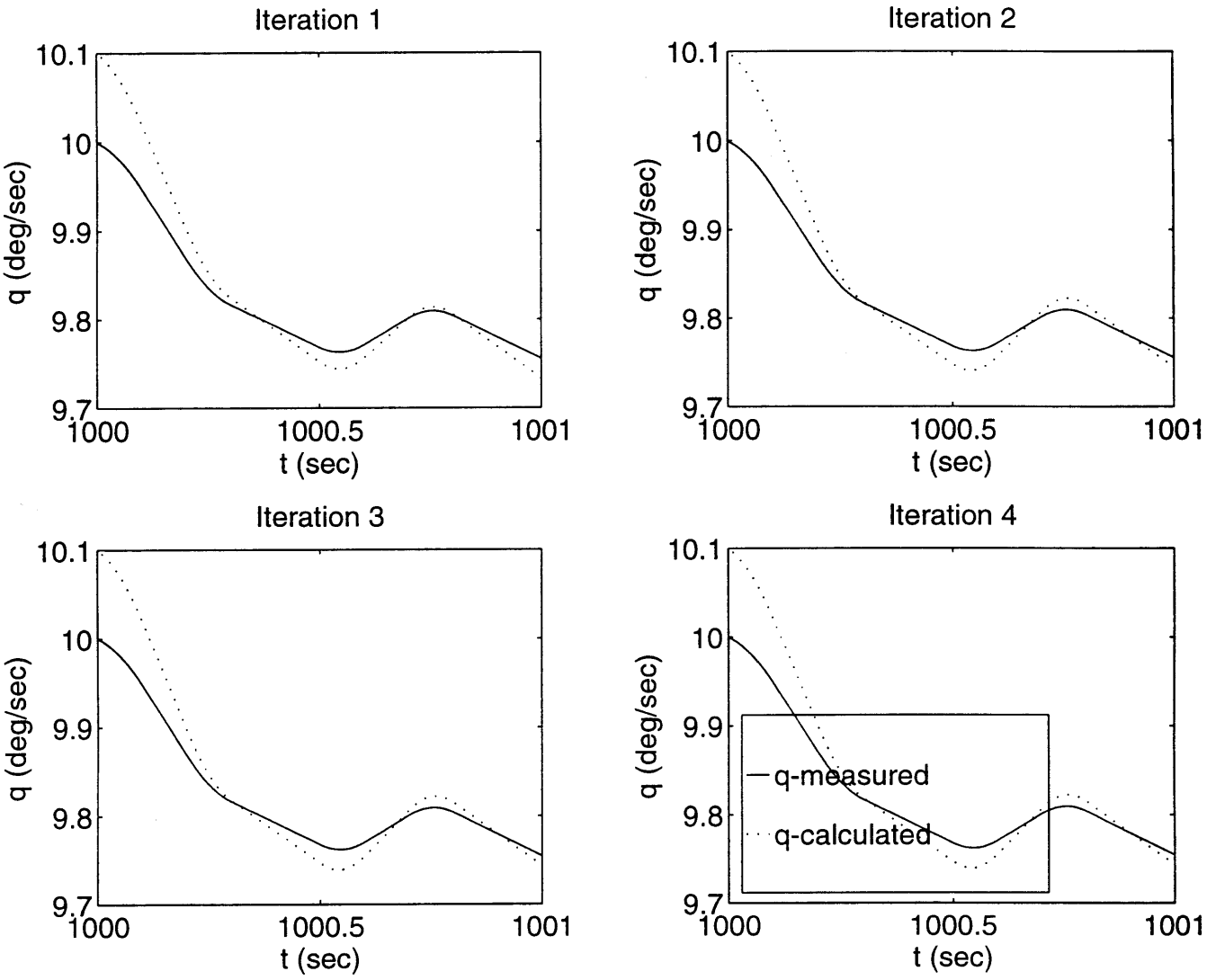

Figure 6-5: Parameter estimation for 1 % error in the initial state

6.4 State Estimation with GMS for Second Order Dynamics

In this section, the results from the GMS method are compared with the results from the direct-integration method in two categories: CPU time vs. maximum error and the CPU time vs. steady-state error (CPU time is based on the IBM RS6000). A second order LTV differential equation, which describes the GHAME vehicle's angle-of-attack perturbation, is used for comparison.

$$\frac{d^2\alpha}{dt^2} + Z_1(t)\frac{d\alpha}{dt} + Z_0(t)\alpha = 0 \tag{6.14}$$

Fig. 6-6 illustrates the accuracy of the GMS solution with comparison to the direct-integration solution. The direct-integration method with step size $\Delta\xi = 20$ is used as a reference case. Figs. 6-7 and 6-8 show the relationship between the CPU time and step size, maximum error and step size, and steady-state error and step size. In order to get accurate results from the direct-integration method, the step size has to be at least $\Delta\xi = 154$. The CPU time which corresponds to this run is 23 seconds. In contrast, the GMS method can use step size $\Delta\xi = 7150$ without significant increased maximum error and steady-state error. The CPU time which corresponds to this run is 1.64 seconds. As a consequence, the GMS method is 14 times faster than the DI method. From Table 6.5, the comparison between the GMS solution with step size $\Delta\xi = 7150$ and the reference case shows that the GMS case is 419 times faster

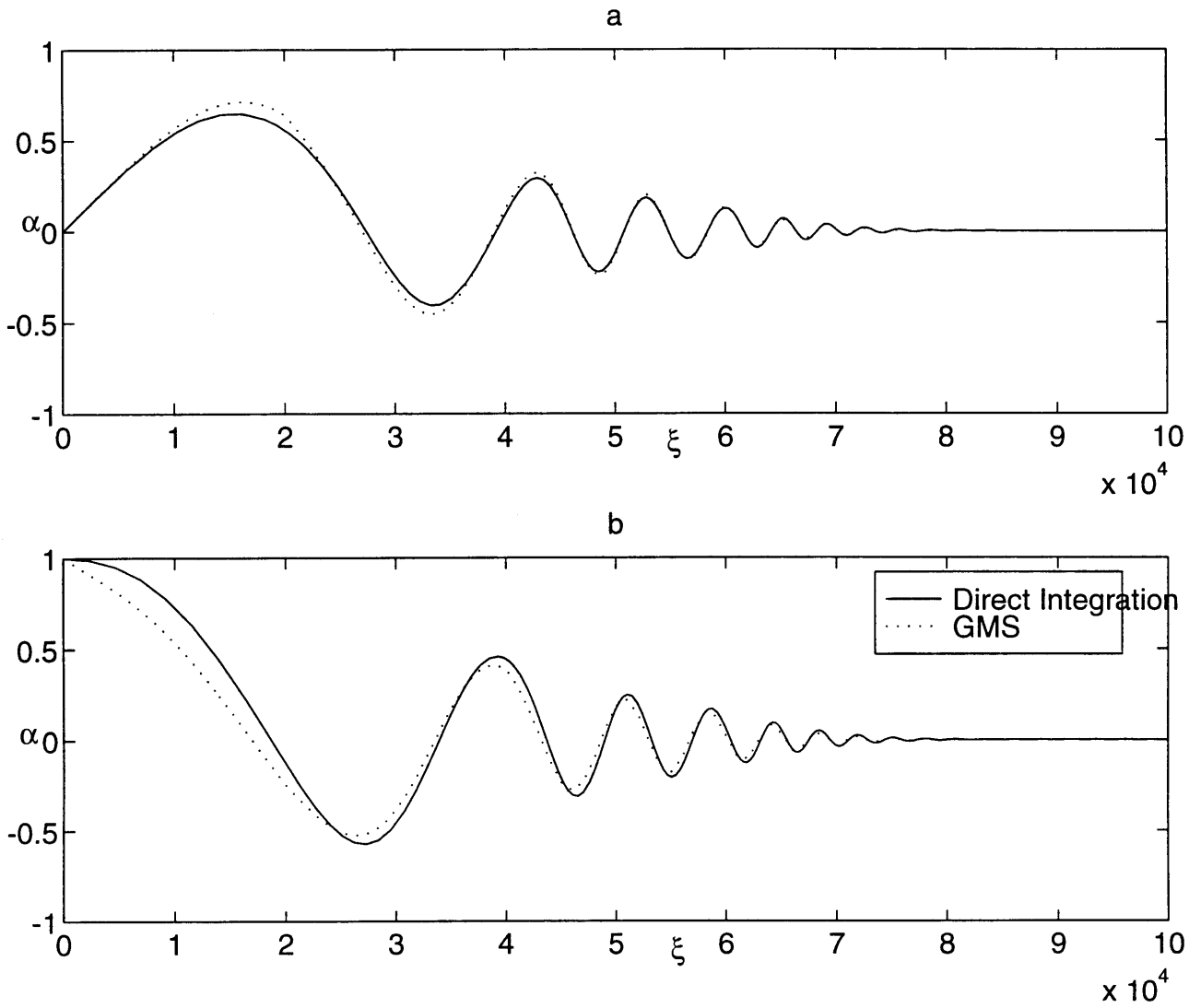

Figure 6-6: Comparison between Direct-Integration and GMS solutions for (a) Sine-like case, (b) Cosine-like case

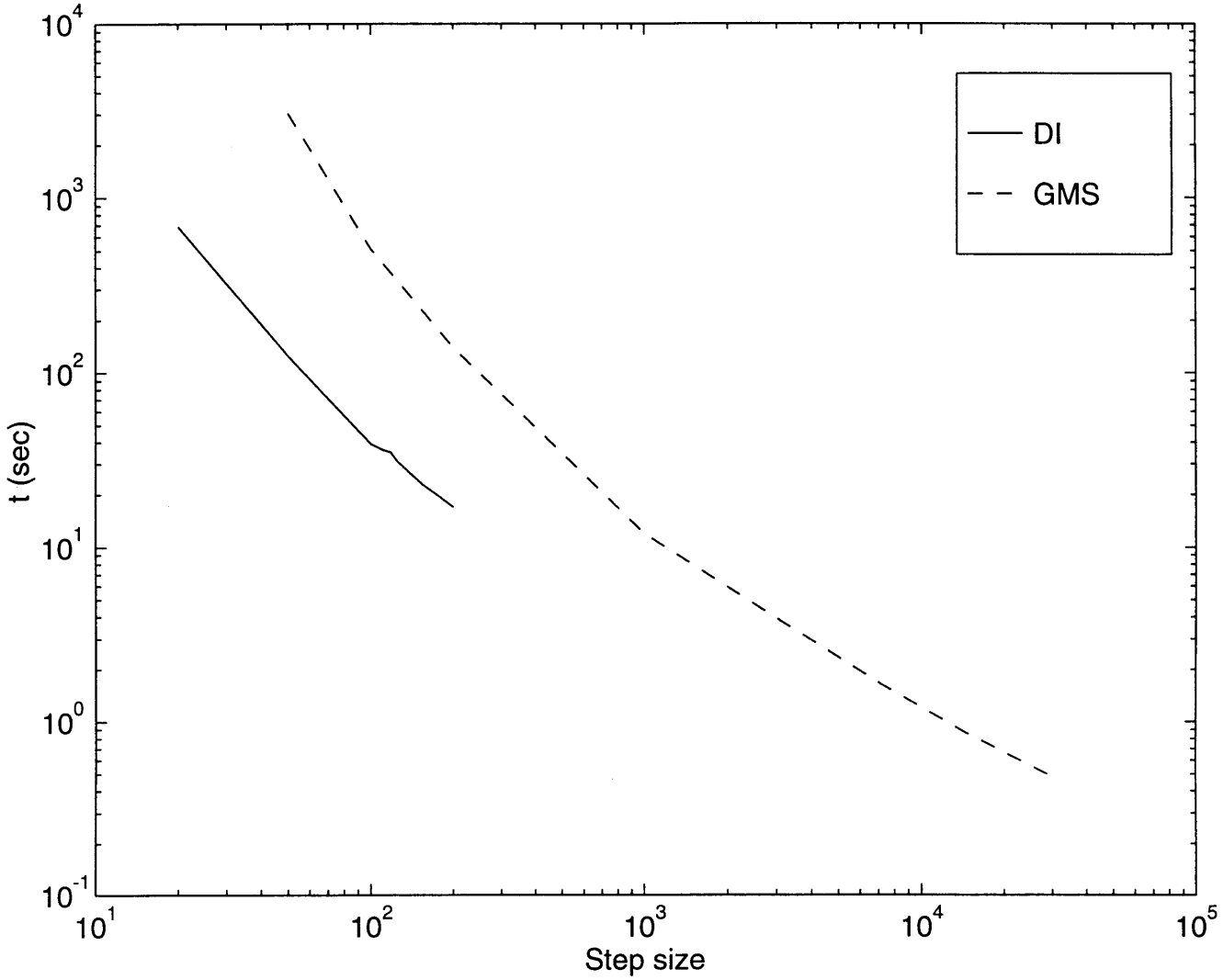

Figure 6-7: CPU time vs. Step Size for Direct Integration and GMS approach

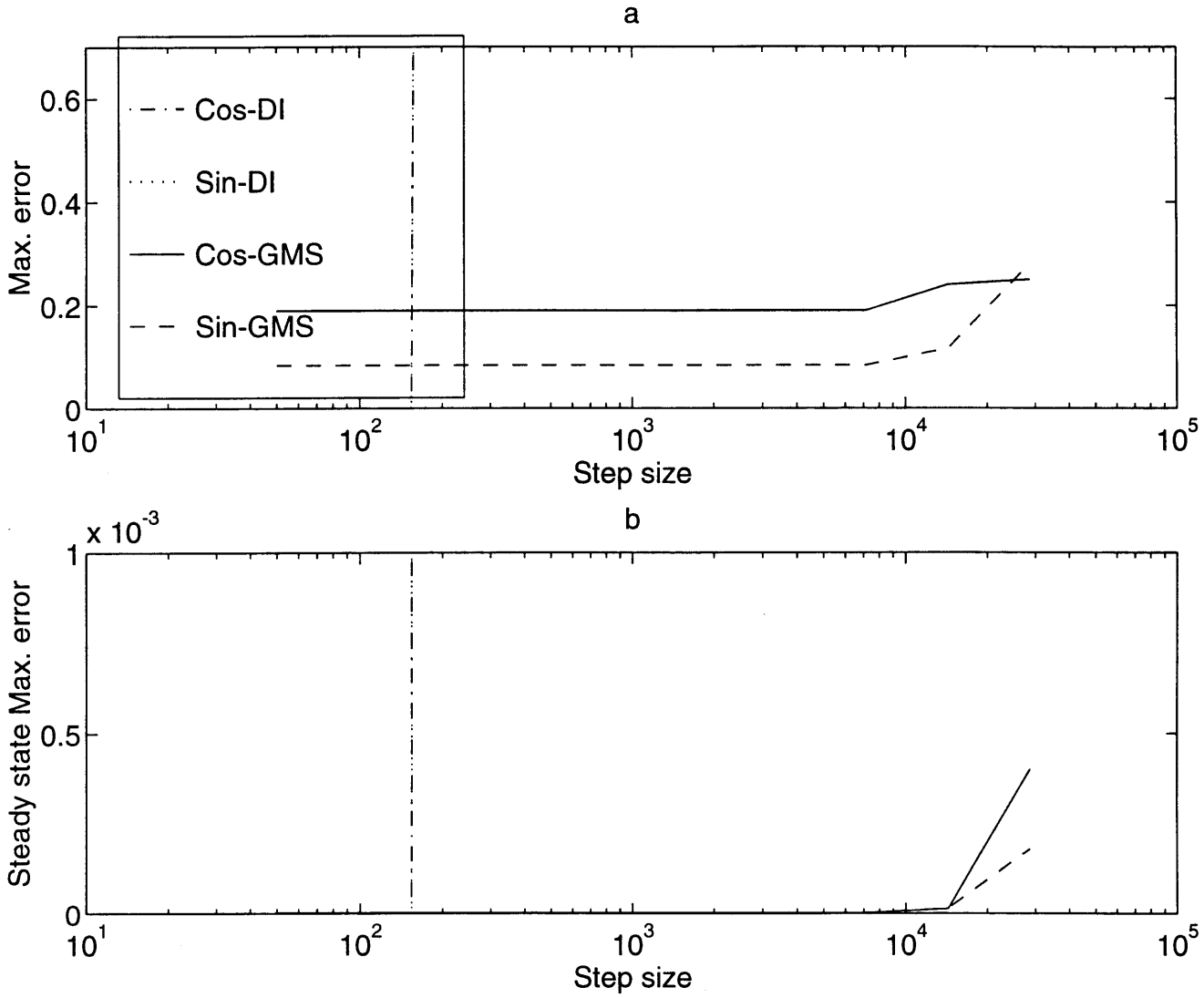

Figure 6-8: (a) Maximum Error vs. Step Size, (b) Steady State Maximum Error vs. Step Size for Direct Integration and GMS solutions

Table 6.5: Comparison between GMS and Direct-Integration

Method	CPU time (Sec.)	S.S. Error		Max. Error	
		Cos	Sin	Cos	Sin
D.I. $\Delta\xi = 20$ (Reference Case)	687	-	-	-	-
D.I. $\Delta\xi = 40$	190	8.6×10^{-12}	3.3×10^{-11}	5.9×10^{-8}	4.9×10^{-8}
D.I. $\Delta\xi = 50$	125	2.2×10^{-11}	8.6×10^{-11}	1.5×10^{-7}	1.3×10^{-7}
D.I. $\Delta\xi = 100$	39	4.2×10^{-10}	1.5×10^{-9}	2.5×10^{-6}	2.1×10^{-6}
D.I. $\Delta\xi = 111$	36	9.3×10^{-9}	2.2×10^{-8}	3.8×10^{-6}	3.3×10^{-6}
D.I. $\Delta\xi = 118$	35	1.2×10^{-8}	2.7×10^{-8}	4.7×10^{-6}	4.1×10^{-6}
D.I. $\Delta\xi = 125$	31	1.5×10^{-8}	3.5×10^{-8}	6.1×10^{-6}	5.3×10^{-6}
D.I. $\Delta\xi = 154$	23	3.5×10^{-8}	8.0×10^{-8}	1.4×10^{-5}	1.2×10^{-5}
D.I. $\Delta\xi = 182$	19	7.0×10^{-2}	7.0×10^{-2}	5.5×10^{0}	5.5×10^{0}
D.I. $\Delta\xi = 200$	17	1.0×10^{84}	1.0×10^{84}	2.5×10^{36}	2.5×10^{36}
GMS $\Delta\xi = 50$	3042	2.3×10^{-6}	1.3×10^{-6}	1.9×10^{-1}	8.4×10^{-2}
GMS $\Delta\xi = 100$	511	2.3×10^{-6}	1.3×10^{-6}	1.9×10^{-1}	8.4×10^{-2}
GMS $\Delta\xi = 200$	140	2.3×10^{-6}	1.3×10^{-6}	1.9×10^{-1}	8.4×10^{-2}
GMS $\Delta\xi = 1000$	12	2.3×10^{-6}	1.3×10^{-6}	1.9×10^{-1}	8.4×10^{-2}
GMS $\Delta\xi = 2000$	5.9	2.3×10^{-6}	1.3×10^{-6}	1.9×10^{-1}	8.4×10^{-2}
GMS $\Delta\xi = 2860$	4.11	2.3×10^{-6}	1.3×10^{-6}	1.9×10^{-1}	8.4×10^{-2}
GMS $\Delta\xi = 7150$	1.64	2.5×10^{-6}	1.6×10^{-6}	1.9×10^{-1}	8.4×10^{-2}
GMS $\Delta\xi = 14300$	0.87	1.5×10^{-5}	1.65×10^{-5}	2.4×10^{-1}	1.16×10^{-1}
GMS $\Delta\xi = 28600$	0.5	4.0×10^{-4}	1.8×10^{-4}	2.5×10^{-1}	2.8×10^{-1}

6.5 State Estimation with GMS for GHAME Vehicle

6.5.1 State Estimation with GMS for Longitudinal Dynamics

In this section, the results from the GMS method are compared with the results from the direct-integration method in fourth order longitudinal dynamics of the GHAME vehicle. A fourth order LTV differential equation, which describes the GHAME vehicle's longitudinal dynamics is used.

$$\frac{d^4y}{dt^4} + Z_3\frac{d^3y}{dt^3} + Z_2\frac{d^2y}{dt^2} + Z_1(t)\frac{dy}{dt} + Z_0(t)y = 0 \tag{6.15}$$

Due to the 'turning point' in the phugoid mode, the first 300 seconds of the longitudinal dynamics are used for comparison. Fig. 6-9 illustrates the accuracy of the GMS solution with comparison to the direct-integration solution in case 1 ($y(0)=0$, $y(0)^{(1)}=0$, $y(0)^{(2)}=0$, $y(0)^{(3)}=0.1$). The direct-integration method with step size $\Delta t = 0.1$ is used as a reference case. Figs. 6-11 and 6-12 show the relationship between the CPU time vs. step size and maximum error vs. step size. The DI method becomes unacceptable with step size Δt greater than 2 seconds. However, the GMS method does not increase the maximum error up to step size Δt= 20 seconds. In Table 6.6, the comparison between the GMS method with step size Δt = 20 seconds and the reference case shows that the GMS case is 125 times faster.

Fig. 6-10 illustrates the accuracy of the GMS solution with comparison to the direct-integration solution in case 2 ($y(0)=0$, $y(0)^{(1)}=1$, $y(0)^{(2)}=0$, $y(0)^{(3)}=0$). The direct-integration method with step size $\Delta t = 0.1$ is used as a reference case as before. Fig. 6-13 and 6-14 show the relationship between the CPU time vs. step size and maximum error vs. step size. The result is very similar to the result from case 1. The DI method becomes unacceptable with step size Δt greater than 2 seconds. However, the GMS method does not increase the maximum error up to step size Δt=

20 seconds. In Table 6.6, the comparison between the GMS method with step size $\Delta t = 20$ seconds and the reference case shows that the GMS case is 141 times faster.

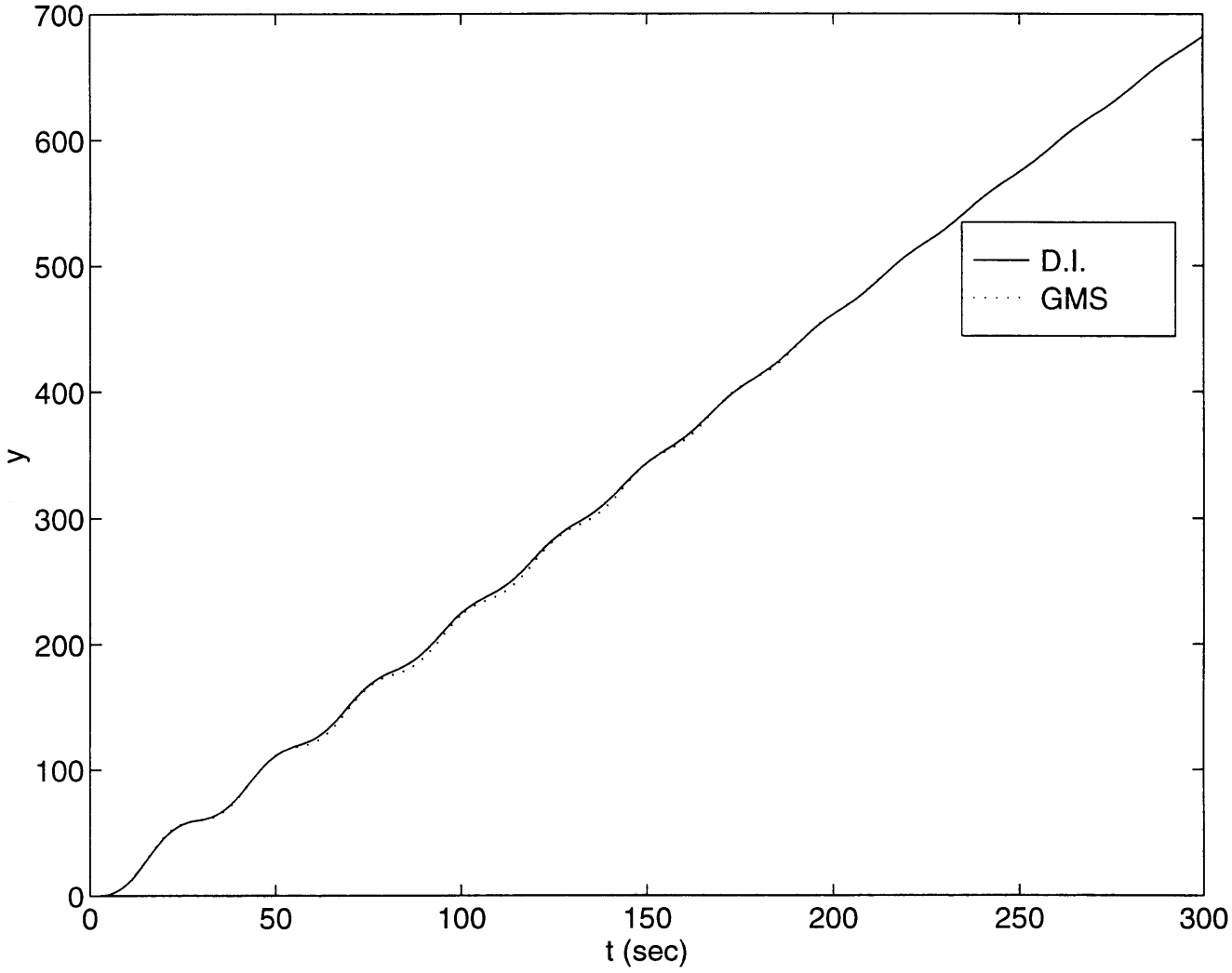

Figure 6-9: Comparison between Direct-Integration and GMS solutions for Longitudinal Fourth Order Dynamics: Case 1 [$y(0)=0$, $y(0)^{(1)}=0$, $y(0)^{(2)}=0$, $y(0)^{(3)}=0.1$]

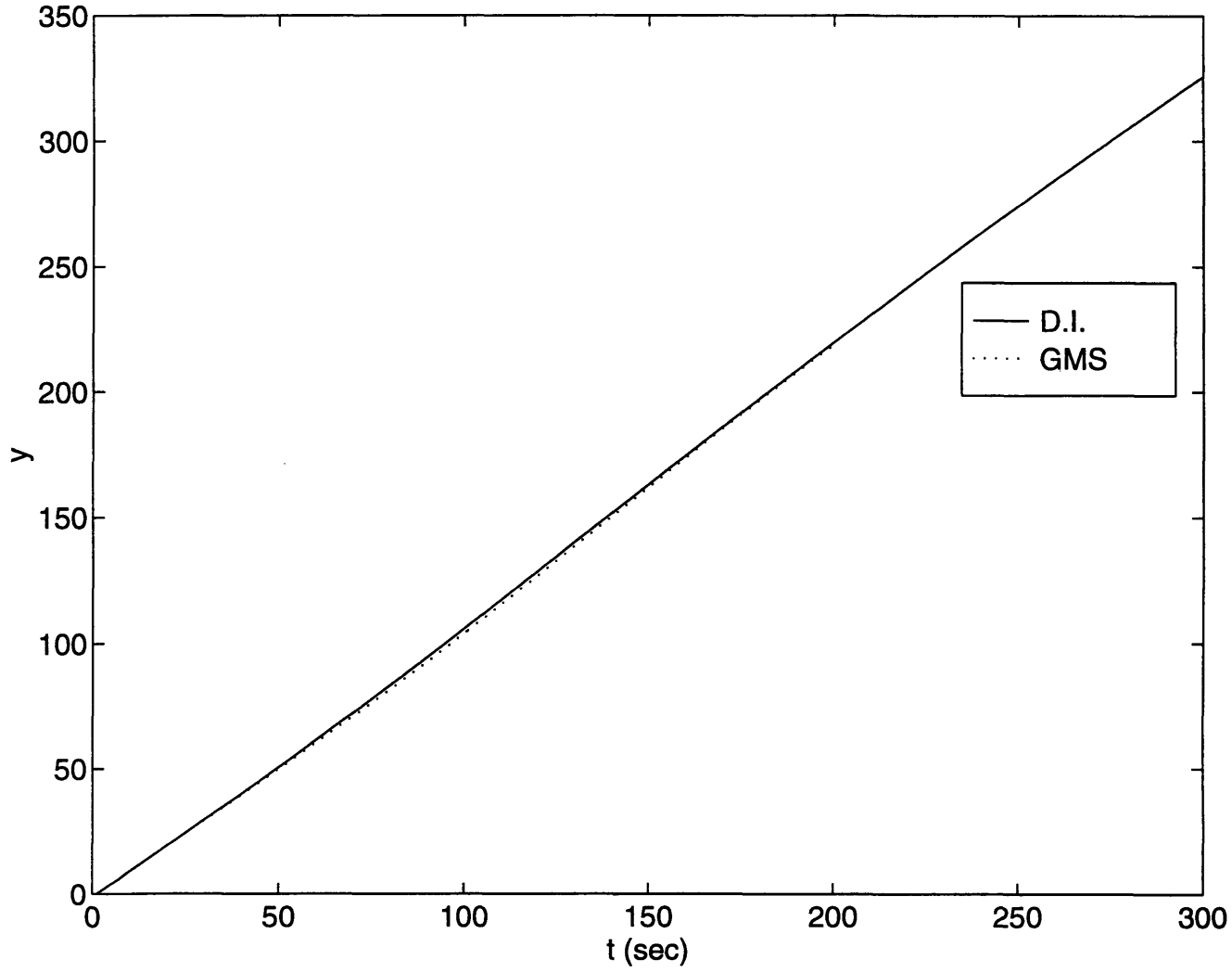

Figure 6-10: Comparison between Direct-Integration and GMS solutions for Longitudinal Fourth Order Dynamics: Case 2 [$y(0)=0$, $y(0)^{(1)}=1$, $y(0)^{(2)}=0$, $y(0)^{(3)}=0$]

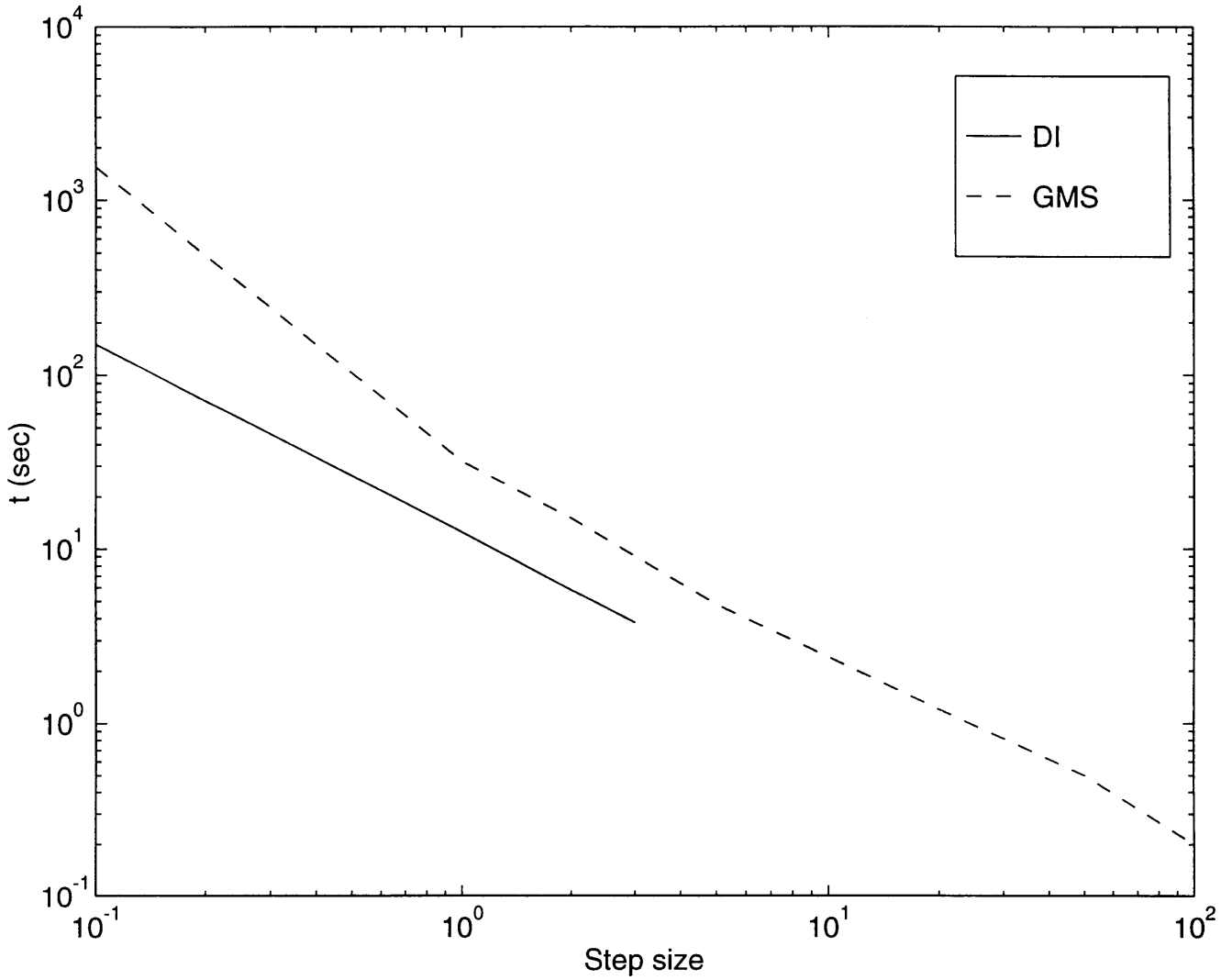

Figure 6-11: CPU Time vs. Step Size for Direct Integration and GMS approach: Case 1

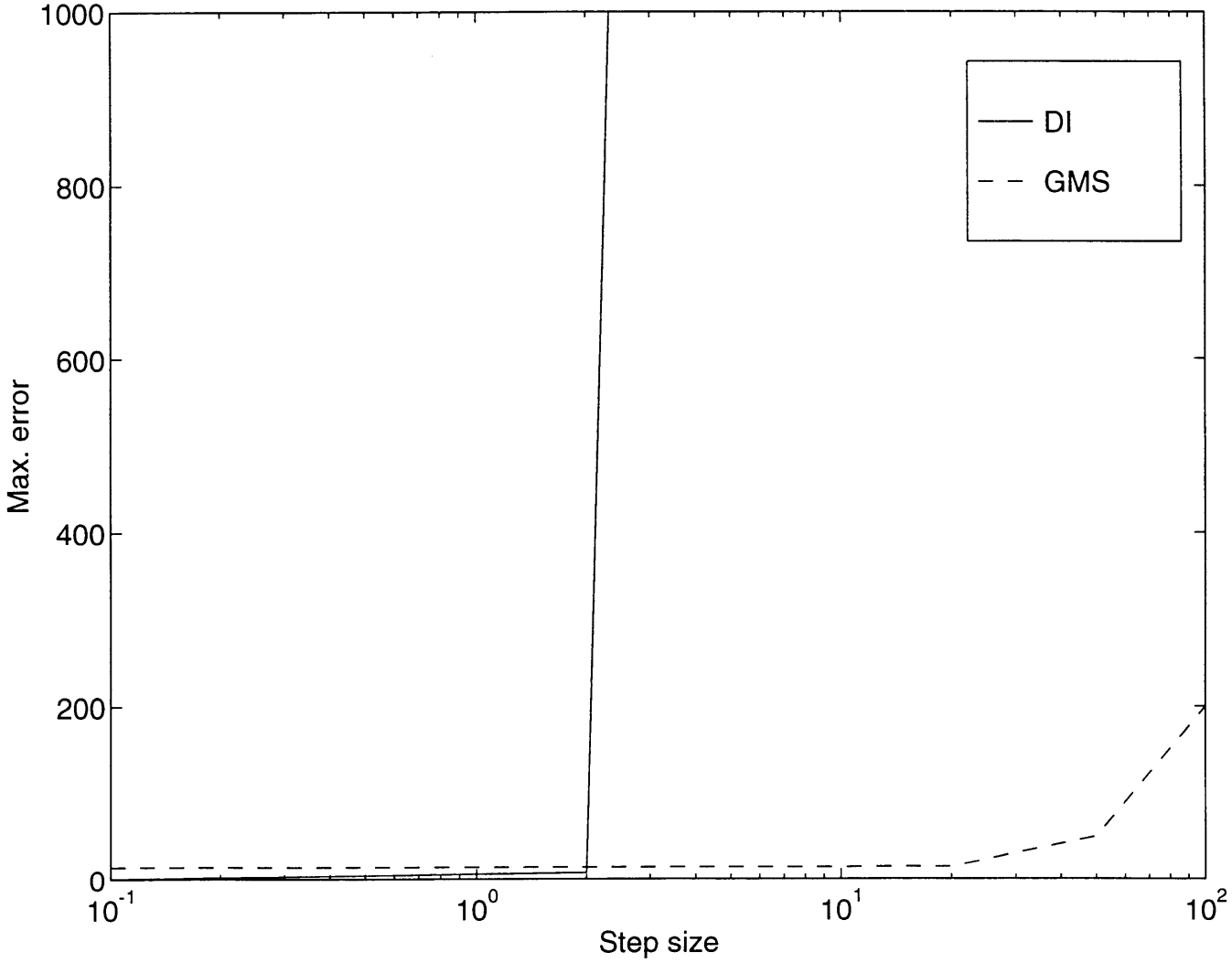

Figure 6-12: Maximum Error vs. Step Size for Direct Integration and GMS approach: Case 1

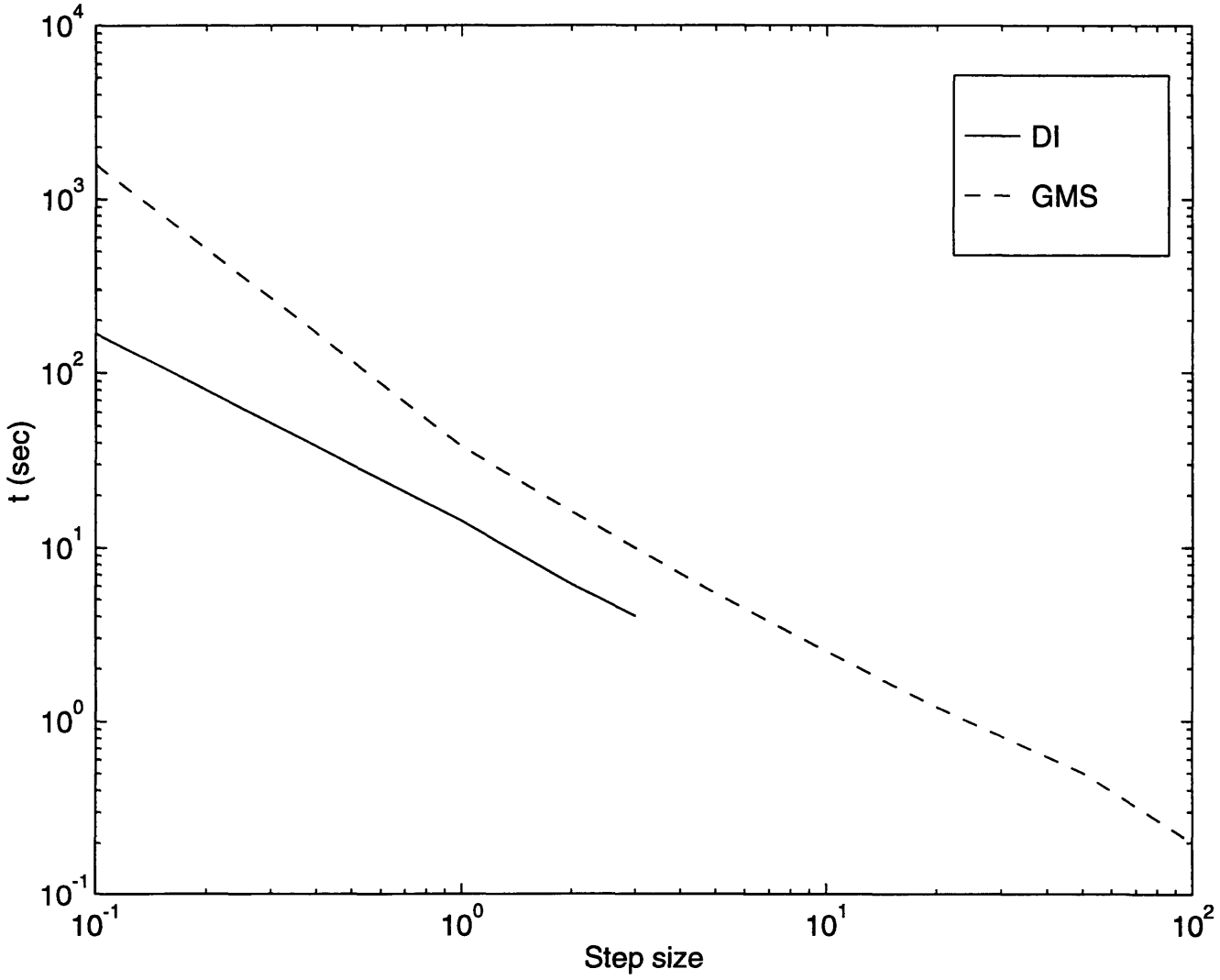

Figure 6-13: CPU Time vs. Step Size for Direct Integration and GMS approach: Case 2

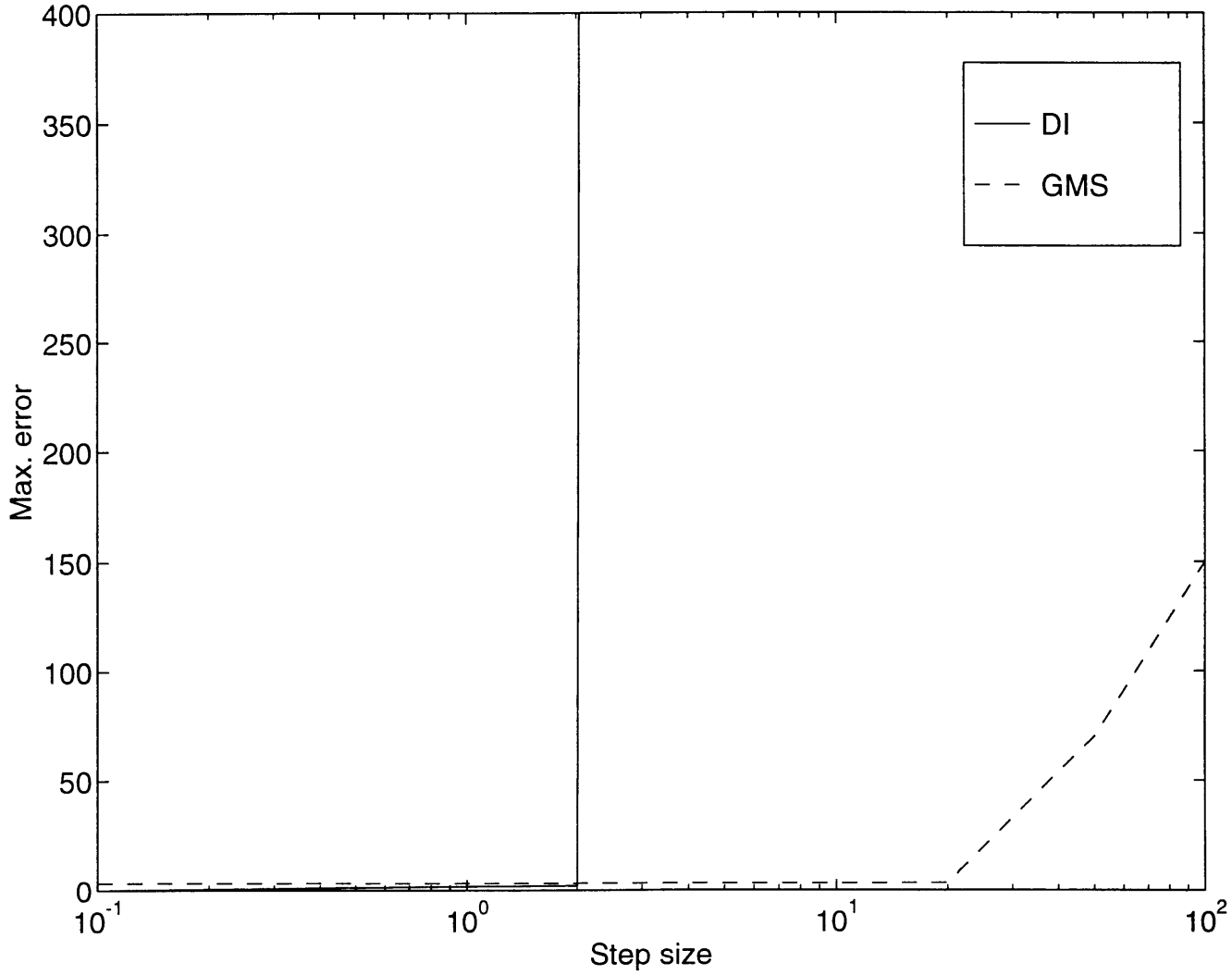

Figure 6-14: Maximum Error vs. Step Size for Direct Integration and GMS approach: Case 2

Table 6.6: Comparison between Direct-Integration and GMS for Longitudinal Fourth Order Dynamics(0 to 300 sec): Case 1 [$y(0)=0$, $y(0)^{(1)}=0$, $y(0)^{(2)}=0$, $y(0)^{(3)}=0.1$] & Case 2 [$y(0)=0$, $y(0)^{(1)}=0$, $y(0)^{(2)}=1$, $y(0)^{(3)}=0$]

Method	Case 1		Case 2	
	CPU time (sec)	Max Error	CPU time (sec)	Max Error
D.I. $\Delta t = 0.1$ (Reference Case)	150.5	-	168.6	-
D.I. $\Delta t = 1$	12.5	6.5×10^{0}	14.2	1.9×10^{0}
D.I. $\Delta t = 2$	5.8	8.2×10^{0}	6.1	2.2×10^{0}
D.I. $\Delta t = 3$	3.8	2.7×10^{3}	4.0	8.5×10^{3}
GMS $\Delta t = 0.1$	1550.6	1.4×10^{1}	1580.7	3.3×10^{0}
GMS $\Delta t = 1$	32.3	1.4×10^{1}	36.4	3.3×10^{0}
GMS $\Delta t = 2$	15.0	1.4×10^{1}	16.1	3.3×10^{0}
GMS $\Delta t = 5$	4.8	1.4×10^{1}	5.4	3.3×10^{0}
GMS $\Delta t = 10$	2.4	1.4×10^{1}	2.5	3.3×10^{0}
GMS $\Delta t = 20$	1.2	1.5×10^{1}	1.2	3.5×10^{0}
GMS $\Delta t = 50$	0.5	5.0×10^{1}	0.5	7.0×10^{1}
GMS $\Delta t = 100$	0.2	2.0×10^{2}	0.2	1.5×10^{2}

6.5.2 State Estimation with GMS for Lateral Dynamics

In this section, the results from the GMS method are compared with the results from the direct-integration method in fourth order lateral dynamics of the GHAME vehicle. A fourth order LTV differential equation, which describes the GHAME vehicle's longitudinal dynamics is used.

$$\frac{d^4y}{dt^4} + Z_3\frac{d^3y}{dt^3} + Z_2\frac{d^2y}{dt^2} + Z_1(t)\frac{dy}{dt} + Z_0(t)y = 0 \tag{6.16}$$

Fig. 6-15 illustrates the accuracy of the GMS solution with comparison to the direct-integration solution in case 1 ($y(0)=0$, $y(0)^{(1)}=0$, $y(0)^{(2)}=0$, $y(0)^{(3)}=1$). The direct-integration method with step size $\Delta t = 0.1$ is used as a reference case. Figs. 6-17 and 6-18 show the relationship between the CPU time vs. step size and maximum error vs. step size. The DI method becomes unacceptable with step size Δt greater than 2 seconds. However, the GMS method does not increases the maximum error up to step size Δt= 20 seconds. In Table 6.7, the comparison between the GMS method with step size Δt = 20 seconds and the reference case shows that the GMS case is 378 times faster.

Fig. 6-16 illustrates the accuracy of the GMS solution with comparison to the direct-integration solution in case 2 ($y(0)=0$, $y(0)^{(1)}=1$, $y(0)^{(2)}=0$, $y(0)^{(3)}=0$). The direct-integration method with step size $\Delta t = 0.1$ is used as a reference case as before. Figs. 6-19 and 6-20 show the relationship between the CPU time vs. step size and maximum error vs. step size. The result is very similar to the result from case 1. The DI method becomes unacceptable with step size Δt greater than 2 seconds. However, the GMS method does not increase the maximum error up to step size Δt= 20 seconds. In Table 6.7, the comparison between the GMS method with step size Δt = 20 seconds and the reference case shows that the GMS case is 447 times faster.

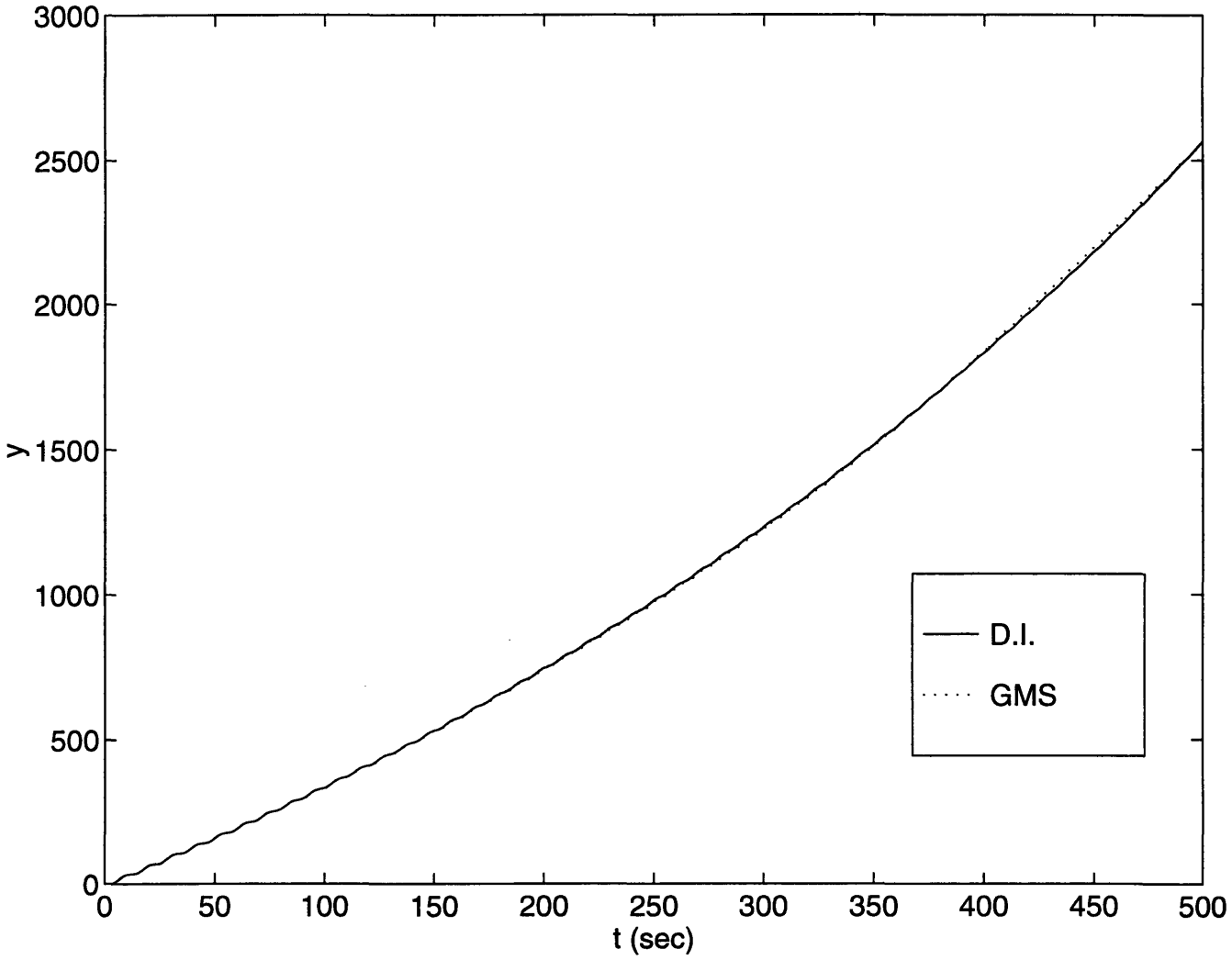

Figure 6-15: Comparison between Direct-Integration and GMS solutions for Lateral Fourth Order Dynamics: Case 1 [$y(0)=0$, $y(0)^{(1)}=0$, $y(0)^{(2)}=0$, $y(0)^{(3)}=1$]

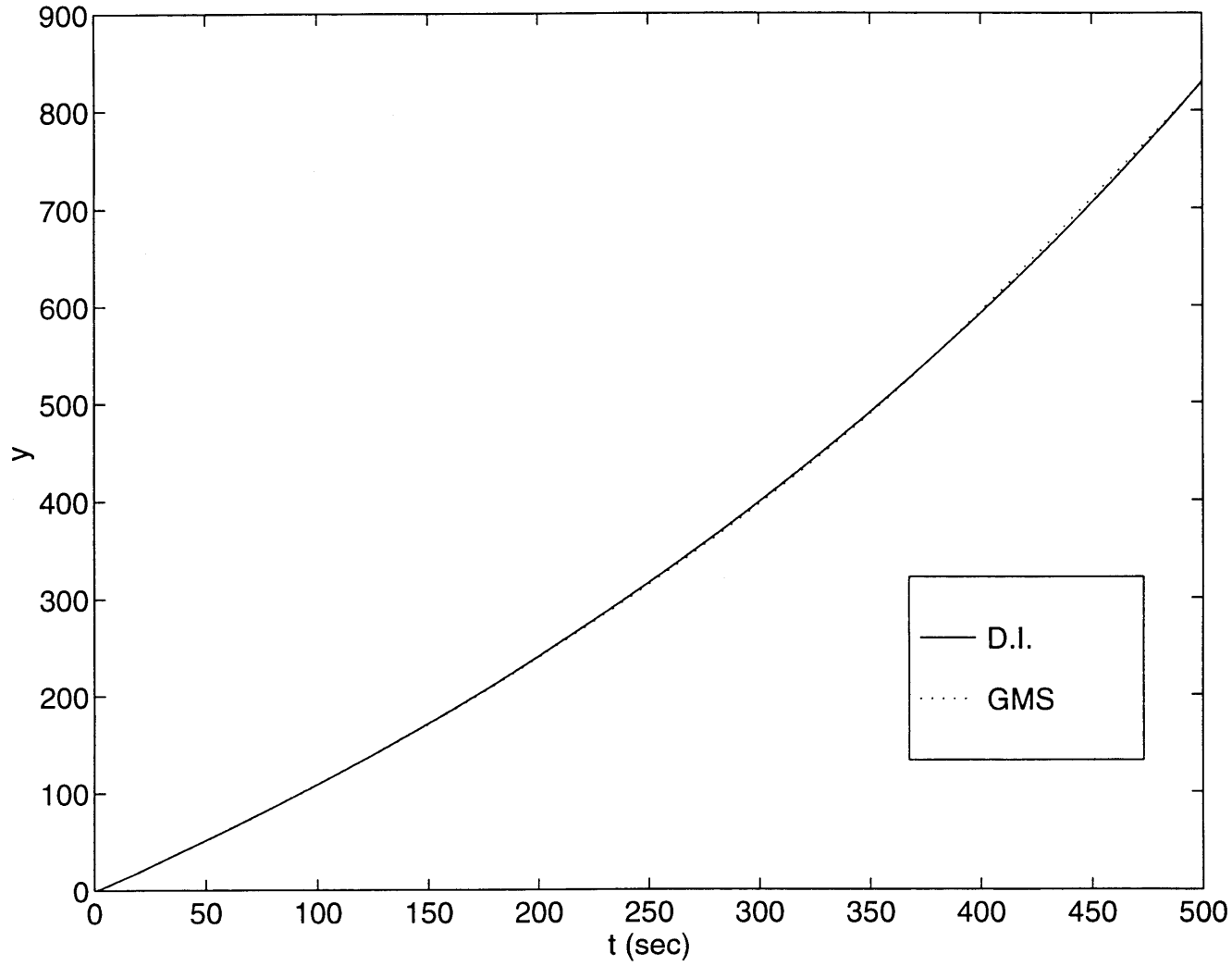

Figure 6-16: Comparison between Direct-Integration and GMS solutions for Lateral Fourth Order Dynamics: Case 2 [$y(0)=0$, $y(0)^{(1)}=1$, $y(0)^{(2)}=0$, $y(0)^{(3)}=0$]

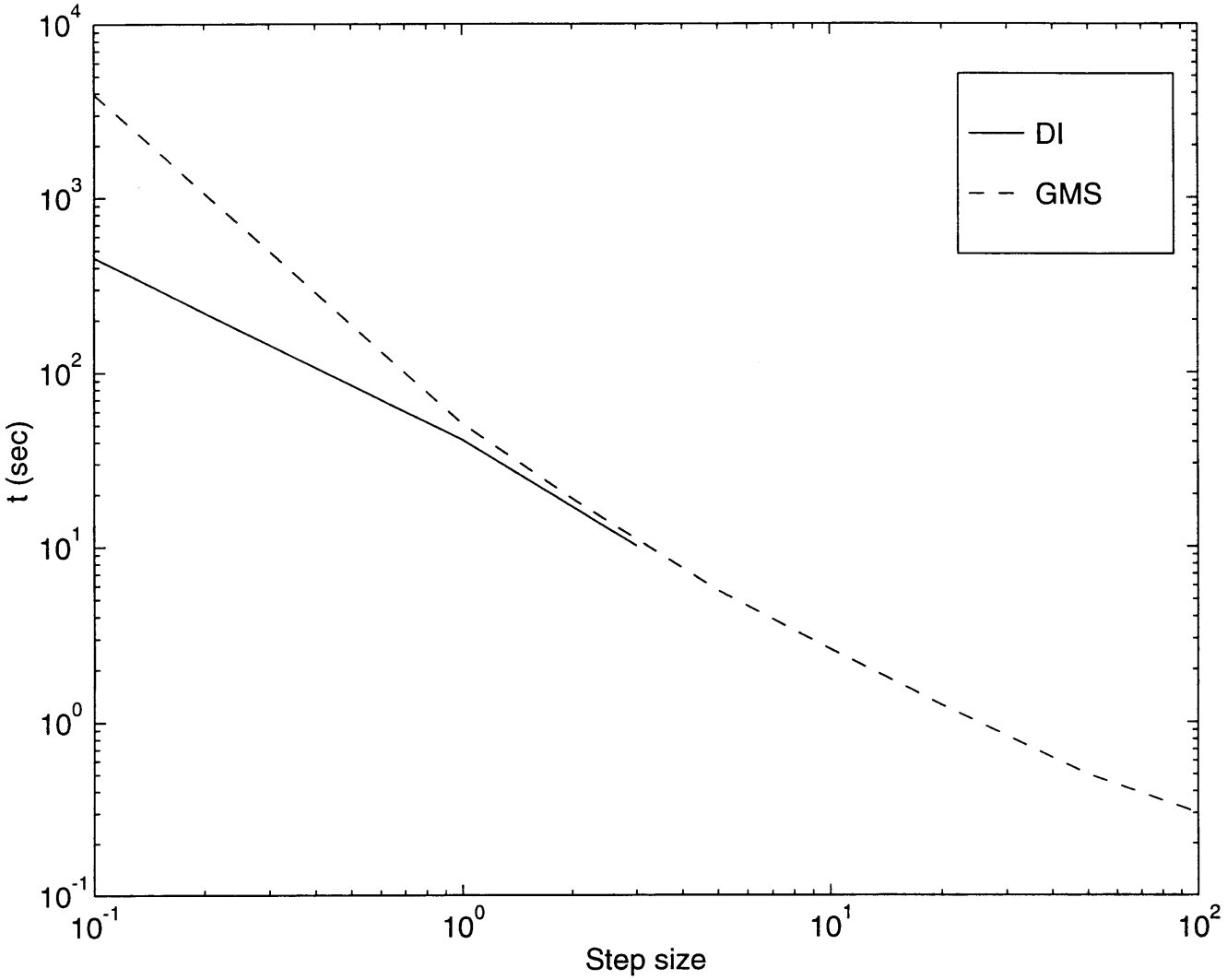

Figure 6-17: CPU Time vs. Step Size for Direct Integration and GMS approach: Case 1

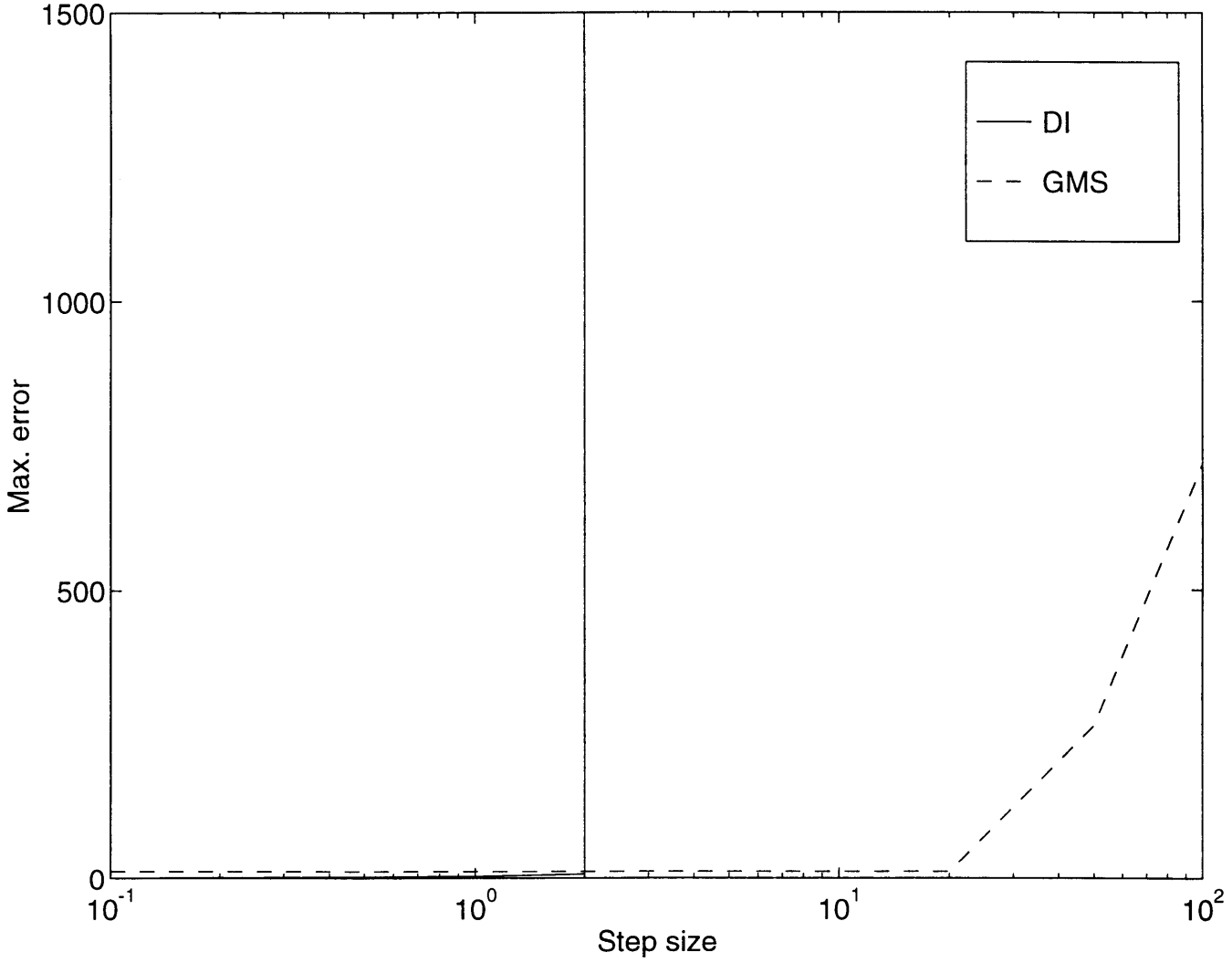

Figure 6-18: Maximum Error vs. Step Size for Direct Integration and GMS approach: Case 1

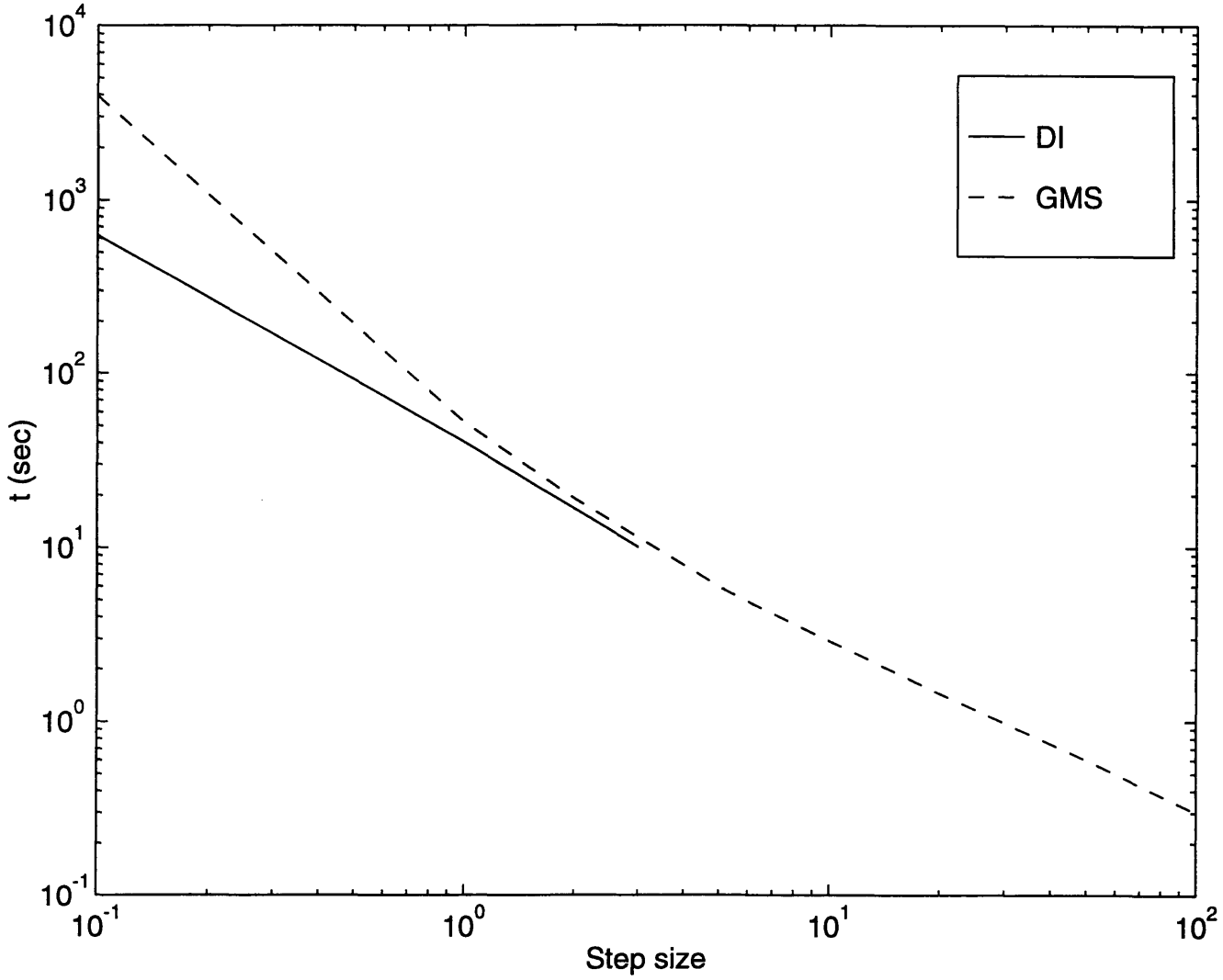

Figure 6-19: CPU Time vs. Step Size for Direct Integration and GMS approach: Case 2

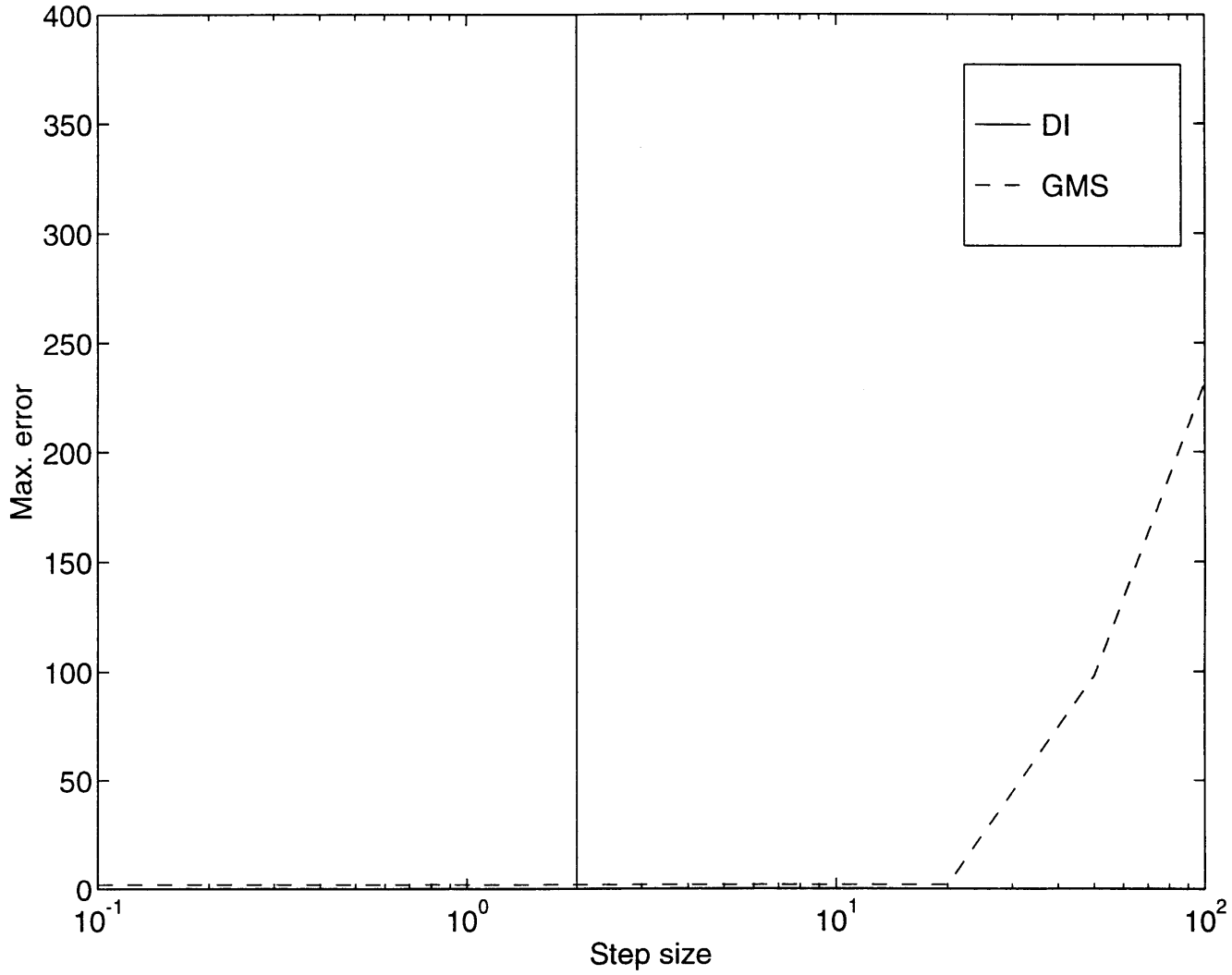

Figure 6-20: Maximum Error vs. Step Size for Direct Integration and GMS approach: Case 2

Table 6.7: Comparison between Direct-Integration and GMS for Lateral Fourth Order Dynamics (0 - 500 seconds): Case 1 [$y(0)=0$, $y(0)^{(1)}=0$, $y(0)^{(2)}=0$, $y(0)^{(3)}=1$] & Case 2 [$y(0)=0$, $y(0)^{(1)}=1$, $y(0)^{(2)}=0$, $y(0)^{(3)}=0$]

Method	Case 1		Case 2	
	CPU time (sec)	Max Error	CPU time (sec)	Max Error
D.I. $\Delta t = 0.1$ (Reference Case)	453.5	-	625.6	-
D.I. $\Delta t = 1$	41.2	3.5×10^{0}	40.9	3.9×10^{-1}
D.I. $\Delta t = 2$	17.1	7.9×10^{0}	16.7	8.9×10^{-1}
D.I. $\Delta t = 3$	10.1	2.7×10^{7}	10	8.5×10^{5}
GMS $\Delta t = 0.1$	3936.6	1.2×10^{1}	3945.7	1.9×10^{0}
GMS $\Delta t = 1$	51.3	1.2×10^{1}	52.4	1.9×10^{0}
GMS $\Delta t = 2$	18.9	1.2×10^{1}	19.0	1.9×10^{0}
GMS $\Delta t = 5$	5.6	1.2×10^{1}	6.0	1.9×10^{0}
GMS $\Delta t = 10$	2.6	1.2×10^{1}	2.9	1.9×10^{0}
GMS $\Delta t = 20$	1.2	1.2×10^{1}	1.4	1.9×10^{0}
GMS $\Delta t = 50$	0.5	2.6×10^{2}	0.6	9.8×10^{1}
GMS $\Delta t = 100$	0.3	7.2×10^{2}	0.3	2.3×10^{2}

6.6 Discussion on Parameter Estimation with GMS Method

From previous sections, the saving of the computational time on the initial state estimation is substantial with the GMS method, and the parameter estimation requires accurate initial state estimation. If the GMS method is used for the initial estimation, which will be used in the parameter estimation, then the saving of the computational time will be significant. For example, the GMS method is 378 -447 times faster than the conventional direct-integration method in the fourth order lateral cases (0 - 500 seconds). The longer the range of the state estimation, the greater the saving on the CPU time. For example, the fourth order longitudinal cases are 125 - 141 times faster because they are investigated only for 0 - 300 seconds. The maximum error is also smaller with lateral cases. The longitudinal cases have 2.1 % maximum error for case 1 and 1.1 % maximum error for case 2. The lateral cases have 0.46 % maximum error for case 1 and 0.23 % maximum error for case 2. As a consequence, the use of the GMS method will expedite the parameter estimation, and the longer the range of the state estimation, the greater the saving on the computational time. The concept of the GMS method with maximum-likelihood process is shown in Fig. 6-21. In conclusion, the GMS solution gives significant savings on the CPU time, and the combination of the maximum-likelihood estimation process with the GMS solution will expedite the parameter estimation process.

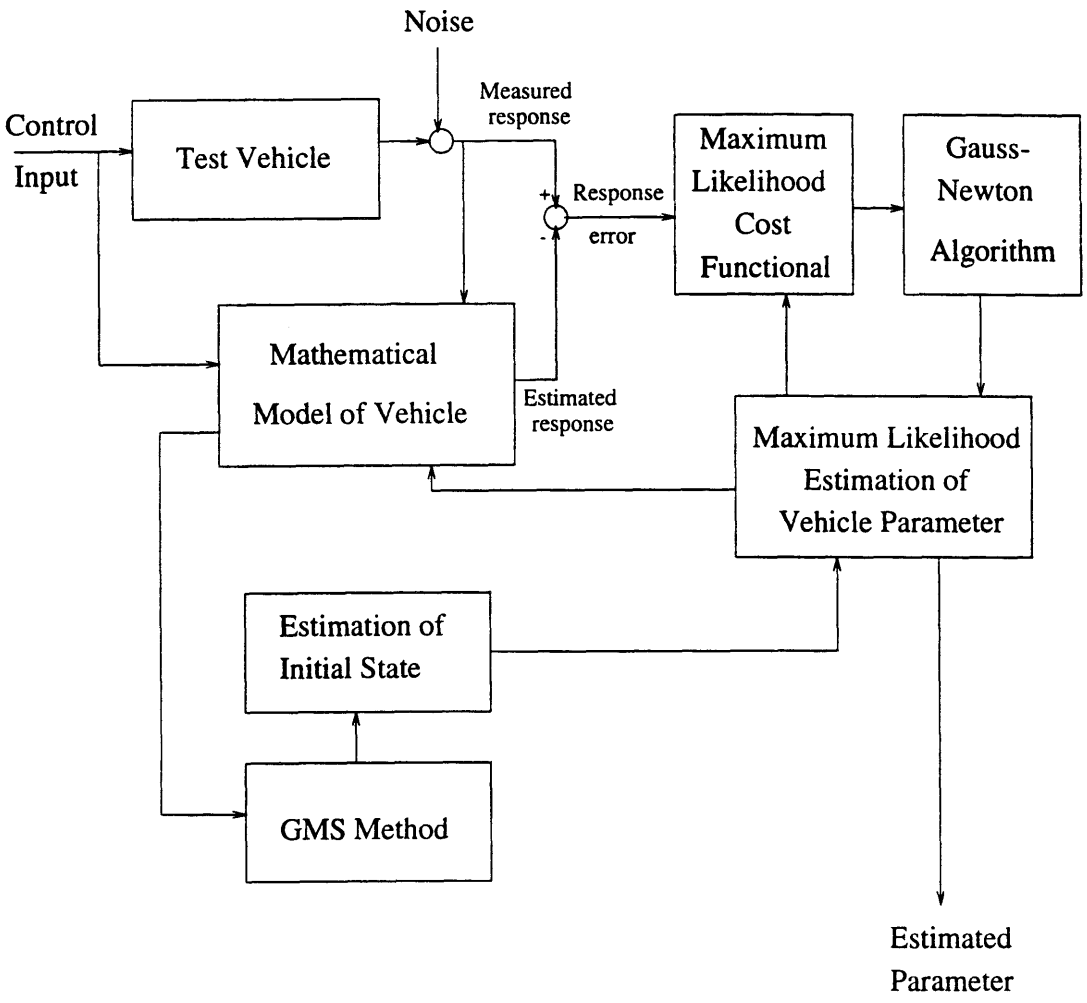

Figure 6-21: Maximum-likelihood estimation with GMS method

Chapter 7

Summary and Conclusion

In this thesis, the longitudinal stability and flying qualities as well as a parameter estimation problem of the Generic Hypersonic Aerodynamic Model Example (GHAME) vehicle are investigated along an optimal trajectory which had been designed for the Space Shuttle orbiter 049 vehicle. The Generalized Multiple Scales (GMS) theory, which was developed by Ramnath, is used throughout this study.

The accuracy of the stability parameter, which was developed by Ramnath, is investigated in two other approaches. One is a numerical solution and the other is the bound of the solution which is derived from the GMS approximate solution. The stability parameter shows that the stability improves as the trajectory progresses. For the numerical solution, the trajectory is divided into six segments and the relative stability is compared among segments. The results agree with the results from the stability parameter. The bound of the solution also gives the same results. The stability parameter provides very accurate stability information based on three simple aerodynamic coefficients and ambient density. Therefore, the stability parameter can be obtained easily with existing flight measurement systems and stability information will be available to the pilot during the flight.

The conventional flying qualities criteria have been based on constant flight conditions. However, the nature of the flight vehicle has changed drastically, and many high speed vehicles have time-varying systems as well as very large flight envelopes. The extended flying qualities criteria (EFQC) are defined based on the GMS theory,

which has analytical solutions for a time-varying system. The EFQC specify flying qualities in terms of variable system responses.

The EFQC are applied to the GHAME vehicle to analyze the flying qualities of the short-period , phugoid, dutch-roll, spiral and roll modes. For the short-period, the flying quality does not meet the Level 3 requirement for the first 900 seconds during 1886 seconds of flight. At the end of the trajectory, the flying quality satisfies only the Level 2 requirement. Therefore, the short-period mode is not controllable for the first half of the flight and the second half of the flight puts an excessive workload on the pilot.

The flying quality of the phugoid mode is not analyzed for the entire trajectory due to the 'turning point'. The flying quality starts from Level 3, then reaches Level 2 and Level 1. However, the flying quality degrades to Level 3 at 312 seconds. Due to the turning point, the flying quality is not analyzed between 312 seconds and 685 seconds. The flying quality remains at Level 1 from 685 seconds until 1670 seconds then the 'turning point' occurs again. The results show that the flying quality of the phugoid mode fluctuates between Level 1 and Level 3. Therefore, it will be very useful to have the flight display window for the pilot to provide flying qualities information especially for the phugoid mode.

For the dutch-roll mode, the flying quality satisfies only Level 3 requirements. Therefore, the workload for the pilot will be excessive. The flying quality of the spiral mode satisfies the Level 1 requirement throughout the trajectory. However, the flying quality of the roll mode does not meet Level 3 requirements. Therefore, the roll mode will be uncontrollable for the pilot. The spiral mode is the only mode which has adequate flying quality during the entire trajectory.

Based on these analyses, either the GHAME vehicle is uncontrollable for the pilot or the pilot's workload becomes excessive. Consequently, the GHAME vehicle needs augmented control systems and the flight display window would be very useful.

Finally, the parameter estimation with the GMS theory is investigated. The advantages of the GMS method over the direct-integration (DI) method in estimating initial states are investigated.

For the second order dynamics, the relationships between the CPU time and step size, maximum error and step size, and steady state error and step size are investigated. For the DI method, the step size has to be at least $\Delta\xi = 154$ and the CPU time for this run is 23 seconds. In contrast, the GMS method can use step size $\Delta\xi = 7150$ without significantly increasing maximum error and steady-state error, and the CPU time for this run is 1.64 seconds. Consequently, the GMS method is 14 times faster than the DI method with $\Delta\xi = 154$ and 419 times faster than the reference case.

For the fourth order dynamics of the GHAME vehicle, the relationships between the CPU time and step size, and maximum error and step size are investigated.

The longitudinal dynamics are investigated first and then the lateral dynamics. For the DI method in longitudinal dynamics with case 1, the step size has to be at least $\Delta t = 2$ and the CPU time for this run is 5.8 seconds. In contrast, the GMS method can use step size $\Delta t = 20$ without increasing maximum error and steady-state error, and the CPU time for this run is 1.2 seconds. Consequently, the GMS method is 4.8 times faster than the DI method with $\Delta t = 2$ seconds and 125 times faster than the reference case.

In longitudinal cases, the results for case 2 are similar to those of case 1. The step size has to be at least $\Delta t = 2$ for the DI method and the CPU time for this run is 6.1 seconds. In contrast, the GMS method can use step size $\Delta t = 20$ without increasing maximum error and steady-state error, and the CPU time for this run is 1.2 seconds. Consequently, the GMS method is 5.1 times faster than the DI method with $\Delta t = 2$ seconds and 141 times faster than the reference case.

For the DI method in lateral dynamics with case 1, the step size has to be at least $\Delta t = 2$ and the CPU time for this run is 17.1 seconds. In contrast, the GMS method can use step size $\Delta t = 20$ without significantly increasing maximum error and steady-state error, and the CPU time for this run is 1.25seconds. Consequently, the GMS method is 14 times faster than the DI method with $\Delta t = 2$ seconds and 378 times faster than the reference case.

In lateral cases, the results for case 2 are similar to those of case 1. The step size

has to be at least $\Delta t = 2$ for the DI method and the CPU time for this run is 16.7 seconds. In contrast, the GMS method can use step size $\Delta t = 20$ without significantly increasing maximum error and steady-state error, and the CPU time for this run is 1.4 seconds. Consequently, the GMS method is 11.9 times faster than the DI method with $\Delta t = 2$ seconds and 447 times faster than the reference case.

The longer the state estimation, the greater the saving in computational time. Therefore, the benefit of the GMS method in computing time is significant and the GMS method will expedite the parameter estimation process.

Bibliography

[1] Bowers, A. H. and Iliff, K. W., *A Generic Hypersonic Aerodynamic Model Example (GHAME) for Computer Simulation*, Ames Research Center, Dryden Flight Research Facility, August 5, 1988

[2] Deyst, J., Kriegsman, B., and Marcus, F., *Entry-Trajectory Design to Minimize Thermal-Protection-System Weight*, Charles Stark Draper Laboratory, November, 1971

[3] Ramnath, R. V. and Sinha, P., *Dynamics of the Space shuttle during Entry into Earth's Atmosphere*, AIAA Journal, Vol. 13, No. 3, March, 1975.

[4] Tao, Y., *Satellite attitude prediction by multiple time scales method*, Sc.D. Thesis, MIT, 1976

[5] Radovsky, S. E., *Sensitivity analysis of slowly-varying systems as applied to a VTOL airplane*, Master's Thesis, MIT, 1978

[6] Ramnath, R. V. and Sandri, G., *A General Multiple Scales Approach to a Class of Linear Differential Equations*, Journal of Mathematical Analysis and Application, Vol. 28, 1969

[7] Ramnath, R. V., Hedrick, J. K., Paynter, H. M., eds. *Nonlinear System Analysis and Synthesis: Vol. 2-Techniques and Applications*, The American Society of Mechanical Engineer, New York, 1980

[8] Vinh, N. X. and Laitone, E. V., *Longitudinal Dynamic Stability of a Shuttle Vehicle*, Journal of Aeronautical Sciences, Vol. XIX, No. 5, March - April, 1972

[9] Etkin, B., *Longitudinal Dynamics of Lifting Vehicle in Orbital Flight*, Journal of Aeronautical Sciences, Vol. 28, October, 1961

[10] Ramnath R. V., *Advanced Flight Dynamics and Control, Class Lecture Notes*, Massachusetts Institute of Technology, 1992

[11] Poincarè H., *New methods of celestial mechanics*, NASA TF F-450, 1967

[12] Etkin, B., *Dynamics of Flight: Stability and Control*, John Wiley & Sons, New York, 1982

[13] Phillips, W. H., *Flying Qualities from Early Airplanes to the Space Shuttle*, Journal of Guidance, Control, and Dynamics, Vol. 12, No. 4, July - August, 1989

[14] *Military Standard: Flying Qualities of Piloted Aircraft, MIL-STD-1797A*, January, 1990

[15] Harper, R. P. and Cooper, G. E., *Handling Qualities and Pilot Evaluation*, Journal of Guidance, Control, and Dynamics, Vol. 9, No. 5, September - October, 1986

[16] Hagelauer, P. V., *Dynamics and Sensitivity Analysis of a Class of High Speed Aircraft*, Master's Thesis, MIT, 1993

[17] Iliff, K. W., *Parameter Estimation for Flight Vehicles*, Journal of Guidance, Control, and Dynamics, Vol. 12, No. 5, September - October, 1989

[18] Ward D. T., *Introduction to Flight Test Engineering* , Elsevier Science Publisher, New York, 1993

[19] Iliff K. W. and Maine R. E., *Practical Aspect of Using a Maximum-Likelihood Estimator*, AGARD-CP-172, Paper 16, May, 1975

[20] Rediess, H. M., *An Overview of Parameter Estimation Techniques and Application in Aircraft Flight Testing*, NASA TN-7647, Paper 1, April 1974

[21] Suit, W. T. and Schiess J. R., *Lateral Longitudinal Stability and Control Parameters for the Space Shuttle Discovery as Determined from Flight Data*, NASA TM-100555, February, 1988

[22] Maine R. E. and Iliff K. W., *Identification of Dynamic Systems-Application to Aircraft Part I: The Output Error Approach*, AGARD-AG-300-Vol.3, 1986

[23] Maine R. E. and Iliff K. W., *Identification of Dynamic Systems*, AGARD-AG-300-Vol.2, 1985

[24] Maine R. E. and Iliff K. W., *Formulation and Implementation of a Practical Algorithm for Parameter Estimation with Process and Measurement Noise*, SIAM Journal of Applied Mathematics, Vol. 41, No. 3, December, 1981